POLITECNICO DI MILANO

School of Industrial and Information Engineering

Master of Science in Energy Engineering

POLITECNICO
MILANO 1863

Master Thesis

Evaluating performance of Fishbone completions using numerical simulations

Advisor:

Prof. Luigi Pietro Maria Colombo

Industrial supervisor:

Ing. Federica Caresani

Dr. Alberto Cominelli

Candidate:

Andrea Rosa

ID Number 872234

Academic Year 2017-2018

Acknowledgments

Questo lavoro è stato possibile solo grazie alle vicinanza e al sostegno di diverse persone.

Volevo innanzitutto ringraziare il Professor Luigi Colombo per la sua pazienza e per i consigli che mi ha dato durante il mio percorso universitario.

A Federica Caresani e Alberto Cominelli devo tutta la mia gratitudine. Li ringrazio per il tempo dedicatomi e per il prezioso aiuto. Grazie a loro ho cominciato il mio percorso in Eni, in particolare nel mondo delle simulazioni di giacimento. Non posso che ricordare anche i colleghi di ARMS e tutti gli altri ragazzi, incontrati negli uffici o in pausa pranzo, per il loro affetto e simpatia.

Un ringraziamento va anche a tutti i compagni conosciuti nei cinque anni universitari. A tutti loro va il mio in bocca al lupo. In particolare a Daniele, Massimiliano e Riccardo con cui ho condiviso un'esperienza meravigliosa all'estero.

Infine volevo ringraziare coloro che hanno permesso tutto ciò, i miei genitori, Manuela e Marco, per il loro sostegno, i rimproveri e le lezioni. Senza dimenticare mio fratello Lorenzo, compagno di vita, nello studio e nello sport, che ho sempre preso come esempio.

Andrea Rosa

Abstract

The Oil & Gas industry has developed sophisticated technologies to maximize reservoir contact. Hydraulic fracturing (HF) is the most effective stimulation process for tight formations, but there are economic, environmental and operational concerns which constrain its implementation in various contexts, e.g. off-shore conditions or thin reservoirs where fractures may jeopardize cap-rock integrity. Fishbone completion is a newly developed technology that can be considered a cheaper and more reliable alternative to HF. A fishbone completion consists of a sequence of short liners. Each of these houses 3-4 small diameter needles departing in orthogonal directions and contacting the reservoir up to 12 m. Notably, a fishbone completion is usually slightly more expensive than the reference liner completion, this explains why in many brown fields operators implement this stimulation as a trial and error process based on pilot experience. In more challenging environments, where Fishbones can be one of the critical factors that make a project economically feasible, it is necessary to estimate its potential benefits using numerical simulations.

In reservoir simulations, wells are modelled according to the so-called Peaceman's model, which allows to define a well performance indicator. However, this model may not work for Fishbones, because of the complex flow path establishing towards the well in presence of high-density needles. To perform 3D simulations of fishbone completion based field developments, it is necessary to define a proper modelling methodology.

In this work, three different modelling approaches for fishbone completion are investigated: High Resolution Grid (HRG), Embedded-Discrete-Fracture-Model (EDFM) and Finite-Element-Method (FEM). The first two methodologies rely on a finite-volume formulation of reservoir conservation equations: the HRG enhances grid resolution to improve accuracy, while in the EDFM needles are treated as fractures and much coarser grid resolution are used. On the contrary, the FEM approach leverages on the possibility to define a mesh conformal to completion geometry.

The FEM results are benchmarked with analytical solutions, proving the effectiveness of the specific implementation of the method. The three methodologies are then used to evaluate fishbone benefit on production with respect to a conventional completion through sensitivity analysis for single phase problems. Notably, inconsistencies between HRG results on one side and EDFM/FEM results on the other side together with some specific insights indicated that HRG is not a suitable technique for modelling Fishbones. This provided confidence about using EDFM for a field-like application where it could be possible to show that Fishbones largely anticipate production and give 10% more gas than conventional completions in the whole concession period.

Keywords: Fishbone completion, High Resolution Grid, Embedded-Discrete-Fracture-Modeling, Finite Element Method, reservoir simulation, well modeling.

Sommario

L’industria petrolifera ha sviluppato sofisticate tecnologie per massimizzare l’estrazione di idrocarburi aumentando la comunicazione tra giacimento e pozzo. La fratturazione idraulica (HF) è il processo più efficace per stimolare giacimenti a bassa permeabilità, tuttavia ci sono preoccupazioni dal punto di vista economico, ambientale e operativo che possono limitarne l’applicabilità in vari contesti, come in campo off-shore o in giacimenti sottili dove le fratture possono compromettere l’integrità della roccia di contenimento. Il completamento a Fishbone è una tecnologia di recente sviluppo che può essere considerata un’alternativa più economica e più controllabile rispetto a HF. Un completamento a Fishbones è costituito da una serie di liner, ciascuno di questi ospita 3-4 laterali, di diametro ridotto, uscenti in direzioni ortogonali, contattando il giacimento fino a 12 m. Il completamento a Fishbones è leggermente più costoso di uno convenzionale, ciò spiega perché viene spesso installato in giacimenti maturi come tentativo per prolungarne la vita basandosi su test piloti. In situazioni più complesse, dove questo completamento può essere il fattore chiave che rende redditizio un progetto, è necessario stimarne i benefici tramite simulazioni numeriche.

Nelle simulazioni di giacimento, i pozzi sono modellati tramite il modello di Peaceman, che permette di definire un indicatore delle performance di un pozzo. Tuttavia, il modello di Peaceman potrebbe non funzionare per un completamento a Fishbones, visto la complessità del cammino seguito dai fluidi in presenza di laterali ad alta densità. Per svolgere simulazioni 3D di sviluppi di giacimento basati sui Fishbones, è necessario definire un approccio modellistico appropriato.

In questo lavoro, tre diverse metodologie per modellare un pozzo a Fishbones sono analizzate: griglia ad alta risoluzione (HRG), Embedded-Discrete-Fracture-Model (EDFM) e metodo agli elementi finiti (FEM). I primi due approcci si basano su una formulazione ai volumi finiti delle equazioni di conservazione dei fluidi in giacimento: l’HRG aumenta la risoluzione della griglia per migliorare l’accuratezza della soluzione, mentre nell’approccio EDFM i laterali sono trattati come fratture e griglie più lasche possono essere usate. L’approccio (FEM), invece, fa leva sulla possibilità di definire una griglia di calcolo conforme alla geometria del pozzo.

I risultati FEM sono confrontati con soluzioni analitiche, provando la consistenza dell’approccio implementato. I tre metodi sono poi utilizzati per valutare il beneficio, in termini di produzione, di un completamento a Fishbones rispetto ad uno convenzionale, attraverso analisi di sensitività in sistemi monofase. In particolare, le inconsistenze tra i risultati ottenuti con il metodo HRG e i metodi EDFM/FEM, affiancate a specifici approfondimenti hanno indicato che il metodo HRG non è una tecnica in grado di modellare i Fishbones. Ciò ha supportato la scelta di utilizzare l’EDFM per un'applicazione in un campo reale dove è stato possibile dimostrare come un completamento a Fishbones anticipa notevolmente la produzione, dando il 10% in più di gas rispetto a un completamento convenzionale durante tutta la durata della concessione.

Parole chiave: Completamento a Fishbones, griglia ad alta risoluzione, Embedded-Discrete-Fracture-Modeling, metodo agli elementi finiti, simulazione di giacimento, modellistica di pozzo.

Extended summary

Oil and gas resources

Conventional oil and gas reservoirs contain accumulations of hydrocarbons that migrated from source rocks until they are captured by sealing layers acting as a cap-rock. Oil, gas and water fill the porous medium according to density and capillary effects. Hydrocarbon production is achieved with wells drilled from surface to the reservoir. During drilling operations, casing and cement are set in position to guarantee mechanical integrity and isolate high pressure zones from the surface. Well completions, including production tubing, are installed to ensure hydraulic communication between the reservoir and the wellbore. The most common (conventional) completions are: open hole, slotted liner and casing perforations. The productivity index of a well (PI) is defined as the ratio between flow rate and pressure drawdown from reservoir to bottom hole. The PI depends on formation type, pressure regime (above or below bubble point), flow conditions (transient, steady state and semi steady state), and type of completion. Usually, reservoir development is more and more difficult the lower the rock permeability and the hydrocarbon column are. Then, the Oil & Gas industry developed sophisticated drilling and completion technologies aimed at maximizing reservoir contact, reducing pressure drawdown between formation and wellbore, delaying water and gas breakthrough. Notably, the advance of these techniques and tools allowed to include in the oil and gas resources what are now known as unconventional hydrocarbons. These reservoirs, where fluids are segregated in low permeability rocks (below 0.001 mD), take a big share of the global technically recoverable resources. It is worth noticing that the name “reservoir” may be often inadequate for unconventional hydrocarbons, which are often stored inside source rocks characterized by very low permeability, the so called shale oil and shale gas formations. Their economic production cannot be achieved employing simple completions, but only when the permeability is enhanced through stimulation processes these fields can be exploited. Nowadays, tight formations are stimulated by horizontal drilling combined with hydraulic fracturing. This last procedure is a complex, expensive and with high social/environmental impacts. Moreover, fracturing is extremely risky when dealing with high pressure and high temperature reservoirs.

Fishbone Completion

The Norwegian company “Fishbones A.S.” has developed a new type of completion that can be seen as an alternative to hydraulic fracturing. A fishbone completed well consists of a main bore from

which several laterals exit contacting the reservoir in orthogonal directions. A reservoir liner is equipped with short fishbone subs, each of these contains 3-4 small-diameter needles/laterals with length up to 12 meters that extend into the formation, sub spacing is determined by the operator to maximize hydrocarbon recovery. The aim is to create small channels, the needle annuli, departing from the main wellbore where formation fluids can flow. Differently from hydraulic fracturing, the flow path of a fishbone completion is under control, hence, sweet spots are targeted while the contact with water zone or gas cap is avoided. Moreover, HSE issues are drastically reduced.

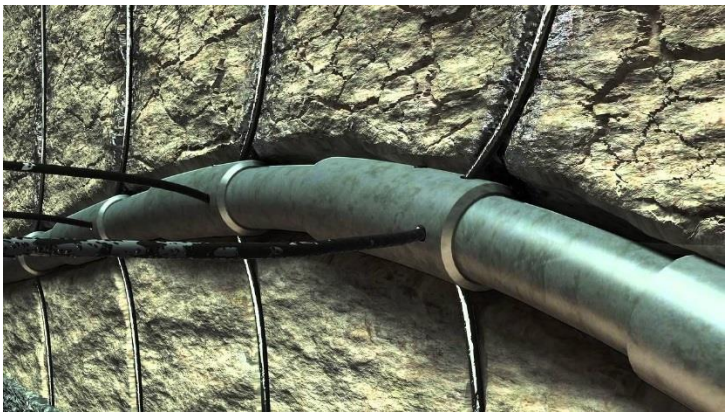

Figure a: A representation of a fishbone completed well. The main bore is equipped with several subs that house laterals which extend into the reservoir in orthogonal directions. Source: (Fishbones AS 2018).

Depending on the formation type, two methods are available to extend the laterals into the reservoir: the Multilaterals Stimulation Technology, recommended for carbonates, and the Multilateral Drilling Stimulation Technique commonly used in sandstone formations. The first technology is performed to install Fishbones subs, made of four needles, while the second is used for Dreamliner subs, made of three needles having 120° phasing.

Fishbones A.S. in collaboration with Oil & Gas companies conduced three pilot tests of the technology. The operators concluded that the downside risk of deploying a fishbone completed well is equivalent as having a conventional (unstimulated) well, while the upside in terms of increased well productivity could be significant. In particular, Fishbones enable the production of marginal and low permeability reservoirs, where hydraulic fracturing can be rejected due to the presence of a gas cap or for the high risks related to harsh environment (high pressure, high temperature).

In general, Oil & Gas companies quantify the benefit of new technologies like Fishbones not only with pilot tests but also with fluid dynamic reservoir simulations. For unconventional resources economic production is not guaranteed, therefore production enhancement estimation is crucial.

Reservoir simulation

Oil & Gas industry exploits 3D numerical reservoir simulators to predict hydrocarbon production profiles for given development scenarios. These profiles are then used to plan investments and operations.

Reservoir simulations rely on mathematical models appropriate to characterize multiphase flow in porous media using a set of Partial Differential Equations (PDEs) which combines Darcy's Law and mass conservation equations. The most common formulation is the Black Oil Model which assumes reservoir fluids consisting of three phases - oil, gas and water - and is based on the conservation of stock tank volumes for each phase.

The system of reservoir PDEs must be solved numerically, therefore discretization in space and time is needed. Following a finite volume formulation, the domain is split in blocks, which generate a computational Corner Point Geometry (CPG) grid, while the fluid and rock systems are characterized using cell-based average properties. Time is discretized in steps: $t_0, t_1, t_2, \dots, t_n \dots t_{n_T}$, where t_0 and t_{n_T} are the beginning and the end of the simulation, while the difference (Δt_n) between two consecutive times (t_n, t_{n+1}) is the time step. Then, cell pressure and saturations – the fractions of pore volume filled by each phase – evolve along a discrete time-line according to inflow/outflow fluxes typically triggered by well operations. To model actual wells in a finite volume grid, the Peaceman's formulation, where the fundamental parameters are well index and cell radius, is used.

The well index is defined assuming radial Darcy's flow and steady state conditions and it is a function of cell permeability, length of the completed interval, well radius and cell radius, that is the distance from the completion where the solution of the well equation equals the average pressure of the block. Notably, the Peaceman's formulation holds for completed cells having dimensions at least one order of magnitude greater than the wellbore diameter. Indeed, if the cell dimensions are comparable to wellbore diameter, the pressure drop between them results to be negligible and the definition of a well index is unnecessary. The Peaceman's formulation integrates also the concept of skin factor, which accounts for near wellbore effects, e.g. mechanical skin and stimulation.

Fishbone completion modelling

The modelling of fishbone completion can be in principle implemented using the Peaceman's formulation by treating laterals as additional completions inside cells which can be already completed by the main bore. However, this may overestimate the benefit of fishbone completion because i) interferences among main bore, laterals, and laterals of the same sub are neglected and ii) the

approximation which is implicit in the Peaceman's model – radial flow near the wellbore – is not true close to needle tips and needle-main bore junctions. This poses challenges in fishbone completion modelling when using the classical simulation technology. For this reason, different solutions were proposed, namely small blocks with extreme permeability to represent wellbore and laterals, the Embedded Discrete Fracture Modelling (EDFM) with an analogy between fractures and needles, and unstructured gridding based on finite volume formulations as available in CFD packages.

In this work, three different approaches were implemented: i) high resolution grid (HRG) following the corner point logic with local grid refinement ii) EDFM and iii) unstructured finite element type gridding. If the last method can be seen – and it was proved to be – the most accurate, only one of the first two options can be implemented in real field workflows. The objective of this work is also to provide motivations for a choice between the first two options in relation to real field applications.

High resolution finite volume simulation

A standard finite volume reservoir simulator, with local grid refinement (LGR) option, can be used to accurately model steep pressure gradients around needles and main bore. Grid refinement is not needed everywhere but only in very limited volumes of the reservoir, in particular near wells, where cells with size comparable to wellbore diameter are used. Because the Peaceman's formulation could not be used for wellbore completions due to cell dimensions, in this work the well index was defined using extremely high values, which essentially say that wellbore fluid and the fluid in the completed cell have the same pressure. As regard the needles, their radius is small enough to allow using Peaceman's model when defining cell radius and well index.

The representative element of a fishbone completion is the "sub": a 12 m main bore section with four needles. Therefore, the minimum distance between two consecutive set of needles is 12 m. In order to minimize their competing effects during production, this distance is increased a little. To make a fair comparison in terms of hydrocarbon production between a conventional well and fishbone sub, the reservoir model is diminished to 20 m along the well orientation. Two assumptions are done when the model employed in this work is considered: i) the relative benefit of the fishbone completion can be scaled to real type installations where several subs are mounted with a regular spacing of 20 m and ii) that the entire surface of main wellbore and fishbone needles is available to flow without local impairment.

With the LGR option, the total number of cells is reduced by an order of magnitude with respect to a uniform main refinement, therefore also computational time decreases at least by one order of magnitude.

The simulations were done with a single hydrocarbon phase since the well productivity is usually referred to a single phase fluid. The effects coming from a multiphase flow model, where the productivity is influenced by relative permeability curves and fluid properties are not considered.

The logic of this analysis was mostly based on the evaluation of the instantaneous benefit of the proposed completion with respect to the conventional one, where the benefit is computed as the ratio between the corresponding flow rates.

Simulations were done at different flow regimes, transient, semi and steady state conditions. Notably, using commercial finite volume simulators it is not easy to implement Dirichlet's boundary conditions, which logically lead to steady state flow. Rather, buffer zones with very high pore volume are used to simulate constant pressures, then steady state conditions are achieved after an initial transient period whose duration depends on the system diffusivity.

During transient flow, reservoir permeability and fluid properties affect the production increment and the fishbone sub can produce also the double of a conventional well, the benefit increases with lower permeability and higher fluid viscosity. During steady state flow, the benefit converges to the same value for different fluids or reservoir permeability. Dirichlet's conditions affect the fishbone benefit, the closer they are and the higher it results to be. In layered reservoirs, where vertical communication can be even absent, a simple horizontal well is penalized. In all the homogeneous cases, the fishbone benefit during steady state resulted to be lower than 2. On the contrary, with high permeability anisotropy, the cumulative fishbone benefit reaches also 4.5. In real field conditions, steady state flow is not usual and, even though the depletion process can be seen as a sequence of steady state flow periods with declining reservoir pressure, it is also interesting to evaluate the benefit in terms of cumulative increment of produced volumes. This analysis showed an anticipation of production measurable in hundreds of days, and a final cumulative production after 500 days doubled in low permeability rocks. In semi steady state conditions, when both the completions are producing at the same rate, the fishbone completion drawdown is much lower than in a conventional well, leading to fewer problems related to sand production and gas/water coning.

The Embedded Discrete Fracture Model

The Embedded Discrete Fracture Model (EDFM) is a technique developed to include flow in a fracture network into a traditional corner point geometry grid developed to model the reservoir matrix. EDFM is used for various reasons: i) it is easy to update the EDFM model with new fracture networks regardless the orientation of the fracture itself with respect to matrix grid, ii) it is computationally efficient, because usually it does require milder refinement in comparison with approaches based on detailed gridding.

To model needles in the EDFM framework, it is necessary to make an analogy between them and high permeability fractures departing from the main wellbore. In the EDFM, the critical point is the flow from a completed cell towards a fracture, which is approximated by defining a transmissibility factor according to a linear pressure drop assumption. This flow should be equivalent to the radial one towards the needles. Hence, a correction based on Peaceman's well index was done to avoid its underestimation. This approach, as for the grid refinement discussed before, can be accepted if in the completed cell both needles and main bore are not present.

A grid sensitivity analysis was done in order to find a suitable grid block dimension able to model the completions with accuracy. Then, sensitivities through the initial transient period and in steady state conditions were performed on fluid types and reservoir permeability, on boundary condition locations and for a layered reservoir. The cumulative fishbone benefit during depletion for primary recovery and semi steady state flow are discussed. The trend of the results obtained with the EDFM methodology was similar to the ones obtained with the high resolution finite volume simulations. However, the values of fishbone benefits found with the EDFM are lower in all the simulations run than the previously discussed methodology. The discrepancy between these two approaches based on finite volume simulators will be discussed once the results obtained with a conformal mesh in a finite element software will be obtained. It should be noticed that differences were seen also when a simple conventional well was analyzed, meaning that one of the two methodologies is not able to model at the same time main bore and needles.

Modelling fishbone completion using conformal mesh

In this chapter, the objective was to model flow around fishbone completions using a detailed gridding as close as possible to the geometry of the completion itself. The natural framework for doing this is the Finite Element Method (FEM) where grids can be built around complex structures, in particular if tetrahedral elements are used. Notably, in reservoir simulations, FEM is not frequently employed because it does not ensure local mass conservation for multiphase flow and high

permeability contrasts, as the finite volume method does. However, in this chapter and in the previous ones, the framework is single phase flow where FEM can work without stability and convergence problems. Having said that, the point is to choose a proper implementation of the FEM and a corresponding gridding package. In this work, the solution of choice was the COMSOL Multiphysics environment, which couples the availability of FEM implementation from a number of physical problems, including Darcy's flow, with sophisticated physically based gridding capabilities.

It is worth noticing that the methods used in the previous chapters lead to results that were somehow inconsistent. Then, a great care was used in order to be confident on the accuracy of the FEM solution. For this reason, a sequence of benchmarks against analytical and semi-analytical solutions were performed to provide the consistency of this methodology. In particular, it was observed that the accuracy of the solution increased with mesh refinement. This allowed identifying a suitable mesh configuration that provided consistent results and acceptable simulation time.

The flexibility of the FEM modelling package allowed the setup of several sensitivities on both reservoir parameters and fishbone geometries/configurations. In particular, the unstructured mesh gave the possibility to investigate problems non-compatible with Cartesian grids, such as the impact on production of the damage zone thickness, of needle exit angle and of the sub type (Dreamliner or Fishbones). It is worth mentioning that the sensitivity on fishbone sub density showed a linear correlation between the number of fishbone and the increment of production, but it also allowed to identify a minimum distance between subs to avoid competing effects. In addition, the impact on production of invasion zone thickness for a conventional and a fishbone completion was compared. While the first has a significant production loss also with thin damage zone, the fishbone completion prevents the well productivity loss.

In addition, the FEM modelling results were used to deeper investigate the differences observed between the High Resolution Grid (HRG) and EDFM approaches. Actually, the EFDM and FEM results were in a very good agreement, while they both differ from the HRG ones. A further insight on the discrepancy is be discussed in the following chapter.

Discussion of the results and application on a real field

The inconsistencies between the results of high resolution grid and EDFM approaches are here investigated. Considering a homogeneous case during steady state flow, the EDFM methodology showed at increasing grid refinement a convergence towards a fishbone benefit value much lower than the one estimated from the HRG. For the same problem, COMSOL solution was in line with

the EDFM ones. In detail, it was observed that the overestimation of the fishbone benefit in the High Resolution Grid solution derived from an underestimation of the main bore production.

To assess the reasons of the differences in the main bore production, a deeper analysis of the HRG approach was performed in a simple 2D grid. It was observed that the completed cell, coincident with the main bore, was allowed to communicate only with the four adjacent cells. On the other side in the EDFM, the Peaceman's model is applied, hence radial flow, much more effective than a cell-to-cell flow, is assumed. The different flow paths towards the well may be the origin of the discrepancies in the well production estimation of the two approaches. This hypothesis is supported by the results of a simple simulation performed imposing, by means of non-neighboring-connections, radial flow towards the well in the HRG implementation. However, deeper investigations are left for future works.

As a consequence, one of the main findings of this work is the assessment of the EDFM fishbone modeling as a suitable approach for finite-volume simulations of real fields. Actually, EDFM was implemented for a real field case as the first available solution to provide fishbone benefit estimation to support business decisions. From the results, Fishbones are expected to provide an increment of 10% in cumulative volumes and a production anticipation of 4 years in the whole concession period.

Conclusions

This thesis work was focused on the implementation of a methodology able to model branched completions, as a fishbone completed well, where the classical well modelling approach may not be optimal.

All the methods highlighted fishbone completion benefits for various combinations of reservoir properties, geometries and flow conditions. In particular, the production increment given by needles inflow with respect to conventional completions increases with an increase in the ratio k_h/k_v. During transient flow a low value of permeability/viscosity ratio enhances the fishbone benefit, while during steady state it does not affect the production increment. In tight formations with viscous fluids, the fishbone completion gives the highest benefit. This increases linearly with the number of subs for a given main bore length, however for high-density needles interferences are present.

It is worth noticing that inconsistencies between HRG on one side and FEM/EDFM on the other side posed questions on the accuracy of the former method. These differences could be ascribed to the limitation related to the use of a Cartesian grid around wellbore in a geometry where cell size is comparable with wellbore diameter (for HRG method) and then, the Peaceman's model, which

accounts for radiality of the inflow in the near-well region, cannot be used. EDFM, on the contrary, provided consistent results with FEM for problems that can be solved with both methods.

The achievements on EDFM motivated the application of this methodology to a real field where hydraulic fracturing is risky. A comparison between the production of a 1 km horizontal well and a fishbone completed well (51 subs spaced by 20 m) was done. The final cumulative production increment due to Fishbones resulted to be 10% higher. than the conventional completion. However, the main advantage for this field is the production anticipation (in the order of 4 years).

Future works can be undertaken to improve accuracy and efficiency in the estimation of fishbone completion benefits. Pressure drops due to friction losses in the annulus and across production valves should be considered to obtain more accurate results. The definition of an abacus that for given cell block dimensions and properties returns a geometric skin factor due to the fishbone completion could be convenient whenever the grid size is too large for implementing fishbone using EDFM.

In conclusion, after a preliminary real field test, the findings of this thesis work will allow to define a fishbone completion based development plan. In fact, since the modified EDFM approach resulted to be accurate and robust also with mild grid refinement, there is the confidence to rely on this methodology once economic decisions must be taken.

Table of Contents

List of Figures

List of Tables

List of acronyms

BHP	Bottom Hole Pressure
CAD	Computer Aided Drafting
CFD	Computational Fluid Dynamic
CPG	Corner Point Geometry
EDFM	Embedded Discrete Fracture Model
FEM	Finite Element Method
FGPR	Field Gas Production Rate
FGPT	Field Gas Production Total
HF	Hydraulic Fracturing
HPHT	High Pressure High Temperature
HRG	High Resolution Grid
HSE	Health, Safety and Environment
LGR	Local Grid Refinement
MDST	Multilateral Drilling Stimulation Technique
MRST	MATLAB Reservoir Simulation Toolbox
MST	Multilateral Stimulation Technique
NNC	Non Neighbouring Connection
NPV	Net Present Value
NTG	Net to Gross
ODE	Ordinary Differential Equation
PDE	Partial Differential Equation
PI	Productivity Index
PVT	Pressure-Volume-Temperature table
RPM	Revolutions per Minutes
STC	Stock Tank Condition
URF	Ultimate Recovery Factor
WI	Well Index

List of symbols

Dimensional

μ	Dynamic viscosity	[cP] or [Pa s]
ρ	Density	[kg/m^3]
$<d_{ff}>$	Fracture to fracture distance	[m]
a	Fracture aperture	[m]
A_{cs}	Needle/fracture cross sectional area	[m^2]
A_{mf}	Matrix to fracture area	[m^2]
B_i	Formation volume factor	[rm^3/Sm^3]
c_i	Compressibility	[Pa^{-1}]
D	Depth	[m]
g	gravity	[m/s^2]
h	Net-pay (reservoir thickness)	[m]
h_{max}	Mesh max element size	[m]
h_{min}	Mesh min element size	[m]
k	Permeability	[mD] or [m^2]
k_d	Altered zone permeability	[mD]
k_{fb}	Needle permeability	[mD]
L or l_f	Fracture length	[m]
l_g	Grid length	[m]
p_{cog}	Gas-oil capillary pressure	[Pa]
p_{cow}	Water-oil capillary pressure	[Pa]
p_f	Friction loss pressure	[Pa]
p_h	Hydrostatic pressure	[Pa]
p_{res}	Reservoir pressure	[Pa]
p_s	Reservoir static pressure	[Pa]
p_{well}	Well pressure	[Pa]
q	Flow rate at reservoir conditions	[rm^3/d]
Q_m	Mass Soucre/sink	[kg/m^3/s]
Q_q	Flow rate at surface conditions	[Sm^3/d]
r_d	Invasion zone radius	[m]
r_e	Reservoir external radius	[m]
r_{fb}	Fishbone radius	[m]
r_o	Peaceman's radius or cell radius	[m]

R_s	Solution gas	[Sm^3/Sm^3]
r_w	Well radius	[m]
T_{ff}	Fracture to fracture transmissibility	[m^3]
T_{mf}	Matrix to fracture transmissibility	[m^3]
v_o	Darcy's velocity	[m/s]
w	Fracture width	[m]
λ	Mobility ratio	[m^2/Pa/s]
Δϕ	Potential difference	[Pa] or [bar]
Δt	Time step	[d]

Non-dimensional

$\tilde{h}$	Partial perforation ratio
G_{max}	Mesh element growth
ψ_i	Basis functions
J(x)	Jacobian matrix
k_r	Relative permeability
R	Residual vector
S	Skin factor
S_{pp}	Skin due to partial perforation
S_α	Saturation of phase alpha
X_j	Mesh nodes
$\Gamma(n)$	Gamma function
γ	Mesh curvature factor
λ	Mesh resolution
ϕ	Porosity

1 Introduction

Reservoirs production is based on wells drilled from surface. Well completions ensure hydraulic communication between the reservoir and the wellbore. The productivity of a well depends on the formation type, pressure regime (above or below bubble point), flow conditions (transient, steady state, semi steady state) and type of completion. The Oil & Gas industry has developed sophisticated drilling and completion technologies that enabled to include in the oil and gas resources what are known as unconventional hydrocarbons. The economic production of these resources cannot be achieved employing simple completion, thus the permeability has to be enhanced. Nowadays, tight formations are stimulated by horizontal drilling combined with hydraulic fracturing. This last procedure is a complex, expensive and with high social/environmental impacts. Moreover it is extremely risky when dealing with high pressure high temperature reservoirs (chapter 2).

Oil & Gas companies are trying to reduce environmental impacts, studying alternative stimulation technologies. One of these is the fishbone technology, a branched liner completion: from the main bore, four small needles depart and perforate the reservoir up to 12 m. The main advantages are the increment of drainage area and the presence of small channels where hydrocarbons easily flow. Two technologies are available according to the rock type. Before installing new technologies in real fields, for Oil & Gas companies is necessary to understand and quantify their benefits in terms of produced flow rates both with pilot tests and numerical simulations. Three preliminary field tests were done to understand fishbone installation feasibility and associated risks (chapter 3).

Reservoir simulation is employed to estimate production profiles from which plan investments. Conservation equations at stock tank conditions and Darcy's velocity are at the core of this model. Reservoir PDEs are solved numerically exploiting a computational grid and a time discretization. Hence, the system is described through cell based average properties and mass conservation is imposed for each block of the corner point grid. Given pressure and saturations at time t for a certain cell, the solution of the equations leads to the updated pressure and saturations at time $t + \Delta t$. The system is influenced by the fluxes that take place with the adjacent cells. These are computed from the pressure gradients and transmissibility between cells. During reservoir simulation, wells are not simply treated as mass source or sink. Usually a linear correlation between flow rate and pressure drop from a completed cell to bottom hole pressure is employed. The link is the well index, which characterizes the connections in the cell *i* between reservoir and wellbore. The well index is defined assuming Darcy's flow and steady state conditions. Notably, the Peaceman's formulation holds for

completed cells having dimensions at least one order of magnitude greater than the wellbore diameter (chapter 4).

Peaceman's model is not suitable to model a fishbone completion due to the absence of radial flow from a completed cell toward the well. Therefore some alternative modelling approaches should be followed. In literature, three studies departing from the classical Peaceman's model can be found: i) small blocks with extreme permeability to represent wellbore and laterals, ii) the Embedded Discrete Fracture Modelling (EDFM) with an analogy between fractures and needles, and iii) unstructured gridding based on finite volume formulations as available in CFD packages. Starting from these, three different approaches were implemented: i) High Resolution Grid (HRG) following the corner point logic with local grid refinement ii) EDFM and iii) unstructured finite element type gridding (chapter 5).

A standard finite volume reservoir simulator, with local grid refinement (LGR) option can be used to accurately model steep pressure gradients around needles and main bore. The Peaceman's formulation can be applied only to needles due to cell dimensions, while the main bore coincides with the completed cells. Simulations were done at different flow regimes with single phase flow. From these, the fishbone benefit, namely the relative production respect a conventional completion is evaluated (chapter 6).

The Embedded Discrete Fracture Model was originally developed to include flow in a fracture network into a traditional corner point geometry grid. EDFM is used for computationally efficient, because usually it does require mild refinement. To model needles in the EDFM framework, it is necessary to make an analogy between them and high permeability fractures. Then, a correction based on Peaceman's well index is done to avoid underestimation of flow towards needle. A grid sensitivity analysis showed a convergence in the results once refinement was increased. Then, sensitivities for different flow regimes are investigated. The values of fishbone benefits found with the HRG and EDFM methodologies showed some discrepancies, that later will be analyzed (chapter 7).

With a Finite Element Method (FEM) approach, the flow around fishbone completions is studied with conformal grids. Notably, in reservoir simulation FEM is not commonly used because it does not ensure local mass conservation for multiphase flow; however, in this thesis the framework is single phase. A sequence of benchmarks against analytical and semi-analytical solutions were done to provide consistency of this methodology. The outcome was the definition of a suitable mesh configuration. The flexibility of the FEM modelling package allowed the setup of several sensitivities on both reservoir parameters and fishbone geometries and configurations, which in some cases are not compatible with CPG grids. Finally, the FEM modelling results were used to deeper investigate

the differences observed between the HRG and EDFM approaches. Actually, the EFDM and FEM results were in a very good agreement, while they both differ from the HRG ones (chapter 8).

The inconsistencies between the results of HRG and EDFM approaches were investigated. The EDFM methodology showed a convergence towards a fishbone benefit value much lower than the one estimated from the HRG. At the same time, COMSOL solution was in line with the EDFM ones. In particular, the overestimation of the fishbone benefit in the HRG solution derived from an underestimation of the conventional completion production. To assess the reasons of the differences in the main bore production, an analysis of the HRG approach was performed in a simple 2D grid. The absence of radiality in the flow towards the well for the HRG can be the origin of the discrepancy. This hypothesis is supported from the result of a simple simulation performed by imposing radial flow towards the well in the HRG implementation. The results were in line with EDFM and COMSOL ones. The EDFM methodology was implemented in presence of a real reservoir geometry where the fishbone completion provides an anticipation of production of 4 years, and a final cumulative gas volume 10% higher (chapter 9).

One of the main findings of this work is the assessment of the EDFM fishbone modeling as a suitable approach for finite-volume simulations of real fields, on which economic decisions can be based. Actually, EDFM was implemented for a real field case as the first available solution to provide fishbone benefit estimation to support business decisions. To improve accuracy on the results, pressure drops due to frictions inside the completion and temperature changes in the reservoir should be considered. Then, the definition of an abacus that for given cell block dimensions and properties returns a geometric skin factor could be convenient whenever the grid size is too large for exploiting EDFM. However these are left for future works (chapter 10).

2 Oil and gas resources

2.1 Hydrocarbon reservoirs

Oil and gas reservoirs are accumulations of hydrocarbons in permeable media contained within some type of trap. Hydrocarbons migrate from source rocks following gravity and then drain permeable formations where pores were originally water saturated. At a continuum scale, porous formations are characterized by porosity (ϕ), i.e. the fraction of a representative bulk volume filled by fluids. The pore space is split amongst three phases, gas, oil and water, and the relative fractions of the pore space filled by the phases are called saturations $\{s_\alpha\}_{\alpha=o,w,g}$. Notably, $s_o + s_w + s_g = 1$.

Figure 2-1 outlines the structure of a generic hydrocarbon reservoir: gas accumulated at the top of the formation, below the cap-rock which seals the reservoir and traps fluids during the migration. Then, an oil leg can be found between the gas cap and a bottom aquifer.

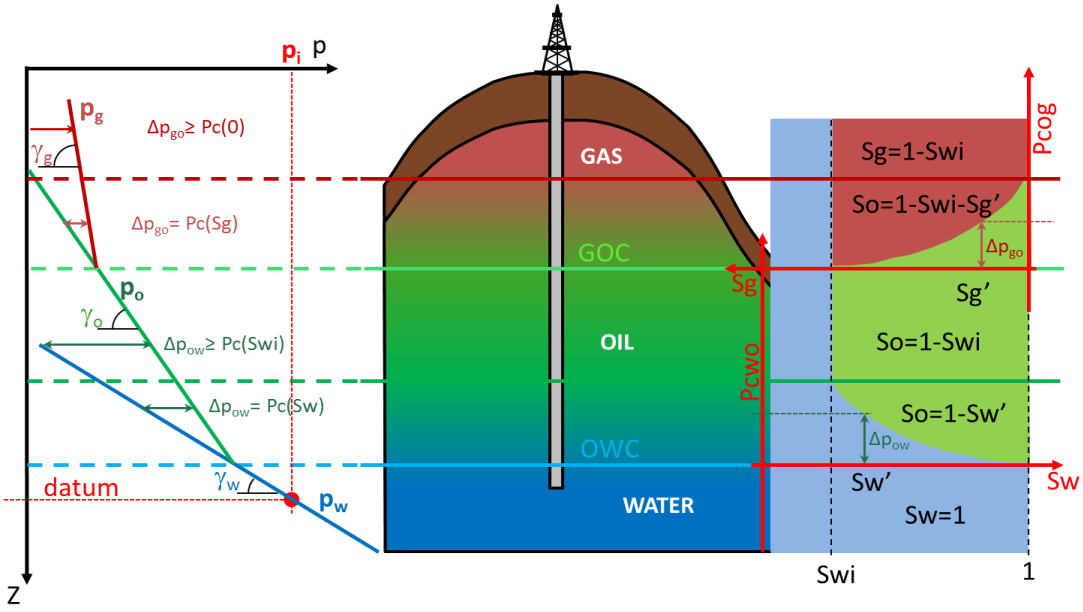

Figure 2-1: Pressure and saturation profiles of each phase according to different depths. At the same depth, each phase has a different pressure due to capillary effect. Source: Eni S.p.A.

Even though the distribution of the fluids is driven by gravity, which segregates fluids according to their densities, the boundary between oil-water and gas-oil may not necessarily be sharp. Rather, capillary effects may lead to transition zones, between oil and water and between gas and oil. The extent of these transition zones derives from capillary pressure between oil and water:

$$p_{cow} = p_o - p_w \quad (2\text{-}1)$$

and between gas and oil:

$$p_{cog} = p_g - p_o \quad (2\text{-}2)$$

Together with the reservoir layout in terms of fluid, Figure 2-1 shows a sketch of the original - pre production - phase pressure along depth in the reservoir: water and oil pressures coincide at the water-oil contact, while oil and gas pressures meet at the gas-oil contact. Because the reservoir is in equilibrium conditions (fluids do not flow) before production, pressure gradients for the different phases are the product of density times the gravity constant.

2.2 Oil and gas wells

Hydrocarbon formations are deep underground; fluids are segregated inside rocks that prevent hydraulic communication with the surface. The connection is established only during the production period throughout wells. A drilling rig is the machine that creates the bores in the earth's subsurface, employing heavy mud to counterbalance the high-pressure fluids encountered.

Wells are usually vertical in the first meters in order to reach the target depth, then they can deviate towards the reservoir. They may be vertical or, most commonly, slanted according to the formation characteristics. The adjective 'horizontal' is used to define wells that follow layer inclination in the formation.

The production potential of a reservoir and the well performances can be expressed by a productivity index term (PI) $\left[\frac{m^3}{sPa}\right]$. It expresses the ratio between surface fluid flow rate and pressure drawdown from reservoir to well bottom hole. It is a function of rock and fluid properties as well as of formation damage around the wellbore.

The productivity index and thus the interactions between well and formation are strongly influenced by the product of formation permeability (k_{eq}) and producing well section. The PI varies according to the well orientation:

- For vertical wells, it is equal to the product between an equivalent horizontal permeability and the completed well section in the reservoir layer: $\sqrt{k_x k_y}h$,
- For horizontal wells, it is equal to the product between an equivalent permeability (in the orthogonal directions with respect to the main bore) and well length in the reservoir layer: $\sqrt{k_z k_y}L$.

Since horizontal wells are much longer than vertical ones ($L \gg h$), their productivity index is significantly greater even if the vertical permeability is usually smaller than the horizontal ones. Horizontal wells lead to an increase of flow rates or to a reduction of drawdown when producing the same amount of fluids of a vertical well.

The typical layout of a well is highlighted in Figure 2-2. Several pipes, called casing, are run in hole to provide mechanical and hydraulic isolation from the overburden. Casing tubes have standard diameters (from 20" at shallow depth till $4_{1/2}$" at target depth), these must be bigger than the production tubing, the small internal pipe (from $4_{1/2}$" to 1" of diameter), placed once drilling is concluded, through which fluids flow to surface during production. All these pipes are hanging from a portion of wellhead called casing hanger.

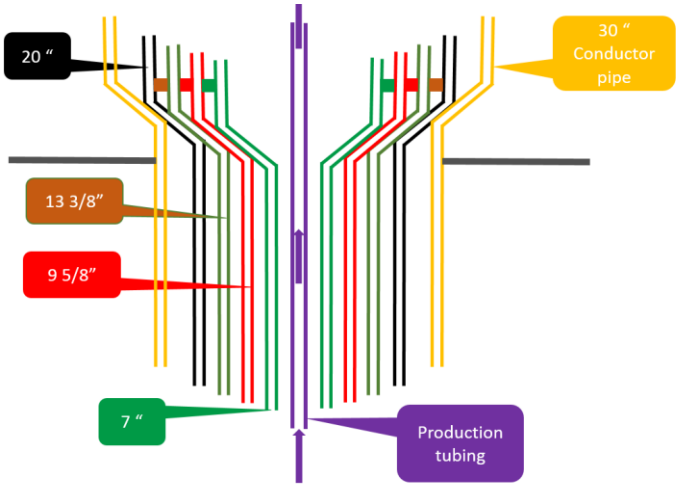

Figure 2-2: Casings and production tube employed to make a well. Source: Eni S.p.A.

The interval that drills the reservoir section, usually the end of the well, is completed in specific ways to allow hydraulic communications with hydrocarbons (see Figure 2-3):

- In an open hole completion (a) neither a casing or a liner are placed across the production zone. In known formations, this section is left entirely bare, while in some cases a sand-control is incorporated. This completion is widespread in horizontal wells, where cemented installations are more expensive and technically more difficult.
- A liner completion (b) can be run in the open hole. A pipe is set to minimize sloughing of the formation into the well bore. Slotted liners are the more common, with several longitudinal slots (2 mm to 50 mm) across their circumference. Liner completions are extensively used in unconsolidated formations to prevent the movement of materials (as sand) into the wellbore. The pressure drop across a slotted liner is negligible, therefore it is usually treated as an open hole completion when the well inflow performances are evaluated.

- A perforated casing completion (c) is the most commonly used technique. The casing is cemented along all the entire reservoir section, then fluid communication is achieved perforating steel, cement and reservoir with a gun.

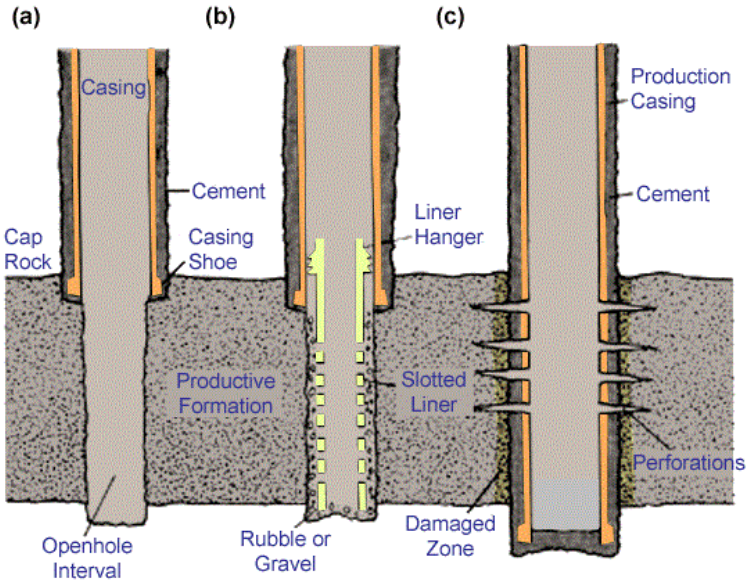

Figure 2-3: Three common reservoir completions: (a) open hole, (b) liner completion, (3) perforated casing. Source: (alien-homepage.de)

Well configurations (internal diameter, skin, valves…) affect the inflow performance (from reservoir to bottom hole) and the vertical flow performance (from bottom hole to wellhead). The following simple equations describe pressure balances from the static reservoir pressure (p_s) to the wellhead pressure (p_{wh}) during production:

$$p_{wh} = p_{wf} - p_h - p_f \quad (2\text{-}3)$$

$$p_{wf} = p_s - \frac{Q}{PI} \quad (2\text{-}4)$$

With p_{wf} the flowing bottom hole pressure, p_h the hydrostatic term and p_f the friction losses proportional to the flow rate.

The hydrocarbons, to reach the surface, must have enough pressure at the bottom hole to counterbalance friction losses, hydrostatic column and valve pressure drops. If they cannot, artificial lift is usually employed to give the necessary energy or reduce their average density and consequently the hydrostatic column.

2.3 Flow conditions and productivity index

The productivity of a well depends on formation type, pressure regime (above or below bubble point) and flow conditions. In the reservoir, three types of flow condition can establish at different time after the start of production and for different boundary conditions applied, see (Dake 1978):

- Transient flow: this condition lasts for a relatively short period after a variation in the well pressure. During this time the pressure wave propagation from the well has not reached any boundaries of the reservoir. The local reservoir pressure is not affected by boundary conditions; therefore the formation appears as infinite. Both pressure and pressure derivative (with respect to time) are function of location and time.
- Semi steady state flow: this condition is reached when the reservoir is produced for enough time that the well experiences the boundary effect. The well is producing at constant flow rate while a Neumann's condition is set on the reservoir boundary, meaning that no flux departs from here. The derivative of pressure with respect to time is constant in the reservoir domain.
- Steady state flow: it is reached after the initial transient period when on reservoir boundary a constant pressure is set. During steady state the well produces at constant rate, while the derivative of pressure with respect to the time is zero in the reservoir domain.

While transient period is always experienced during a depletion process, steady state and semi steady state conditions may never be reached. However, the steady state condition is usually simulated with reservoir software since the surface facility design is based on such conditions.

2.4 Unconventional resources

Recent reservoir discoveries are characterized by low productivity (Freyer, et al. 2011). In the last decades, discoveries of conventional reservoirs at low depth and with good productivity have declined. Shale oil, shale gas, tight oil, tight gas have a significant share in global technically recoverable resources (Kuuskraa, Stevens and Moodhe 2013). These formations are classified as unconventional, meaning that hydrocarbons are segregated in low (0.001 mD to 1 mD) permeability rocks that do not allow natural fluid flow and production. Conventional wells composed only by the main wellbore, do not have enough communication in these low permeability formations to guarantee economic production.

Moreover, other flow restrictions are introduced in the reservoirs once these are perforated. In fact, during the drilling phase, the mud invades the formation altering the porous rock properties, mainly reducing the permeability nearby the wellbore. Thus, the pores result to be plugged and this "skin effect" further reduces the productivity index. Production in unconventional reservoirs can be economical only when stimulation, aimed to obtain a permeability enhancement, is done properly.

In the last decades, know-how improvement, experience built on learning curves and marginal cost reduction of stimulation processes allowed economic production of these complex formations. Technologies, such as horizontal drilling combined with hydraulic fracturing, have unlocked vast unconventional resources, which have dramatically altered the natural gas supply chain in the recent years, particularly in North America (Castro-Alvarez, et al. 2017). This trend is expected to last for the next decades, since about 45 percent of remaining natural gas resources, the "fuel of the future" or the "bridge fuel" towards a decarbonized energy system (Brandt, et al. 2014), are from unconventional fields (ExxonMobil 2018).

2.5 Reservoir stimulation: the state of art

Unconventional fossil fuels are produced using a variety of processes, many of them involve fluid injection (water or acid) at high pressure into the reservoir (Jackson, et al. 2014). Just in few cases produced carbon dioxide is re-injected to enhance the extraction of fossil fuel. In other situations, thermal energy coming from steam is exploited to reduce dynamic viscosity of oil (Farrell and Brandt 2006). In general, unconventional fossil fuel extraction requires leading technologies, more complex, more expensive and with higher environmental impacts than conventional fossil fuels extraction (Rosa, et al. 2018).

The present technology used to stimulate tight formations is horizontal drilling combined with hydraulic fracturing (Freyer, et al. 2011), extensively used in North America, where it drastically changed oil and gas industry and energy economy (Castro-Alvarez, et al. 2017).

High-pressure fluids are pumped into the formation with the aim to create a set of fracture wings that open normally to the lower mean stress. To keep the fractures open, along with a large amount of water, also proppants or acid are injected depending on the rock type and operators (Figure 2-4).

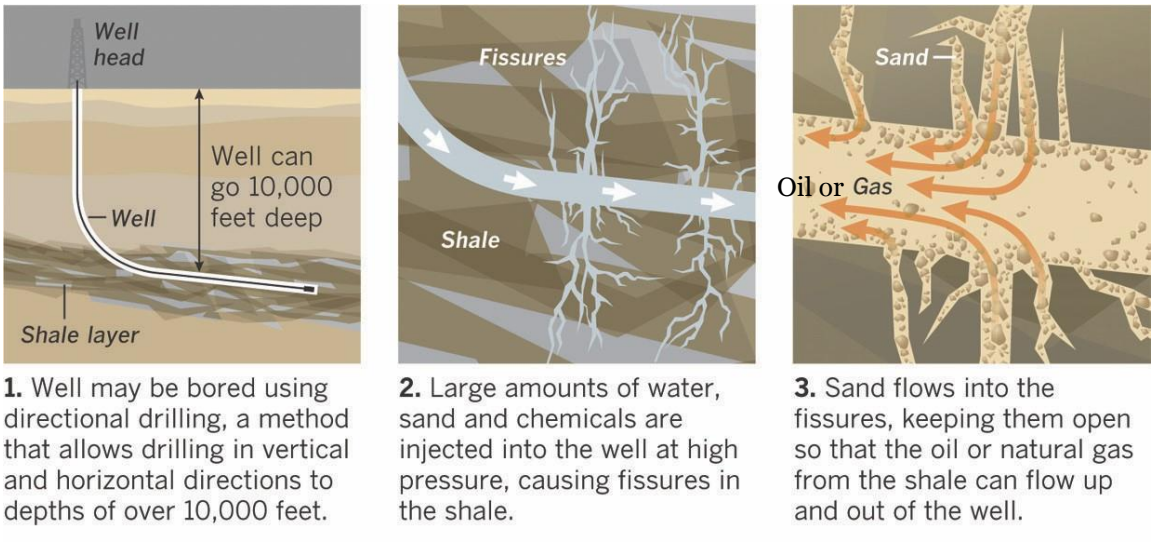

Figure 2-4: Schematic illustration of hydraulic fracturing. Source: (SlideServe)

Even if hydraulic fracturing increases the energy security and provides economic benefits for hosting countries, it brings several problems at the centre of public debates (Jackson, et al. 2014).

Environmental, social and economic consequences can be summarized in the following points:

- Land clearing and water consumption are two of the main consequences that come with the exploitation of unconventional resources. (Castro-Alvarez, et al. 2017).
- Fracking jobs requires high power diesel engines (Figure 2-5) to pump fluids. Thus, emissions of greenhouse gases added to methane leakages from the oil and gas infrastructure can have significant effect on climate (Brandt, et al. 2014).
- Casing is subjected to high pressure during the hydraulic fracturing process, and it can be damaged leading to leakages in atmosphere, groundwater or in the nearby drinkable aquifer (Castro-Alvarez, et al. 2017). Hydraulic fracturing, time and pressure-integrity testing can cause pressure changes that damage the cement or the steel casing (Jackson, et al. 2014). Not only hydrocarbons can flow away, but also injected water (containing acids, scale inhibitors, proppants) can. This situation is crucial since toxic fluids mix with water table used in agriculture or in domestic circumstances.
- The only parameters under control are the pumping rate and the injection pressure, leading to lack of fracture extension knowledge, and the possibility to contact unwanted water, gas cap or reinjection areas. This problematic is enhanced in zones where the learning curve of fracturing works is not available, e.g. off-shore (Freyer, et al. 2011). The main disadvantage of these situations is the early breakthrough of unwanted fluids that reduces hydrocarbon production while increasing costs associated to separation, treatment and disposal.

- After stimulation, hydrocarbon production can start. However, oil and gas come out with large volumes of injected fluids and brine. The so called "flowback and produced water" rate is extremely high in the first production period (Castro-Alvarez, et al. 2017). Thus, the water footprint of unconventional reservoirs should include water injected for fracturing purposes but also water produced along with hydrocarbons, both flowback water and brine (Scanlon , et al. 2016). Waste water management is one of the main drawbacks of hydrocarbon production, in particular when toxic fluid comes back after being injected, as in hydraulic fracturing. Treatments or fluid disposal must be done to respect environmental laws, reducing the economic profitability of the field.

- Unconventional oil and gas production can create new jobs and enhance economic growth, securing energy independency for the hosting countries. However, the unpredictable hydrocarbon rates along with the abrupt production decline after the first years can lead to a huge financial exposure if one considers the high capital and operational costs associated with the development and production of this formation (Rosa, et al. 2018).

- Hydraulic fracturing is a complex, risky and costly activity (Freyer, et al. 2011). Only competent personnel due to the presence of acids and high-pressure fluids can do the workover. Dealing with toxic fluid under pressure or explosive enhance the job risks and its costs.

- No track records exist in the oil and gas industry when dealing with subsea wells fracturing. While onshore fracturing know-how can exploit information coming from thousands of wells, this is not feasible for off-shore fields (Freyer, et al. 2011).

Figure 2-5: Well pad during hydraulic fracturing with trucks carrying pumps for injecting fluids. This evidence the high quantities of required energy. Source: (Drilling Contractor).

To remedy these environmental, economic and social challenges, the oil industry is developing new stimulation procedures. Unconventional reservoirs play a key role in energy supply for the next

decades; research and development are focusing on non-water alternatives for hydraulic fracturing fluid including foams, which can reduce water usage but require more chemicals and extra safety precautions, while limiting the efficiency of hydrocarbon production (International Energy Agency 2016). Among these alternatives, there is the fishbone completion, a new way for stimulate reservoir respecting environmental and economic constraints.

3 Fishbone Completion

The Norwegian company “Fishbones A.S.” has developed a new type of completion that can be seen as an alternative to hydraulic fracturing stimulation (Freyer, et al. 2011). A reservoir liner is equipped with short subs, each of these contains 3-4 small-diameter needles with length up to 12 meters that extend into the formation during few hours of fluid jetting/drilling. The aim is to create hundreds of small channels, the needle annuli, departing from the main wellbore where formation fluids can easily flow (Figure 3-1). The laterals will provide a similar flow path as hydraulic fracturing does, while HSE issues are drastically reduced (Freyer, et al. 2011). Lower working hours, pressure regimes and acid fluids are required and this implies a cost reduction. Moreover, the needle path inside the formation is well known, meaning that sweet spots are targeted while water zone or gas cap are not contacted.

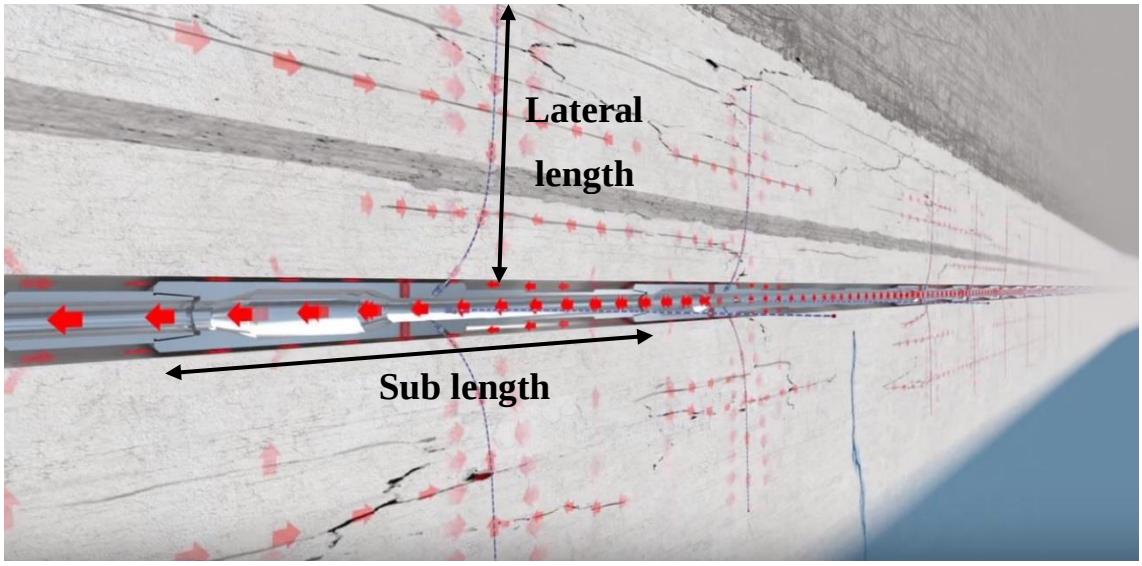

Figure 3-1: A reservoir section contacted by fishbone laterals, the hydrocarbon path during production is shown with red arrows. Source: (Fishbones AS).

The main aim of fishbone completions is increasing reserves per well, this is done mainly contacting layers not reached with conventional (as horizontal well) completions. The productivity index of a well is enhanced since formation damage is by-passed, the apparent well radius is increased, and the creation of highly permeable channels reduce the impact of a low permeability medium. Being the needle path under full control during penetration, contact of unwanted zones, such as aquifer or gas cap (only in the case of an oil field where “gas to market” is not economic), are avoided. Differently from hydraulic fracturing, undesired fluids production can be reduced significantly along with environmental, economic and social impacts. Finally, sweet-spot location errors (in the order of

10 m), due to seismic measurements, can be evaded by the needles, meaning higher hydrocarbon production in fewer time and a higher final recovery factor than a conventional well.

(Freyer, et al. 2011) compared fishbone completions and hydraulic fracturing and found that a well with 160 laterals (each twelve meters long) has the same performances of two fractures in a low permeability gas reservoir (k_h=0.005-0.8 mD, k_v/k_h =0.001-0.01, porosity 2-7%). While the same completion has an equivalent effect of 6 propped fractures (modelled as degrading/closing over time) in a low permeability oil reservoir (k_h = 3.5 mD, k_v/k_h=0.1, high porosity).

Table 3-1 provides a comparison between fishbone completions and hydraulic fracturing. It is deduced gathering information from several articles and websites. It is worth observing that:

- The values regarding fishbone completion are based on a field test performed in a horizontal well along a 704 m completion interval, as reported by (Rice, et al. 2014). In that field test, 60 needles (12 m each) were used to stimulate a carbonate reservoir (tight limestone, 5% porosity, 0.5 mD permeability). The jetting fluid was water containing 15% HCl.
- The values regarding hydraulic fracturing are based on the experience of the Canadian Oil & Gas industry over the past 150 years. The quantities are estimated from a compilation of the most up-to-date information available from regulators, academics and industry (Petroleum Servicies Association of Canada 2018).

Table 3-1: Main aspects that show fishbone completion advantages with respect to hydraulic fracturing.

	Fishbone completion	**Hydraulic fracturing**
Pumping pressure	3000 psi (Fishbones AS n.d.)	10.000-20.000 psi (Jackson, et al. 2014)
Water per well	120 m^3 (Fishbones AS 2018)(1)	On average 15.000 m^3 (Jackson, et al. 2014) range: 500-100.000 m^3 (Petroleum Servicies Association of Canada 2018)(3)
Acid fluid per well	20 m^3 (Fishbones AS 2018)(1)	100 m^3 accounting also biocides, scale inhibitors, friction reducers (Petroleum Servicies Association of Canada 2018)(4)
Proppants per well	None	About 1.500 m^3 (Petroleum Servicies Association of Canada 2018)(4)
Time to complete the job	5 h pumping time (Rice, et al. 2014)(2)	3-4 days (5)
Explosive	No	Perforating gun used to create holes in the steel liner
Workers needed	Normal workers	Specialist
Surface facilities	Rig already employed for drilling	Hydra-frack trucks
Oriented drilling	Yes	No, fractures open perpendicularly to the min stress
Water/gas breakthrough	Few or avoided	Unknown, depends on fracture length and direction
Sweet spot	Targeted	Unknown

Here some clarifications about Table 3-1 are reported:

(1) Consider that if fishbone laterals are drilled instead of been jetted (as described later in chapter 3.1.2), no acid or water is used. Instead, drilling mud is employed.

(2) The completion installation time (time to run the liner in hole) is not considered. In this field, the liner was rotated for more than 10 hours before jetting the fluids (Fishbones AS 2018).

(3) Small volume fractures could require 500 to 2.500 m^3 of water per well, moderate volume fractures 10.000 to 50.000 m^3 per well, while high volume fractures could lie between 50.000 to 100.000 m^3 per well (3 km long, with 300 m reservoir thickness). (Petroleum Servicies Association of Canada 2018).

(4) About 90.0% of the frack-fluid mixture is water and 9.5% sand. The remaining 0.5% consists of chemical additives to enhance the fracturing process (Petroleum Servicies Association of Canada 2018). Those values are based on an average of 15.000 m^3 of water per well.

(5) It accounts for fluids and proppants transportation to the well site, mixing in the blender and injection (Petroleum Servicies Association of Canada 2018). While all the fishbone laterals are created simultaneously, hydraulic fracturing is done in several steps. Once a fracture is created, a plug is set to isolate that liner section, then these operations are repeated until all the well length is stimulated.

It is important to look at the orders of magnitude, not at the exact values reported in Table 3-1, since they are affected by reservoir properties, well length and operator experience.

Before installing new technologies in real fields, for Oil & Gas companies is necessary to understand and quantify the introduced benefits in terms of produced flow rates with pilot tests and numerical simulations.

For the fishbone completion, first pilot tests were conducted to guarantee fishbone success from a mechanical point of view (see 0). Then, to understand fishbone completion potentiality, different procedures should be followed. The completion has been already analysed employing diverse computational methods, as later discussed in 5.1. These studies are taken as starting points for this thesis work, where new approaches are developed (see 5.2).

It is important to notice that a state-of-the-art methodology for modelling Fishbones does not exist, thus each approach has its own advantages and disadvantages.

3.1 Fishbone completion technologies

Fishbone completion is suitable for a large range of reservoirs. Depending on the formation type, two methods are available in order to create the needle annulus: the Multilaterals Stimulation Technology (MST) and the Multilateral Drilling Stimulation Technique (MDST). MST is used in carbonate, coal bed methane or oil sands reservoirs: the needles penetrate by jetting high-pressure fluids or acids. In sandstone and basement type, MDST, known also as Dreamliner is the choice:

needles are equipped with small drill bits powered by turbines driven by mud pumped from surface. Both vertical and horizontal main bores can be completed with fishbones.

3.1.1 Multilateral Stimulation Technology

MST is suitable for formations that can be stimulated simply with a jet. The sub, reported in Figure 3-2, is composed by four needles, each equipped with a jet nozzle at the end (Rice, et al. 2014). The liner, an assembly of several subs and anti-slip anchors, is run in hole with a liner hanger. Once the completion is set in the desired position, acid is pumped from the surface towards the formation (Figure 3-3). Usually, a solution of water and hydrochloric acid is the chosen fluid, able to erode and chemically dissolve the rock. The needles, pushed as hydraulic pistons by a pressure difference between the inner and outer part of the liner, exit from the sub with a 40° angle, reaching 90° at the tip when fully extended. A pressure gauge signals this situation when it records a pressure spike. After few hours of pumping, the system can produce through the two production valves of each sub. The hydrocarbons will flow in the main well annulus and needles annuli but also inside the needles (see Figure 3-4).

As a contingency plan against failures, Fishbones A.S. has developed laterals equipped with an aluminium shield. This is dissolved with acid once the lateral penetration is finished. Finally, the needle will be only composed by a steel slotted tube, able to produce even in presence of hole collapse.

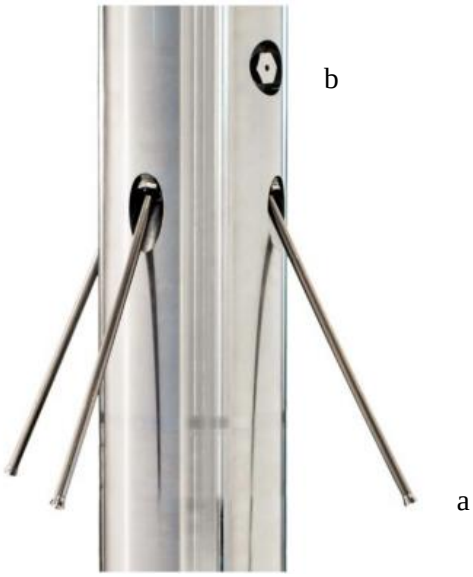

Figure 3-2: Sub where three of the four needles (a) can be seen. In addition, one of the two-production valve (b) is visible. The needles are not fully extent. Source: http://Fishbones.as/news/.

Figure 3-3: Fluid jetting from a lateral during a laboratory test. Source: fishbones.asproducts-2/.

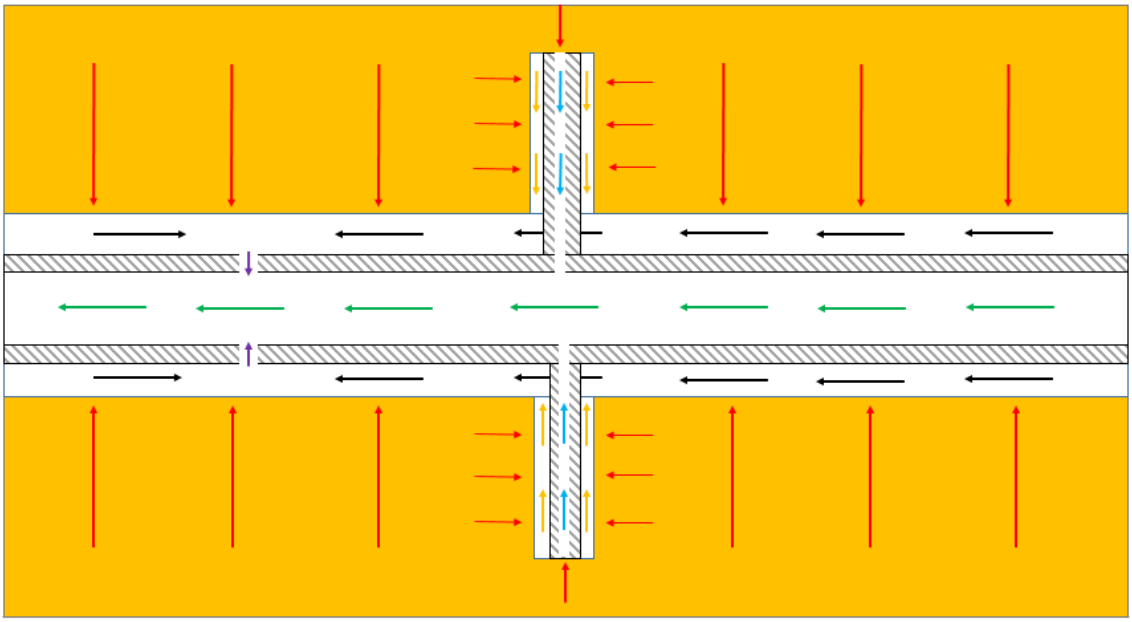

Figure 3-4: Schematic representation of a reservoir and fishbone sub section (geometrical sizes are not respected). The colored arrows label the several flow paths followed by hydrocarbons during production. The red is the flow inside the reservoir towards the well completion, the orange the flow in fishbone annuli, the blue inside needle tubes, the black in the main bore annulus, the violet in the two production valves and the green in the production tubing.

3.1.2 Multilateral Drilling Stimulation Technology

MDST was developed in a joint venture shared by Fishbones AS, Statoil (now Equinor) and Eni Norge, see (Torvund, et al. 2016) as an alternative to MST for sandstone. As shown in Figure 3-5, each sub (called Dreamliner for this technology) contains three needles with rotating drill bits having a 12 mm diameter. A turbine powered by the flow pumped in the main liner drives each of the drill bits. A series of Dreamliner alternated with anchors are run in hole as shown in Figure 3-6, once the anchors are set to avoid axial movement during drilling or due to thermal expansion, a short

pump job begins. The drilling fluid activates the turbines and when the right RPM is reached, the bit drills the formation allowing needle extension. A spike in the pressure gauge indicates the full perforation (around 10 m). Cuttings (the small pieces of rock removed) are circulated as in a standard drilling procedure. Once the tubing is set, production can start. Formation fluids flow in the needle annuli and in the main annulus towards the two production valves placed in each sub (as in Figure 3-4).

To avoid production decrease due to mechanical failure of valves, the first part of the liner is usually slotted (perforated) as a contingency plan (LR Senergy 10/06/2015). In this case, the formation fluids will flow in the main well annulus towards the first perforated section. Moreover, such geometry allows the fluids to by-pass the production valve in the first section, where a lot of pressure is dissipated due to high velocity in such a restriction.

In case of partial needle elongations, a milling tool is used to clean the internal pipe path from obstacles. The amount of fluid used, the working hours and the pumping horsepower are strongly affected by the formation porosity.

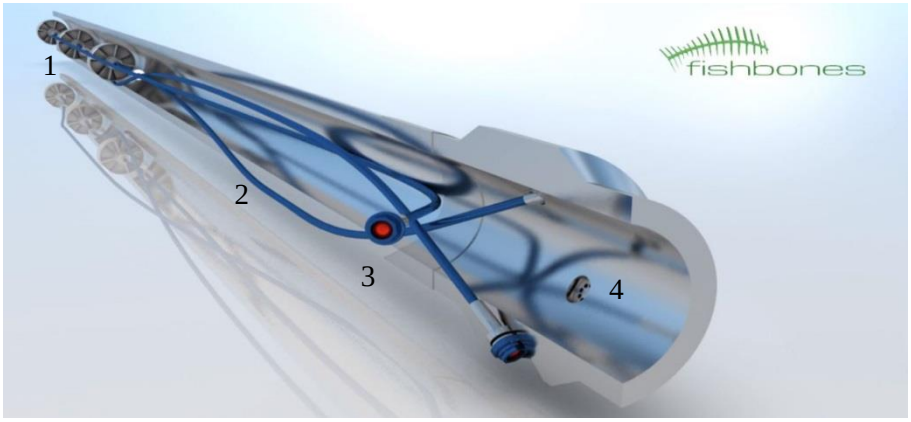

Figure 3-5: Dreamliner with turbines (1), needles (2) equipped with drill bits (3), and a production valve (4). Source: http://Fishbones.as/videos/.

Figure 3-6: Subs alternated with an anchor (1). It is also possible to see the pumped fluid path (red arrows). Source: http://Fishbones.as/videos/.

3.2 First documented fishbone installations (and pilot tests)

Fishbone technology was initially tested and discussed in three different fields. According to the type of formation, Fishbones (MST) were analysed in a coal bed methane (Fishbones AS) and in a chalk oil reservoir (Rice, et al. 2014), while Dreamliner (MDST) in a tight sandstone formation (Torvund, et al. 2016):

- On November 2013, nearby Sumatra Island (Indonesia) for the first time a vertical well was completed using fishbone technology (Fishbones AS 2018). The coal bed formation required the use of jetting needles to create fishbone annuli. The wellbore was completed with an 8.5" open hole through the contacted reservoir length (180 m). As shown in Figure 3-7, the pilot test was finished with two fishbone subs, slotted liners in the bottom and water swelling packers (sealing devices) for isolating the coal beds. The fishbone completion was hung off with the liner hanger, while the 12 m long needles were jetted with filtered water at 3000 psi. After few hours of penetration, the pumping pressure increment evidenced the full extension of the needles. Only 49 bbl of filtered water was employed for the operation. The flow rate resulting in the first days of production was four times higher with respect to the existing vertical cemented completion.

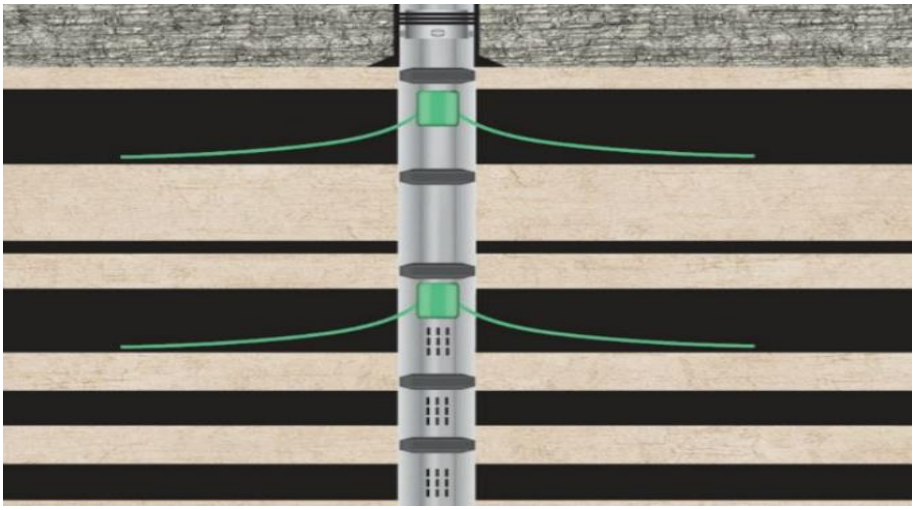

Figure 3-7: Schematic well completion composed of a vertical open hole with two subs, five water swelling packers and the three slotted liners on the bottom. The needles penetrate the thickest layers that range from 7m to 13m. Source: http://Fishbones.as/case-study-first-coal/.

- On April 2014, in Texas the first pilot installation in a horizontal well exploiting fishbone jetting was done in the Austin Chalk carbonate reservoir (Rice, et al. 2014), a Cretaceous formation which may act both as reservoir and source rock. The project was aimed at better understanding the technology and its risks in order to be later applied off-shore on the Norwegian and Danish continental shelves. The test was run on an existing open hole well producing for 20 years from a limestone formation with porosity 5% and 0.5 mD permeability and candidate for abandonment. Since the formation nearby was thought to be fully depleted, the test was done only to check the mechanical integrity of the assemble. According to laboratory tests on formation samples, 810 bbl with 15% HCl acid were chosen to jet the needles annuli. The installation required a workover rig. After the liner was set in the right position with packers, the acid was pumped to extend the needles into the formation. As shown in Figure 3-8, 15 subs with four needles each were inserted in the open hole and to avoid axial movement of the liner, three anchors were set. The pumping job lasted only 5 hours and the fully extension of the needles was highlighted by a spike in pumping pressure. At the end, 875 bbl of acid solution was required. The only flow rates monitoring allowed to safely perforate hard formations such as carbonate ones. Even if the reservoir was thought to be fully depleted, the needles increased the apparent wellbore radius and contacted new zones: cumulative production during the first 30 days increased by 8.3 times if compared with production before shut-in.

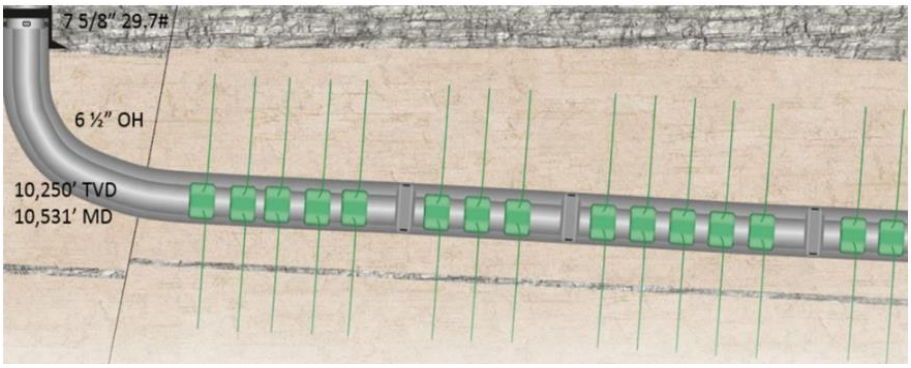

Figure 3-8: Schematic completion showing the horizontal open hole well with the 15 subs. Source: http://Fishbones.as/case-study/.

- In July 2015, in the Norwegian Sea one of the two lateral wells in the Smørbukk South reservoir was completed with fishbone subs (Torvund, et al. 2016) as illustrated in Figure 3-9. The hydrocarbons result to be saturated, thus a gas is present in the reservoir top. The tight sandstone formation targeted, the Halten Terrace, was thought to be a good example of several marginal reservoirs in the Norwegian Continental Shelf. The project was aimed to earn knowledge about marginal and low permeability reservoir rocks and to demonstrate productivity of this type of formations. The hydraulic fracturing alternative was rejected in order to avoid gas cap contact due to uncontrolled fracture growth. The tight sandstone formation required needles equipped with small drill bits to create fishbone annuli. With a semi-submersible rig, the liner was run in hole and 144 laterals, departing from 48 subs, where drilled in few hours circulating low solid oil-based mud, increasing the original permeability. To evaluate the relative contribution of each branch, oil sensitive inflow tracers were installed. This method is affected by inaccuracy, but a production log made on September 2017, after two years of production, confirmed that the fishbone branch was producing twice the rate compared to the lateral with pre-drilled liner.

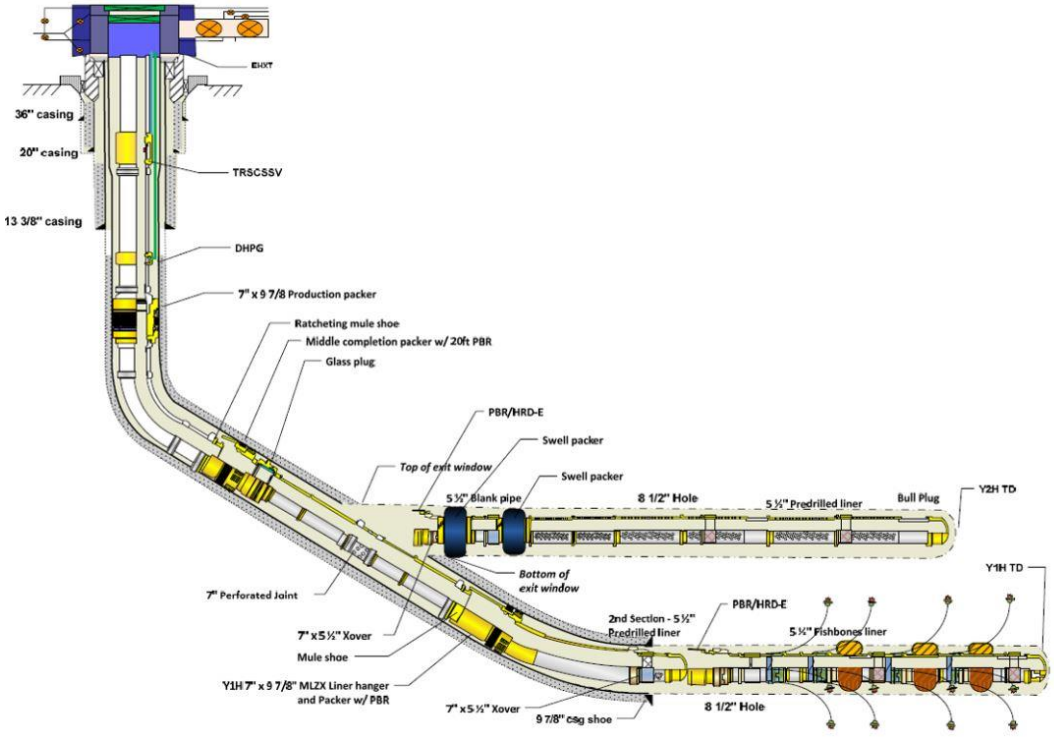

Figure 3-9: Well completion made of two lateral legs: on top a pre-drilled liner, on the bottom the bore is completed for 200m with 48 subs, with an initial slotted liner section. Source: http://Fishbones.as/news/.

These first installations were focused on proving the mechanical stability of the completions, evaluating the additional risk with respect to conventional wells. The operators were surprised by the small amount of workover needed and the low risk of mechanical failure added to classical drilling procedures. Furthermore, they showed that laterals increase the productivity of the well making also marginal and low permeability reservoirs economically producible. All these aspects can be summarized in what the operators deduced after the preliminary installations, that the downside risk of deploying Fishbones is equivalent as having a conventional (unstimulated) well, while the upside could be significant.

4 Reservoir simulation

Oil & Gas industry exploits 3D numerical reservoir simulators to predict hydrocarbon production profiles for given development scenarios. These profiles are used to plan investments and operations in the different assets, including the choice of completion solutions: the ultimate objective is to maximise economic return. In this chapter, an introduction to the state-of-the-art technology that characterizes reservoir simulation as an industrial process is provided, with some emphasis on the modelling of interactions between wells and porous media.

Reservoir simulations are based on mathematical models suitable to characterize multiphase flow in porous media by means of a set of partial differential equations (PDEs) including Darcy's Law and conservation equations. Reservoir PDEs can be solved analytically only for very simple problems, hence numerical solutions based on discretization in space and time are needed. Space discretization relies on the definition of a computational grid: the reservoir is split into N blocks (see Figure 4-5) usually called cells, thus the fluid system is characterized using cell-based average properties, e.g. pressure/saturations. Time is discretized in steps: $t_0, t_1, t_2, \dots, t_n \dots t_{n_T}$, where t_0 and t_{n_T} are the beginning and the end of the simulation, while the difference (Δt_n) between two consecutive times (t_n, t_{n+1}) is the time step. The state of the reservoir fluids at time t_i is defined by means of $N_c \times N$ primary variables (with N_c given by the number of conservation laws, while N by the number of blocks). At any time t_i a set of $N_c \times N$ cell-centric non-linear conservation equations is solved in order to evolve with time and get state properties at t_{i+1}. Notably, fluid properties change because of well activities, which include withdrawal and injection of fluids. Non-linearity is managed by means of Newton-Raphson method, with many linear systems solved at each time-step.

4.1 The black-oil model

The Black-Oil model, see (Aziz and Settari 1979) for an insight, is the most common used formulation in the oil and gas industry. According to this model, reservoir fluids consist of three components – oil, gas and water at stock tank conditions – flowing in the porous media as oil, gas and water phases. The conserved quantities are volumes of oil/gas/water at stock-tank conditions (from now on STC), under the assumption that stock tank densities of the fluids can be considered constant. Hence, conservation equations for oil, gas and water components at STC can be written as:

$$\frac{\partial}{\partial t}\left(\frac{\phi S_o}{B_o}\right) = -\nabla \cdot \left(\frac{v_o}{B_o}\right) \tag{4-1}$$

$$\frac{\partial}{\partial t}\left(\frac{\phi S_w}{B_w}\right) = -\nabla \cdot \left(\frac{v_w}{B_w}\right) \tag{4-2}$$

$$\frac{\partial}{\partial t}\left[\phi\left(\frac{S_g}{B_g} + R_s\frac{S_o}{B_o}\right)\right] = -\nabla \cdot \left(\frac{v_g}{B_g} + R_s\frac{v_o}{B_o}\right) \tag{4-3}$$

Where:

- $\phi(p)$ is the porosity of the rock defined with respect to a reference pressure [-],
- $S_{o,w,g}$ are the phase saturations [-],
- $B_{o,w,g}(p)$ represent the formation volume factors, thus the ratio between reservoir volume and surface volume [rm^3/Sm^3] (see the example in Figure 4-1),
- $R_s(p)$ is the solution gas, hence the dissolved gas in the oil solution at any pressure [Sm^3/Sm^3] (see the example in Figure 4-2),
- $v_{o,w,g}$ are the velocities of the phases in the medium [m/s].

In eq. (4-1), (4-2) and (4-3) the unknowns are the phase pressures and saturations, which are the quantities that describe the state of the reservoir system. Fluid properties (B_o, R_s, μ_o) depend on pressure. In particular, typical trends for an oil case are illustrated in Figure 4-1, Figure 4-2 and Figure 4-3:

- Below bubble point (undersaturated oil), decreasing the pressure more and more gas liberates from oil. R_s decreases according to its definition; at the same time B_o goes down since the reservoir volume of oil (with lower and lower gas content) approaches the surface volume. The viscosity increases since the oil has less content of light components as gas.
- Above bubble point (saturated oil), increasing the pressure no more gas can dissolve in the oil. Thus, the dissolved gas R_s keeps constant. For what concerns the formation volume factor, it slightly decreases. The saturated oil behaves like a liquid, thus increasing the pressure, the reservoir volume reduces according to compressibility effects. Viscosity grows a little since at fixed gas content the oil occupies less volume.

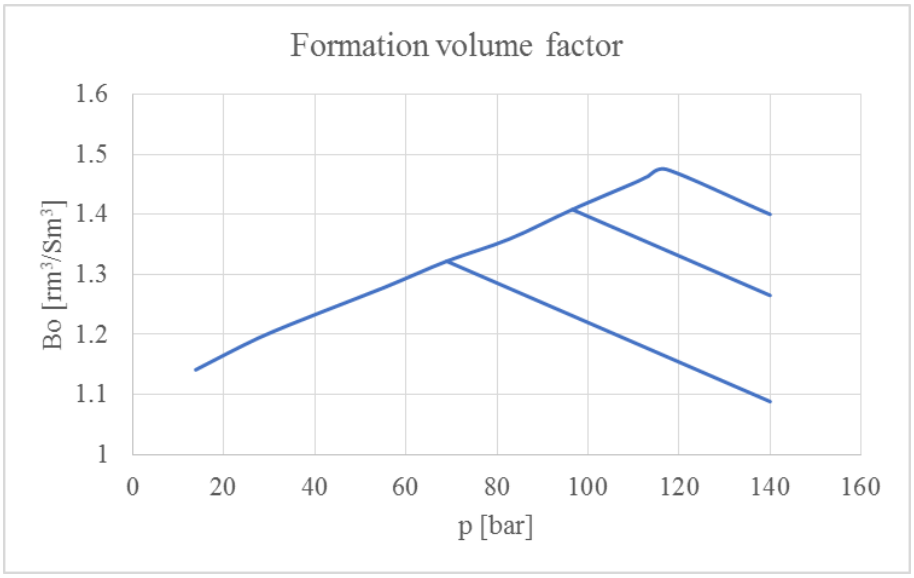

Figure 4-1: Oil formation volume factor curves for a black oil at different bubble pressures.

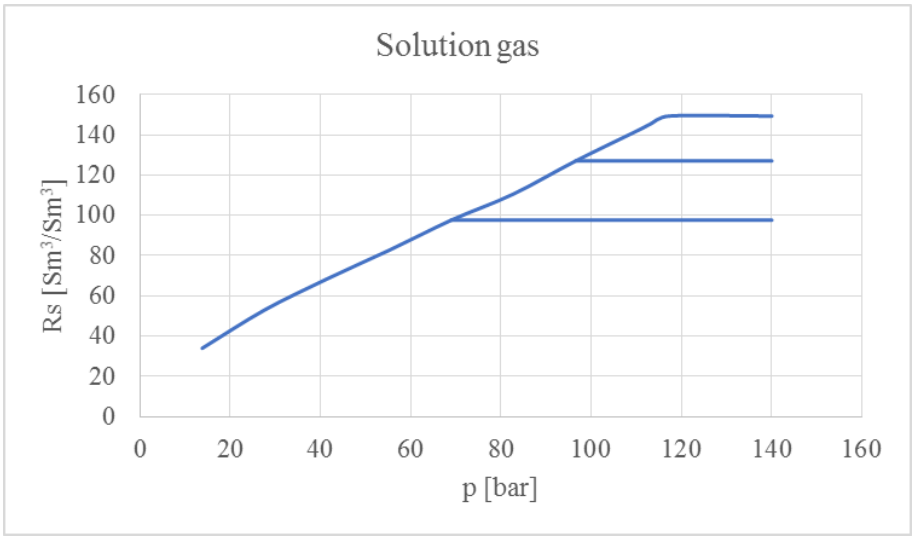

Figure 4-2: Solution gas curves of a black oil at different bubble pressures.

The phase velocities $v_{o,w,g}$, are defined according to a proper multi-phase extension of Darcy's Law:

$$v_\alpha = -\frac{k}{\mu_\alpha} k_{r\alpha} \nabla(p_\alpha) \qquad \alpha = o, g, w \tag{4-4}$$

Where:

- p_α the phase α pressure [Pa],
- k is the rock permeability [m^2],
- $\mu_\alpha(p)$ is the dynamic viscosity of phase α [Pa s] (see the example in Figure 4-3),
- $k_{r\alpha}$ is the relative permeability [-] of phase α (function of its saturation), (see the example in Figure 4-4).

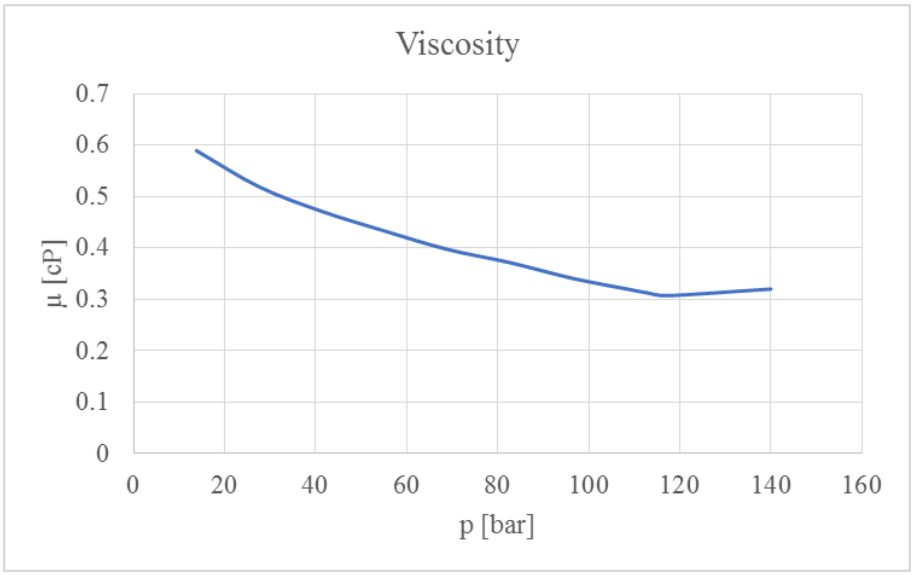

Figure 4-3: Viscosity of a black oil having a bubble pressure of 117 bar.

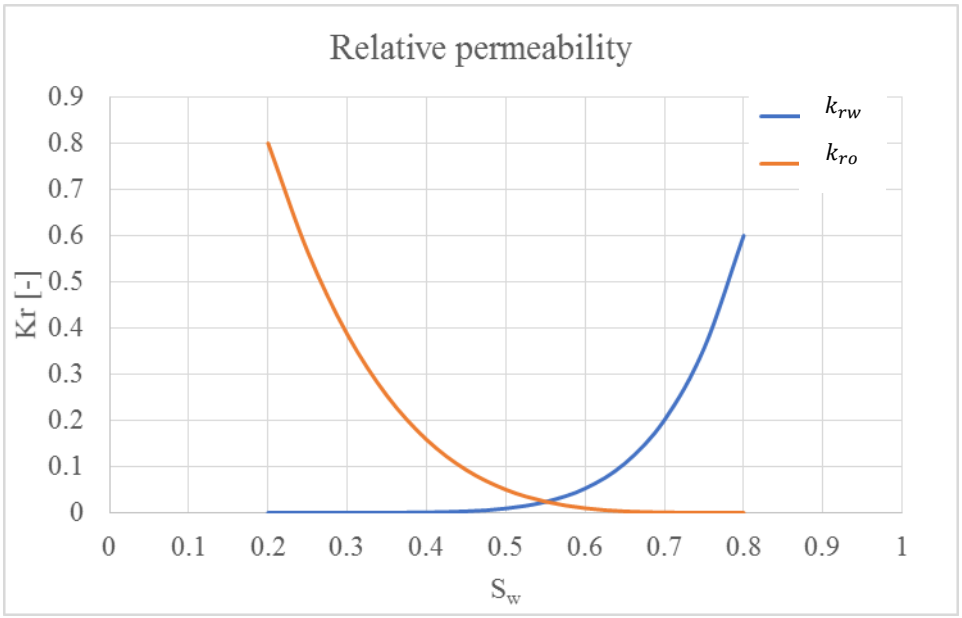

Figure 4-4: Example of relative permeability curves for oil and water phases.

It is worth comparing relative permeability with pressure dependent properties like formation volume factors, solution gas and viscosity. Relative permeability functions are highly non-linearly dependent on saturation and this leads to abrupt change in phase velocities in a very short scale. For instance, in a water injection process of an oil reservoir, water relative permeability is zero where the porous media has not been flooded and close to one few hundreds meter apart, where the reservoir has been irrigated. On the contrary, formation volume factors, solution gas and viscosities are smooth functions of pressure. This is particularly true for undersaturated oil properties. In this case, B_o can be written as:

$$B_o = B_{o,bp}(1 - c_o \Delta p_o) \quad (4\text{-}5)$$

Where $B_{o,bp}$ is the formation volume factor at the bubble point pressure p_{bp}, $\Delta p_o = p_o - p_{bp}$ and c_o, the undersaturated oil compressibility, is characterized by orders of magnitude of $10^{-4} - 10^{-5}$ bar^{-1}. Notably, linearity in pressure dependency holds in most of the cases also for porosity, which can be similarly written as:

$$\phi = \phi_{ref}(1 + c_\phi \Delta p_o) \quad (4\text{-}6)$$

Where ϕ_{ref} is the porosity at reference pressure p_{ref}, $\Delta p_o = p_o - p_{ref}$, and c_ϕ is the pore compressibility, with orders of magnitude similar to c_o. In reservoir problems, non-linearity is then associated to saturation changes in the reservoir, e.g. between injection and production wells, while volumetric properties and viscosities change mildly across the reservoir. In case of single-phase liquid flow, linearity of pressure dependent variables gives the possibility to simplify the system as a more manageable diffusion problem for pressure.

Using the Darcy's law eq. (4-4) to replace velocity in equations (4-1), (4-2) and (4-3), a system of three non-linear partial differential equations is obtained. The oil equation, see eq. (4-7), highlights the general structure of the system:

$$\frac{\partial}{\partial t}\left(\frac{\phi S_o}{B_o}\right) = -\nabla \cdot \left[-\frac{K}{\mu_o B_o} k_{ro} \nabla(p_o)\right] \quad (4\text{-}7)$$

Similar balances can be derived for gas and water, remembering to include the contribution of dissolved gas in the hydrocarbon liquid phase. The Black-oil model consists then in a set of three partial differential equations where the unknowns are three primary variables, namely one pressure (usually the oil pressure) and two saturations (for water and gas phase). Notably, Black-oil model equations can be solved analytically only for very simple problems, while real (or realistic) reservoir studies are solved numerically. In the oil industry, the state-of-the-art solution for reservoir simulation is the finite volume formulation, which relies on the definition of a computational grid and a time discretization.

4.2 Reservoir grid

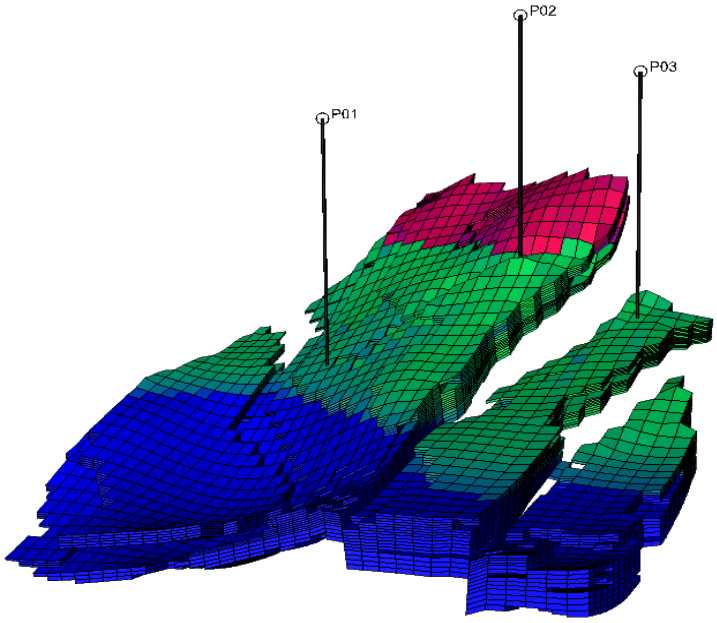

Figure 4-5: A reservoir model split into several hexahedral cells. More blocks mean more accuracy but higher computational time. The discretization is done for numerically solve non-linear PDEs. The phases are shown with different colors: blue (water), green (oil), and red (gas). The three vertical lines represent the wells.

According to a finite volume formulation, the reservoir domain is split in *N* blocks (see Figure 4-5), usually called cells, which allow to characterize the system by using cell based average properties, e.g. pressure/saturations and porosity/permeability. The mass conservation equation is defined for any cell, hence ensuring a strong (local) formulation.

State-of-the-art grids have a corner point geometry (CPG) (as in Figure 4-5): cells are hexahedral and are identified by a unique set of coordinates (*i*,*j*,*k*).

Typical reservoir simulation jobs span hours and projects require thousands of simulations. Thus, it is necessary to apply coarse cells with dimensions of 100 m, 100 m (X, Y directions) in order to have reasonable time frames. The cells are more refined in the Z direction (1 - 2 m) in order to capture the high vertical heterogeneity of formations.

Challenges persist with irregular geometries as fractured reservoirs or multilateral well completions. Complex and non-homogeneous domains should be modelled with a more detailed grid around the well; anyway, also the time spent to reach a solution builds up. To reduce run time, some commercial simulators, like ECLIPSE and Intersect, are designed to be run also through super computers, where several simulations are done at the same time. It is worth noticing that often high resolution is not needed everywhere but rather in very limited volumes of the reservoir, in particular near wells. For this reason, it is a common practice in the Oil & Gas industry to use Local Grid Refinement (LGR)

approach, see (Wasserman 1987), (Quandalle and Besset 1985), (Quandalle 1983) and (Heinemann, et al. 1989). As the name suggests, with LGR a baseline coarse model is modified by splitting a relatively small portion of the cells into smaller cells as shown in Figure 4-6.

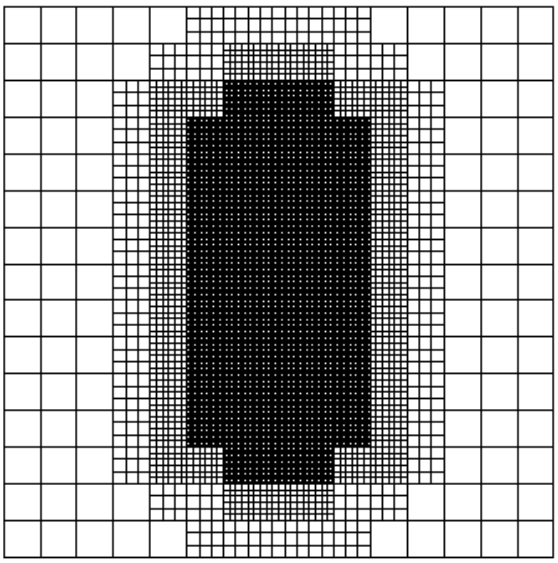

Figure 4-6: Slice of a 3D grid with a local grid refinement around well. External cell dimensions are 15x15 m, while the ones close to the well are in the order of a main bore diameter (about 0.2 m).

In this way, it is possible to increase resolution only where it is needed. Local Grid Refinement was developed in the 80's and 90's, it is now a standard in all commercial reservoir simulators and its popularity increased a lot in the last 10 years because of the development of hydrocarbon resources in extremely tight systems, such as shale oil and shale gas formations.

4.3 Numerical solution

Referring to a computational grid as those presented in chapter 4.2, where a reference cell is labelled as *i* and a generic adjacent cell is labelled as *j*, the time and spatial discretization of the conservation equation (4-7) for a component *c* can be written as:

$$R_{ic} = \frac{\Delta M_{i,c}}{\Delta t_n} + \sum_j F_c^{ij} + Q_c^w = 0 \qquad (4\text{-}8)$$

Where *c* labels oil, water or gas at stock tank condition. The discretized conservation equation is written in a residual form ($R_{ic} = 0$) and STC volumes are actually conserved.

Considering the oil component equation, variation of STC volumes in the cell can be detailed as:

- $\Delta \mathrm{M_{i,o}} = \Delta \left(\frac{\mathrm{V_b}\phi S_o}{B_o}\right)_i$ with $\mathrm{V_b}$ the bulk volume of the cell *i*,

- $\frac{\Delta M_{i,o}}{\Delta t_n}$ is the accumulation term inside the cell *i*, thus the variation of oil volumes at STC in the time step Δt_n,
- $\sum_w Q_o^{iw}$ is the sum of flows into the cell *i* from external source or sink *w*, for instance a well:
  - For a non-vaporized oil $Q_o = \frac{q_o}{B_o}$, with q_o the volume at reservoir condition,
  - For a gas, also the dissolved amount in the oil has to be considered, thus: $Q_g = \frac{q_g}{B_g} + R_s \frac{q_o}{B_o}$,
- $\sum_j F_o^{ij}$ is the sum of inter-cell oil flow into the cell *i* from a generic adjacent cell *j*.

Given pressure and saturation at time t, solution of equations like (4-8) for oil/gas/water in the grid cells lead to the updated pressure and saturations at time $t + \Delta t$. The unknowns in these equations depend on the way fluxes are evaluated.

The state-of-the-art solution for the evaluation of the fluxes among adjacent cells is the so-called two-point-flux approximation, which links the fluid flow to the pressure gradient by means of a transmissibility term:

$$\sum_j F_o^{ij} = \sum_j \frac{T_{ij} k_{r,o}}{B_o \mu_o} \Delta\Phi_{o,ij} \qquad (4\text{-}9)$$

Where:

- $\Delta\Phi_{o,ij}$ is the potential difference, defined as $\Delta\Phi_{o,ij} = (p_{o,i} - \rho_{o,i} g h_i) - (p_{o,j} - \rho_{o,j} g h_j)$,
- T_{ij} is the transmissibility between cells *i* and *j*. Considering flow along x-direction, T_{ij} is defined as:

$$T_{i,j} = \left(\frac{2}{\frac{1}{k_{x,i}} + \frac{1}{k_{x,j}}} \right) \frac{\Delta y \Delta z}{\Delta x} \qquad (4\text{-}10)$$

Where $k_{x,i}$ and $k_{x,j}$ are the x-permeability of cell *i* and *j*, and $\Delta x, \Delta y, \Delta z$ are the block dimensions. Eq. (4-10) is derived from Darcy's law and it is formally correct only for k-orthogonal grids (for example, Cartesian grids with a diagonal permeability tensor). The equation makes a harmonic average, as in the Ohm's law, of the parameter that obstacles the flow. In particular, the movement is impeded where there is a high permeability contrast (analogy permeability-resistance).

The two-point approximation defines the mass change in the current cell as a function of the fluid properties (pressure and saturations) in a local stencil. In particular, if the grid is Cartesian, the stencil consists of seven cells, that is to say the central cell and the six neighboring cells. Notably, to maximize efficiency and stability, reservoir simulators use a fully implicit approach, where fluxes are evaluated using cell pressures and saturations at time $t + \Delta t$.

Referring again to eq. (4-9) and (4-10):

- the quantities $k_{r,o}$ and μ_o are estimated with a so called "up-stream weighting rule", that takes the values from the up-stream cell of the flow direction:

$$\left(\frac{k_{ro}}{\mu_o}\right)_{i+1/2,j} = \begin{cases} f\left(S_{w,i,j}, p_{o,i,j}\right) & \text{if } p_{o,i,j} \geq p_{o,i+1,j} \\ f\left(S_{w,i+1,j}, p_{o,i+1,j}\right) & \text{if } p_{o,i,j} < p_{o,i+1,j} \end{cases} \quad (4\text{-}11)$$

  While viscosity is mildly influenced by pressure changes, relative permeability is strongly affected by small saturation changes, thus an accurate estimation of this last variable is crucial,
- B_o at the boundary is the value found with the average pressure of the two adjacent cells.

4.4 Numerical well models

In a reservoir simulator, wells cannot be simply represented using sinks or sources. In real wells (see 2.2), fluid pressure profile from sand face to wellhead characterizes operations. For instance, in production wells fluid flows in the wellbore according to the pressure drop between reservoir and bottom-hole fluid, then pressure drops due to friction and densities characterize fluid movement to wellhead: it is then necessary not only to compute cell pressure but it is also required to provide estimate of fluid pressure in the wellbore till the wellhead. For this purpose, first it is necessary to define models linking pressure values computed in the reservoir cells with bottom hole well pressure and inflow/outflow rates.

These models are based on Darcy's equation, which usually establishes a linear dependency between flow rates and pressure drops from cells to wellbore. Then the availability of a simulated bottom-hole pressure allows performing some fundamental analysis, such as estimate the deliverability for certain completions, which is incidentally one of the main purposes of this study. In this thesis work, the purpose is to investigate the effectiveness of various completion, thus the critical pressures are reservoir and bottom-hole well ones. Pressure losses along the tubing are not then taken into consideration.

The simplest model describes a well completed in a single cell i. The volumetric rate at reservoir condition $q_{\alpha i}$ of fluid injected/produced into/from the block can be written as (Holmes 2005):

$$q_{\alpha i} = WI_i \lambda_\alpha (p_i - p_w - H) \quad (4\text{-}12)$$

where:

- $\lambda_\alpha = \frac{k_{r\alpha}}{\mu_\alpha}$ represents the mobility ratio of phase α at the grid block connection i,

- p_w is the flowing bottom hole pressure (BHP) of the well calculated at the reference depth (D_{ref}),
- $H = \rho_{avg} g(D_i - D_{ref})$ is the hydrostatic pressure difference in the wellbore between reference depth (D_{ref}) and the well completion depth in the cell i (D_i). It is based on the mixture average density,
- Eq. (4-12) and (4-13) are rigorous for slightly compressible fluids, thus in presence of a linearity in pressure drops. It is less rigorous for gas cases, where non-linearity affects pressure drops,
- WI stays for "well index" which characterizes the connections in the cell *i* between reservoir and wellbore, regardless of time and fluid saturations.

The well index is defined assuming Darcy's flow and steady state conditions. Under these assumptions, Peaceman (D. Peaceman 1978) proposed the following definition:

$$WI_i = \left(\frac{2\pi kh}{\log\left(\frac{r_o}{r_w}\right)} \right)_i \tag{4-13}$$

In eq. (4-13), r_o is the Peaceman's radius defined as the distance from the well where the radial solution of the well equation equals the average pressure of the block (D. Peaceman 1978):

$$p(r) = p(r_0) + \frac{q_w \mu}{2\pi kh} \ln\left(\frac{r}{r_0}\right) \tag{4-14}$$

With h the well penetration length. Peaceman's definition, eq. (4-13) and (4-14), are valid for an isotropic and homogeneous reservoir where top/bottom grid cell faces are squares (see Figure 4-7).

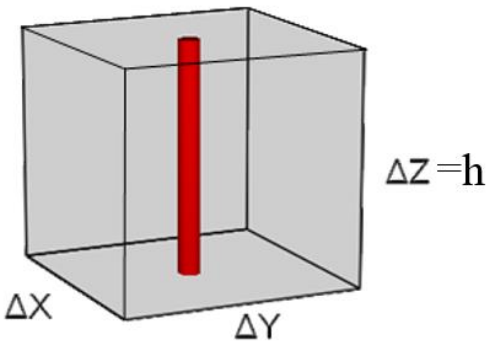

Figure 4-7: Example of a grid block fully penetrated by a vertical well slice. Source: (Shu 2005).

More generally, for a well oriented in the z-direction, with permeability heterogeneity and non-squared grid blocks (D. W. Peaceman 1983):

$$WI_i = \left(\frac{2\pi\sqrt{k_x k_y}h}{\log\left(\frac{r_o}{r_w}\right)} \right)_i \tag{4-15}$$

$$r_o = 0.28 \frac{\left[\Delta x^2 \left(\frac{k_y}{k_x}\right)^{0.5} + \Delta y^2 \left(\frac{k_x}{k_y}\right)^{0.5} \right]^{0.5}}{\left(\frac{k_y}{k_x}\right)^{\frac{1}{4}} + \left(\frac{k_x}{k_y}\right)^{\frac{1}{4}}} \tag{4-16}$$

where Δx and Δy are the x- and y-dimensions of the grid block, and k_x and k_y are the x- and y-direction permeability.

The assumptions for developing eq. (4-16) are:

- full penetration of the block by the well, perpendicularly to two faces of the cell,
- radial flow close to the well,
- no other wells in the vicinity that can affect the radial flow convergence.

In case of squared regular grid ($\Delta x = \Delta y$) and isotropic orthogonal permeability ($k_x = k_y$), $r_o = 0.2\Delta x$.

Notably, the definitions of eq. (4-15) and (4-16) are for a cell much larger than the wellbore: the Peaceman's definition of the well index makes sense only if cell dimensions are at least one order of magnitude larger than wellbore diameter. According to eq. (4-13) or (4-15), the Peaceman's radius loses its physical sense if it is lower than the wellbore radius. If these two values are close to each other's, it means that the cell coincides with the well, resulting in a negligible pressure drop between them. In this situation, it is unnecessary to compute the well index.

Peaceman's model is valid for a well that completely penetrates a block, with steady states radial flow towards it; however, in some situations these conditions are not fulfilled:

- well not completed through the entire reservoir block (spherical flow at the tip),
- wells closely spaced, thus each one affects the other's inflow.

Fortunately, Peaceman's model is suitable for reservoir drilled with simple conventional well, allowing to use coarse grid and significantly reduce computational time.

It is worth noting that the well index defined in eq. (4-13) using the Peaceman's model can easily accommodate the impact of local near wellbore effects such as damage or stimulation. In the oil industry these effects are characterized by means of a skin factor *S*, a non-dimensional parameter that takes into account additional pressure drops between reservoir and wellbore. In particular, a mechanical skin is associated to damaged or stimulated zones, while geometrical skin is associated to partial penetration and deviation with respect to layer bedding. Notably, mechanical skin due to damaged zone is always present since during drilling the rocks are crushed and mud filtrates into the

reservoir around the well affecting the original permeability. Damages are usually rectified by re-perforating, injecting acid or fracturing, leading to a productivity regain. If the radius r_d of the altered (damaged or stimulated) zone and the ratio between reservoir permeability and altered permeability (k and k_d) are known, S can be written according to Hawkins' equation (Hawkins 1956):

$$S = \left(\frac{k}{k_d} - 1\right) \ln \frac{r_d}{r_w} \tag{4-17}$$

A positive value of S means additional pressure drop, while a negative value indicates a region with higher permeability than the original one (Figure 4-8).

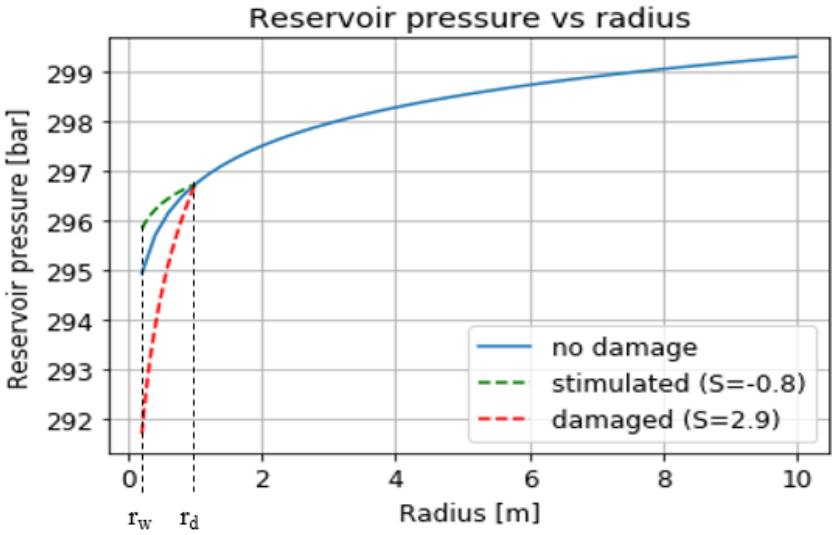

Figure 4-8: The chart shows the pressure inside a reservoir and in the altered zone. In case of reduced permeability (S= 2.9) the pressure drop near the well is more significant. While with stimulation (S= -0.8), there is a reduction of pressure drop with respect to the original permeability case.

The skin factor can be included in the Peaceman's well index (eq. (4-13)):

$$WI_i = \left(\frac{2\pi\sqrt{k_x k_y}h}{\log\left(\frac{r_o}{r_w}\right) + S}\right)_i \tag{4-18}$$

Eq. (4-18) holds for vertical, fully penetrating wells. If the well fully penetrates cells along the X axis, then the definition of well index and Peaceman's radius is easily generalized as:

$$WI_{ix} = \left(\frac{2\pi\sqrt{k_z k_y}\Delta x}{\log\left(\frac{r_o}{r_w}\right) + S}\right)_i \tag{4-19}$$

$$r_{o,x} = 0.28\frac{\left[\Delta z^2\left(\frac{k_y}{k_z}\right)^{0.5} + \Delta y^2\left(\frac{k_z}{k_y}\right)^{0.5}\right]^{0.5}}{\left(\frac{k_y}{k_z}\right)^{\frac{1}{4}} + \left(\frac{k_z}{k_y}\right)^{\frac{1}{4}}} \tag{4-20}$$

Well index and Peaceman's radius for a fully penetrating well oriented along Y axis, WI_{iy} and $r_{o,y}$, can be similarly defined.

Well index and Peaceman's radius can be generalized for a well which completion inside the given cell can be represented as in Figure 4-9. The solution suggested by (Holmes 2005) and (Shu 2005) is based on the projection of the completion segment along the cell axis. Using L_x, L_y, L_z (as in Figure 4-9) it is possible to compute axis referred well indexes (WI_x, WI_y, WI_z) and Peaceman's radii $r_{o,x}$, $r_{o,y}, r_{o,z}$.

The projection along X axis in the gridblock *i* gives:

$$WI_{x,i} = \left(\frac{2\pi\sqrt{k_y k_z}L_x}{\log\left(\frac{r_{o,x}}{r_w}\right) + S}\right)_i \tag{4-21}$$

$$r_{o,x} = 0.28\frac{\left[\Delta z^2\left(\frac{k_y}{k_z}\right)^{0.5} + \Delta y^2\left(\frac{k_z}{k_y}\right)^{0.5}\right]^{0.5}}{\left(\frac{k_y}{k_z}\right)^{\frac{1}{4}} + \left(\frac{k_z}{k_y}\right)^{\frac{1}{4}}} \tag{4-22}$$

Similarly, eq. (4-21) and (4-22) should be applied for Y and Z projections. The overall cell connection factor is given by:

$$WI_i = \sqrt{WI_x^2 + WI_y^2 + WI_z^2} \tag{4-23}$$

The pressure equivalent radius r_o of the slanted well is finally given by (Schlumberger 2009):

$$r_o = r_w e^{\frac{2\pi kh}{WI_i} - S} \tag{4-24}$$

Where $kh = \sqrt{(k_y\, k_z)L_x^2 + (k_x\, k_z)L_y^2 + (k_x\, k_y)L_z^2}$.

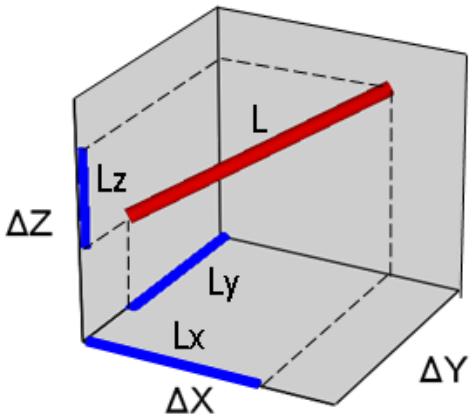

Figure 4-9: A slanted well penetrating a grid block and its projection in the three dimensions. Source: (Shu 2005).

More generally, a well intersecting a grid-cell can always be seen as a sequence of vectors as in Figure 4-10, thus the overall well connection factor is given by the sum of the connection factors calculated for each vector.

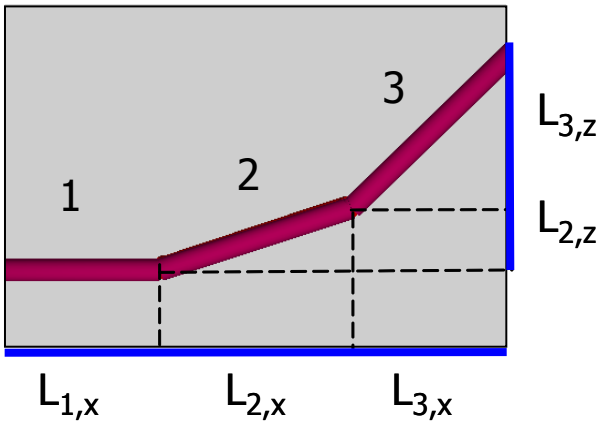

Figure 4-10: A generic well in a cell can always be seen as a sequence of vectors. Source: (Shu 2005).

Using SI units, the well index measure is cubic meter. In the Oil & Gas industry well indexes are defined as the ratio between rate time viscosity and a pressure drop: $\mu Q \ / \ \Delta p$. Then, well index is routinely reported as $[Sm^3 cP] \ / \ [bar \ day]$ or $[stb \ cP] \ / \ [psi \ day]$.

4.5 Going forward in time

In a reservoir simulation the time-line is discretized in a sequence of time steps Δt, and a new set of fluid properties at time t_{i+1} is computed using values at time t_i and inflow/outflow conditions of wells established using well models and well inflow/outflow performances. Following a black-oil framework, $N \times 3$ (with N the number of grid blocks) non-linear conservation equations are

assembled at the generic time-step $i+1$, (see equation (4-8) and the discussion there), to give a non-linear system, which can be written in a compact form as:

$$\boldsymbol{R}\left(\boldsymbol{p}^{\boldsymbol{T}}, \boldsymbol{S}^{\boldsymbol{T}}\right) = \boldsymbol{R}(\boldsymbol{x}) = \mathbf{0} \tag{4-25}$$

Where $\boldsymbol{R}$ is the residual vector, $\boldsymbol{p}$ and $\boldsymbol{S}$ are pressure and gas/water saturations for N cells at time - step $+1$, $\boldsymbol{x} = \left(\boldsymbol{p}^{\boldsymbol{T}}, \boldsymbol{S}^{\boldsymbol{T}}\right)$ is a $N \times 3$ lines vector and $\mathbf{0}$ is a $N \times 3$ lines vector of zeros. A solution for the system (4-25) can be found using the Newton-Raphson iterative method, where at each iteration a correction $\delta\boldsymbol{x}$ is computed by solving:

$$\boldsymbol{J}(\boldsymbol{x})\delta\boldsymbol{x} = -\boldsymbol{R}(\boldsymbol{x}) \tag{4-26}$$

Where $\boldsymbol{J}(\boldsymbol{x})$ is the Jacobian matrix of the residual $\boldsymbol{R}(\boldsymbol{x})$ with respect to x. Reservoir simulation splits the time T in a convenient number of N_t steps, where the value of N_t is a combination of field development update frequency (e.g. wells rate given on a monthly basis) and non-linearity of the model (the stronger is the non-linearity of the problem, the shorter is the time-step). At each time-step, many linear systems as in (4-26) are solved, and these computations, which represent about 90% of the time needed for a reservoir simulation, scales as the number of cells N. In operational work - flows, where reservoir simulation is used to evaluate in a robust manner the benefit of different field development or re-development plans, it is necessary to run thousands of simulations usually in a relatively short time, say few months. This poses limitations to the number of cells that can be used and, ultimately, on the resolution of the grid. This explains why reservoir models are built using an average lateral cell spacing of 100 m, 100 m and a thickness of some meters (usually few): finer grids are unpractical even with the current parallel computing capabilities available in all commercial simulation packages (Casciano, Cominelli and Bianchi 15/09/2015).

5 Fishbone completion modelling

In this chapter, some methodologies implemented in this work to quantify the benefit of fishbone completions using numerical simulations are outlined. To perform these simulations, it is necessary to depart at some stage from the well modelling described in section 4.4. The traditional well modelling used in reservoir simulation studies is based on Peaceman's model, which holds in principle for wells that are completed with some distance in terms of cell numbers from boundaries and other wells. In the industry practice, these constraints are often relaxed and the so-called projected Peaceman's model is systematically used. Nonetheless, the implementation of this model for fishbone completions is questionable.

The issues related to the use of Peaceman's model for fishbone completions can be highlighted using a simplified case where a horizontal well is completed along the reservoir with four additional needles that penetrate the formation for 10-12 meters. Adopting a commonly used block geometry for simulations (100 m, 100 m for x- and y- direction, 5-10 m along depth), the well layout for a single sub with respect to the grid system can be highlighted as in Figure 5-1.

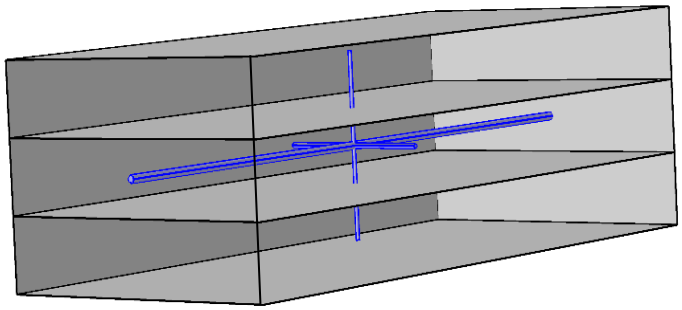

Figure 5-1: A section of a fishbone completed well with a single sub of four needles. The main wellbore penetrates the central cell, as horizontal needles do, while vertical needles partially penetrates the grid blocks. This leads to three completed cells.

With reference to the grid blocks in Figure 5-1 and to the values reported in Table 5-1, applying the Projected Peaceman's model (eq. (4-21) and (4-22)), the well indexes of a fishbone completion (with 9 subs) and of a conventional well are compared. Their ratio results to be: $\frac{WI_{FishCompl}}{WI_{ConvWell}} = 2.55$, meaning that fishbone completion more than duplicates the steady state production in an isotropic reservoir. This value leads to an overestimation of the benefits if compared to results found in literature.

Table 5-1: Parameters employed to compute the ratio of well indexes between a conventional well and a fishbone completion.

Cell dimensions	100 m,100 m, 10 m (X,Y,Z)
Main well length	100 m
Main well radius	0.19 m
Needle length	10 m
Needle radius	0.01 m
Number of subs along the main bore	9
Permeability	1 mD (isotropic)

The actual flow path generated by fishbone completions can be highlighted using some pictures which anticipate methodologies and results described in upcoming chapters. Figure 5-2 and Figure 5-3 show pressure contours near needles and between subs and highlight that even in these simple conditions the flow is no more radial with respect to the well bore; rather, radial flow-paths can be seen towards the needles or the wellbore far from the needle-wellbore junctions. Moreover, with reference to the grid cell in Figure 5-1, the partial penetration of the needles into the blocks introduces a "tip effect" due to the fluid flowing into the lateral annulus also from the tip.

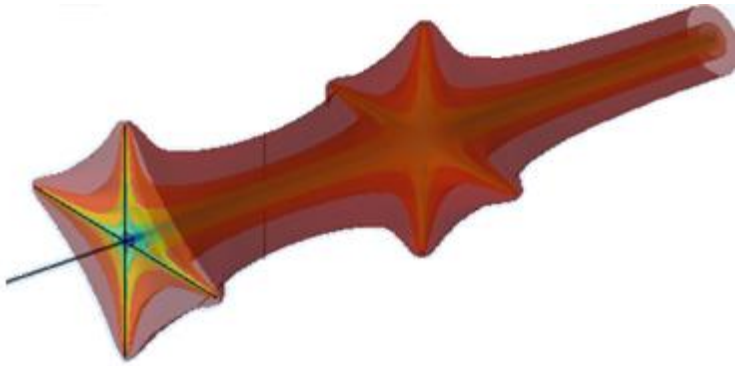

Figure 5-2: Isobars around a fishbone completed well. Radiality is present only far from needle-main bore junctions.

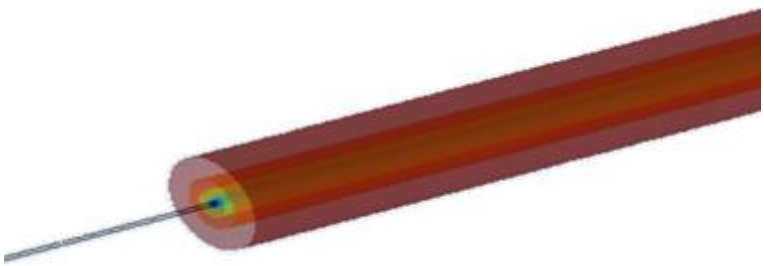

Figure 5-3: Isobars around a conventional well. Radiality is present along the entire main bore.

Then, to estimate fishbone completions benefits for simplified but representative geometries and both steady state and transient conditions, it is not possible to use the Peaceman's model as it is and run 3D simulations with coarse grid blocks.

In this work, different solutions for numerical modelling and benefit evaluation of fishbone completed wells are implemented and compared. Before discussing in detail these approaches (see 5.2) an overview of the studies that can be found in literature is given in chapter 5.1. Being Fishbones a relatively young technology, few studies on their performance were made before.

5.1 Review of previous studies and modelling in literature

5.1.1 High resolution Cartesian grids (Klovning 2016)

In 2016, Carl-Ivar Klovning published his Master Thesis on fishbone completions. The purpose of his work was to find the best way to model fishbone completions and to evaluate their benefits with respect to conventional completions in very simple geometries.

From a geometrical viewpoint he considered fluid flow occurring around completions in a cubic reservoir sector with 100 m of side length and homogeneous properties. The reservoir grid has variable resolutions, in particular gridblocks are smaller in proximity of the well position.

Klovning investigated the pros and cons of modelling fishbone laterals as numerical wells or as fractures. In both cases, a comparison in terms of productivity is performed with respect to conventional wells. Simulating needles as numerical well is done by applying Peaceman's model. In these cases, the main wellbore is not modelled to avoid the presence of many completions in close vicinity which would affect the radiality of flow. This method comes with two problems: an area with a high completion density that actually creates a non-radial inflow path; the partial perforation of needles, introducing important errors when Peaceman's connection factor is used. When fishbones are modelled as fractures, the grid in the well regions is refined so that cells have the same cross-sectional area of laterals. Fractures are given arbitrary high permeability (10^7 mD) to resemble flow in the pipes. Also the main wellbore is modelled as a fracture, but high permeability is given to a number of cells that altogether have an area equivalent to the cross-sectional area of the well itself.

After some sensitivities on grid refinement and fracture permeability, the author concluded that modelling fishbones as highly permeable channels is the best method. The several completion keywords adopted for simulating the fishbones as laterals generated overestimated flow rates or weird results, while the fracture model had just some inaccuracies that could be accepted. Thus,

Klovning continued his work of estimating fishbone performances with the "lateral as fractures" model. Several sensitivities on permeability, grid refinement, fishbone length and density were done. Increasing grid refinement and fracture permeability the flow rates converged towards some values, however a trade-off between computational time and accuracy was applied. The completion with a single sub gave a production increment up to 60% with respect to a conventional open hole.

5.1.2 EDFM

EDFM (Embedded Discrete Fracture Model) is the state-of-the-art method for discrete fracture network modelling with commercial simulators. The method hierarchically subdivides the fractures according to their length with respect to the grid size (Cavalcante and Shakiba 2015). Short fractures ($l_f/l_g<<1$) are thought to influence only matrix properties such as porosity and permeability, while long fractures ($l_f/l_g>>1$) are responsible for fluid flow since they are the preferential path that interconnects well and reservoir zones (Li, Lee and Chevron Enegy Technology 2008). In such way, EDFM is able to model the fracture network without increasing too much the model complexity, since it explicitly works only with the more impacting fractures. Short fractures are taken into account editing grid block conductivities in which are included (Li, Lee and Chevron Enegy Technology 2008). Long fractures are substituted as auxiliary cells added to the grid. The different connections of these new degrees of freedom are defined via cell non-neighboring connections (NNC). In EDFM, fractures are characterized by two kind of connectivity: matrix-fracture (describing the flow from the matrix towards the fractures) and fracture-fracture (describing the flow inside fracture planes).

A long fracture behaves like a high conductivity channel; therefore, it is equivalent to a small well in the reservoir, where fluids easily flow. Due to their small radius and length, the needles can be seen as fractures that communicate with the reservoir and the main well, having the same flowing properties of the needles. (Cavalcante and Shakiba 2015) applied EDFM concepts to Fishbones, in particular by defining the traditional EDFM connectivity as: (Figure 5-4):

- Matrix to lateral: according to a Peaceman's equation, for a lateral in x- direction:

$$T = 2\pi\left(K_y^{matrix}K_z^{matrix}\right)^{0.5}\Delta x_{fb}\frac{1}{\ln\left(\frac{r_o}{r_{fb}}\right)} \tag{5-1}$$

  Where $K_y^{matrix}, K_z^{matrix}$ are the cell permeability in y- and z- directions, Δx_{fb} is the lateral penetration in the block along the x- direction and r_o is similar a Peaceman's radius:

$$r_o = 0.28\frac{\left(K_y^{matrix}\Delta z^2 + K_z^{matrix}\Delta y^2\right)^{0.5}}{\left(K_y^{matrix}\right)^{0.5} + \left(K_z^{matrix}\right)^{0.5}} \tag{5-2}$$

With $\Delta z \; and \; \Delta y$ block's dimensions. For a lateral along other directions than x-, the previous equations should be modified by similarity.

- Between lateral blocks:

$$T = \frac{A_{fb} k_{fb}}{< d >_{fb}} \tag{5-3}$$

where the cross-section area of a lateral is $A_{fb} = \pi r_{fb}^2$, k_{fb} is the equivalent fracture permeability and $< d >_{fb}$ is the distance between the centers of two equivalent fractures.

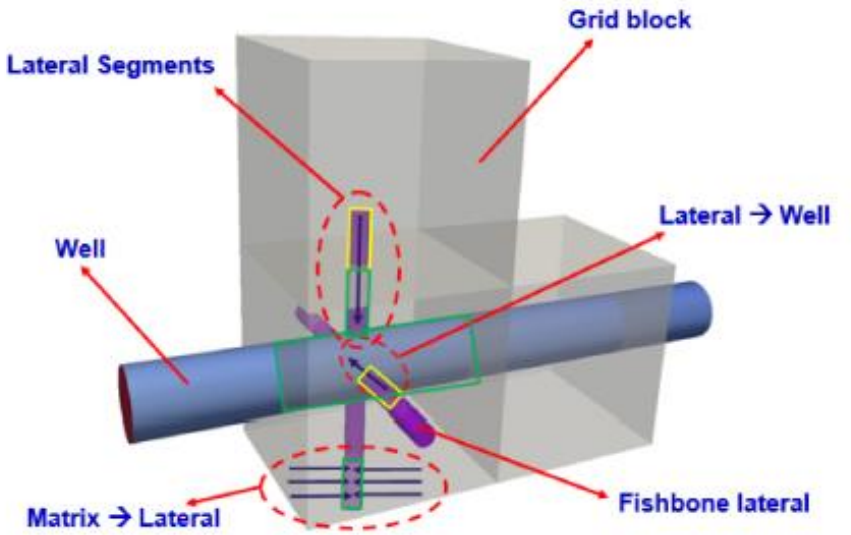

Figure 5-4: Schematic representation of the connections used in the model. (source: (Cavalcante, et al. 2015)).

Cavalcante, changing the number of subs, identified the "fishbone production saturation point", or the maximum number of subs that gives a sensible production increase. Accordingly, from an economic point of view, he plotted the NPV (net present value) against the number of subs. Where the NPV curve reaches a maximum, it means that the cost of an additional sub is not repaid by the further production increment. The author also evaluated the benefits of this completion in different reservoirs (isotropic, anisotropic and fractured), showing that this technology is worthy in several conditions.

5.1.3 CFD simulators: CFD (Senergy and Sintef)

A totally different approach consists in exploiting a CFD (computational fluid dynamic) software and its ability to model complex geometries. This way of simulating physical problems is increasing its share with respect to conventional software mainly due to two aspects. First of all, the computational power of new computers allows to run complex analysis, moreover CFD, with the help of a CAD (computer aided drafting) module and the fine mesh allows to represent all the small

details in the system. This software is based on refined and unstructured meshes (up to 10 million of cells) that can be customized in order to be more or less accurate in specific zones (Figure 5-5).

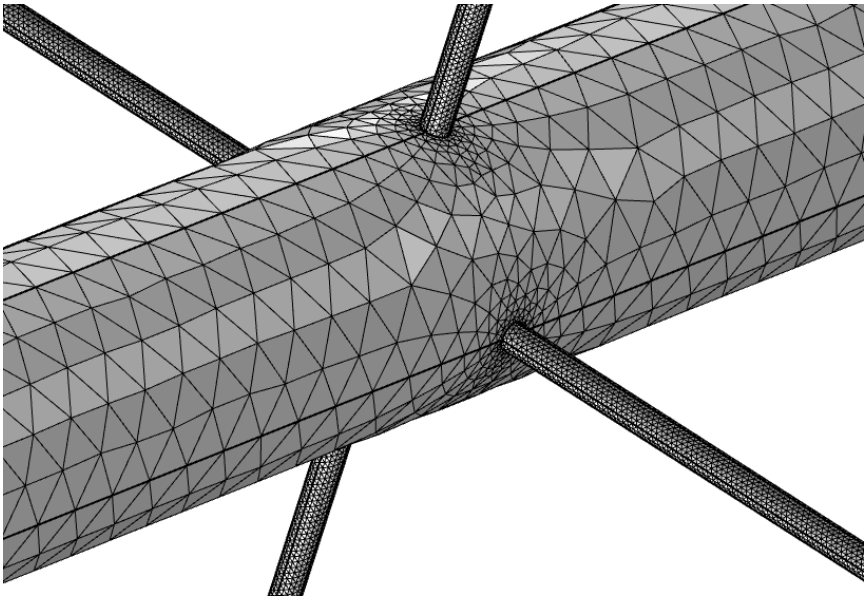

Figure 5-5: A classical mesh employed by a CFD simulator: a main well of 0.19 m diameter and three laterals of 0.02 m diameter can be seen. The minimum element size of the mesh is set to 0.001 m so that tetrahedrons can shape with good quality also small domains (made with COMSOL Multiphysics).

A CFD software, called Wellscope™, was developed and used by LR Senergy to predict the performances of Fishbones. The field under study was the Smørbukk Sør, in the Norwegian North Sea, owned by Statoil (now Equinor). The potentiality of Wellscope™ is the ability to describe in detail the processes that take place in the reservoir, near the well and inside the completion (LR Senergy 10/06/2015). The study was aimed to assess the impact of formation damage, pressure drawdown, failure of some completion parts such as production valves or needles, and the potentiality of installing a slotted liner in the first section. The complex well geometry, considering main bore, needles, production valves and slotted liner was firstly modelled with an extremely refined mesh. Unfortunately, the high number of meshing elements generated numerical instabilities and unpractical run times. Thus, Senergy instead of modelling the well in all its length (two branches of about 2000 m each), just considered a section of it, one single sub of approximately 50 m (see Figure 5-6). This simplification was done according to the assumption that one sub does not influence the production of the near subs due to their big distance and to the low permeability of the formation. Another simplification of the model was considering a smaller reservoir radius, made possible by rescaling the drawdown between well and reservoir boundaries. Later, applying symmetry and proportionality, the result found for this small model was applied to the full geometry. This shows that CFD software should be applied only with small geometry extension to avoid unfeasible simulation time. On the other part, the results are accurate and can be modified and properly scaled to the full model. Wellscope™ was also able to evaluate pressure distribution nearby the needles,

inside them and across the production valves. This was the first time that pressure drop due to needles presence was evaluated, things that conventional software cannot do, anyway the value found can be considered negligible. Finally, Senergy investigated the effect of valve or annulus failures as the worst scenario. Thanks to the slotted liner, the loss of production with respect to a conventional well was of few percent (2%), while with non-damaged Fishbones the maximum increment was about 20%.

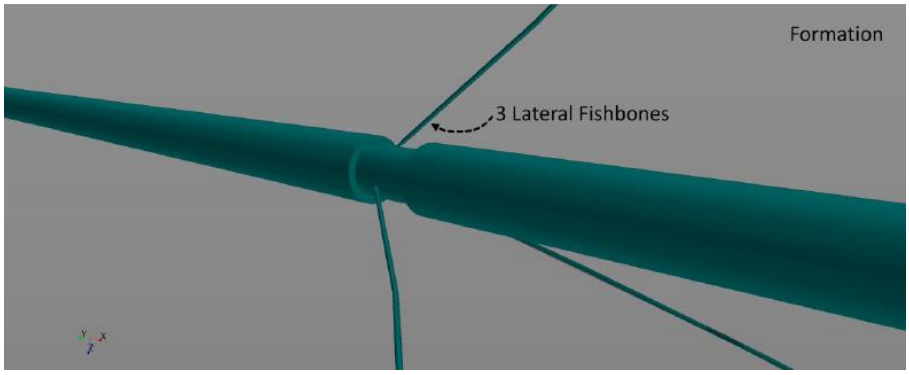

Figure 5-6: Senergy considered only one sub with three needles.

Also Sintef, in collaboration with Fenix Consulting Delft, exploiting the MATLAB Reservoir Simulation Toolbox (MRST), developed a program named Simfish with the purpose of fishbone design optimization (Sintef.no 2015). They compared fishbone and open hole production capacities on a simplified grid, estimating the relative increment and productivity index. The software requires short run times (in the order of few minutes) and it has the benefit to generate wellbore completions readable with ECLIPSE, allowing to do a deeper analysis also with reservoir software.

5.2 Implementations

In this work, three different solutions for modelling fishbone completed wells in order to evaluate their benefit are implemented and compared. These three solutions can be labelled according to the key technology used in the process: High Resolution Grid (HRG), Embedded Discrete Fracture Model (EDFM) and Finite Element Method (FEM). In short, these solutions can be described as follows:

- **High resolution finite volume simulation**

  Borrowing some ideas from (Klovning 2016), a possible way to study the benefit of fishbone completions consists in developing high resolution grid based on Cartesian geometry. The drivers are the geometry of the wellbore and of the needles. In this work, grid resolution is increased up to the scale of the wellbore, using for the wellbore region cubic cells of 0.2 m of

side. In the cells completed by the main bore, the Peaceman's model cannnot be implemented because their cell radius is smaller than the wellbore radius. Near needles, grid resolution is not increased further, hence given the typical needles annulus radius, the Peaceman's model is used to derive needles completion well indexes from cell radius. In principle, this solution may detail steep pressure gradients developed in vicinity of wellbore and needles, in particular near junctions. Moreover, using LGR option (see chapter 4.2 and 6), it is possible to coarse the grid near the external boundaries where pressure variations are milder. Exploiting the potentiality of the ECLIPSE simulator, both the main bore and fishbone laterals are modelled with completion keywords. In the way fishbone laterals are modelled, leveraging on local grid refinement, lays the main difference between this work and the one done by Klovning.

- **EDFM approach**

  The EDFM (Embedded Discrete Fracture Model) was developed for fractured reservoirs characterized by large-scale fracture corridors (Cavalcante, et al. 2015) (Panfili, Cominelli and Eni E&P 2014) as an effective way to incorporate fractures into corner-point geometry grids. Then, (Cavalcante and Shakiba 2015) suggested to reformulate EDFM to reflect the possibility to model fishbone completions, essentially turning the fracture elements into needles and the connections between fractures and host matrix cells into a transmissibility between needles and related cells. This method is implemented in chapter 7, where needles are substituted with modified fractures. The innovative step introduced in this work is the customization and the use of an Eni-proprietary EDFM plug-in of commercial geomodelling software.

- **Finite Element modelling approach**

  A detailed and accurate modelling of fluid flow towards wellbore and needles can be achieved using computational packages where partial differential equations are discretized using finite element schemes (Quarteroni and Valli 2008). In this way, it is possible to use unstructured grids based on tetrahedral elements and achieve an enhanced resolution around completions that cannot be obtained using conventional simulation technology. It is worth noticing that FEM are not commonly used in reservoir simulation because of their formulation: it is not easy to derive local conservation equations suitable for fully implicit solution regardless the number of component and phases. Moreover, reservoir grids are developed to follow depositional processes and describe formation where lateral extents may range tens of kilometres while thickness may span tens of meters. Using tetrahedrons in such geometries would require a gigantic amount of elements or unreasonably skewed geometries. However, in this work the target is to numerically evaluate the benefit of fishbone completions on well productivity using single phase simulation

and thus the benefit given by FEM in terms of geometrical accuracy is valuable. In chapter 8, FE modelling is implemented using the COMSOL Multiphysics packages.

These three solutions were run and their results were evaluated to define the best way to estimate the increment in the well productivity associated to fishbone completions. Adopting a classical reservoir simulator (ECLIPSE) and a CFD software (COMSOL Multiphysics) the completion performances are evaluated. In all the approaches innovative ways that improve the ones used in the literature can be found, as described in the following sections.

Notably, it should be highlighted that since the installation cost of a fishbone completion is similar to the one of a conventional well, their comparison is based just on produced flow rates. Economics are strongly affected by time, thus a production anticipation or delay (in term of months or years) impacts both the NPV and the internal rate of return of a project, two of the main parameters that show the profitability of a field development. Therefore, from here on, the two completions are analyzed in terms of production increment and anticipation.

6 High resolution finite volume simulation

In this section, fishbone completion performance is simulated using a standard finite volume reservoir simulator as described in chapter 4, with LGR option to increase resolution in the grid and then model as accurately as possible steep pressure gradients around needles and well main bore. The benefit of a locally refined grid in comparison with a coarse grid is shown in Figure 6-1, where the field pressure appears to be completely different, in particular close to the completions.

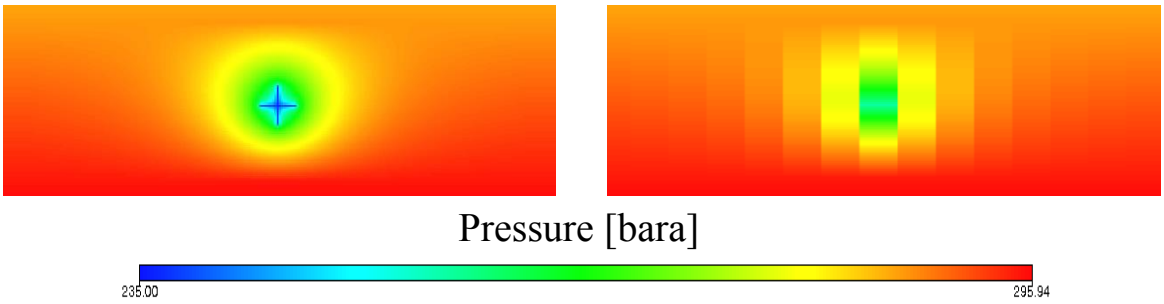

Figure 6-1: Field pressure after depletion with a fishbone completed well (100 m main well and four laterals of 10 m) producing at 250 bar (with respect to the reference depth). On the left a refined grid is employed, while on the right the accuracy is lost due to a coarse grid.

6.1 Model definition

In this chapter, the key scale elements are wellbore radius and needle annulus radius. Peaceman (D. Peaceman 1978) (see 4.4) gave a method to define a connection between well pressure and grid-block to account for large grid blocks typically used in reservoir simulation. One of the key points is to detail flow behavior near completions and in particular differences between flow towards needles and towards main wellbore. This motivated the choice of very fine grid cells; in particular, the fundamental grid size is dictated by the wellbore diameter: the main well is simulated using cell completions with an area comparable to the wellbore cross-section. The net consequence of this choice is that one of the Peaceman's assumptions, $\Delta X_{cell} \gg r_w$, is no more valid because well-bore and completed cells coincide. Then, the logic used in this work is to replace the well indexes in the wellbore completions with sufficiently large values to obtain a negligible pressure drop between a wellbore connection and the corresponding cell. It is worth noticing that this approach is equivalent to use very large permeability – say 10^7 mD – in the completed cells. In fact, because of the harmonic average of permeability used in the definition of transmissibility (see eq. (4-10) at page 33), such extreme values of permeability have no effect in the fluid flow between cells but only in the definition of the well indexes.

Following the above quoted logic, the core of the grid is characterized using very small cells – essentially cubes with 0.2 m of side – comparable with wellbore diameter. As regard the needles, it is worth noticing that their radius – 0.01 m – is small enough to allow using Peaceman's model when defining cell radius (r_o) and well index.

Moving away from the completions, cells increase their dimensions as reported in Figure 6-2, until they achieve (20 m x 20 m x 10 m) extensions near the borders. It is worth observing that the grid is suited to simulate performance of a horizontal well with one sub located at the center of the grid.

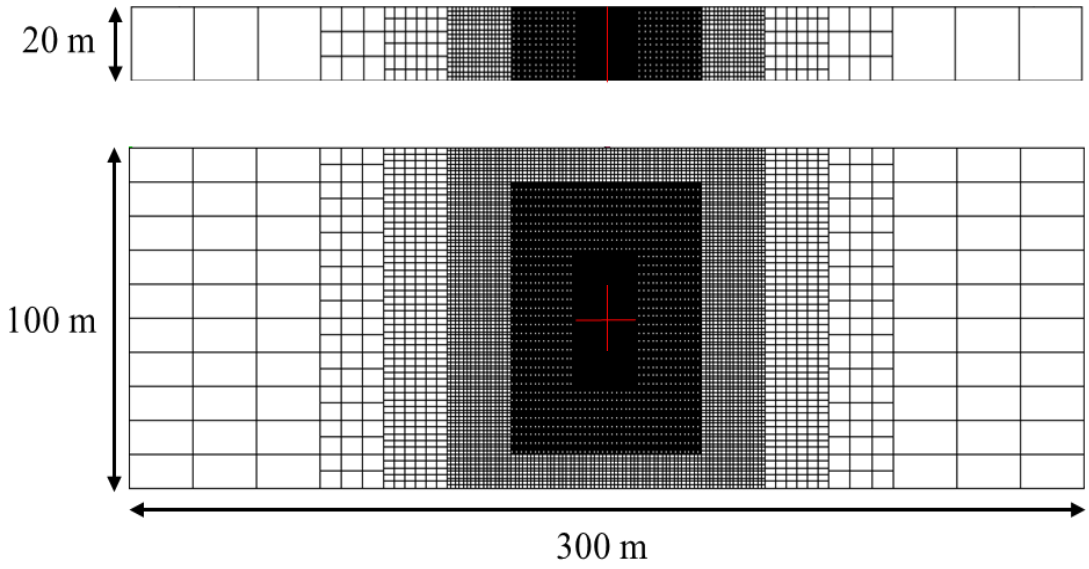

Figure 6-2: Local grid refinement around the wells (in red). The cells close to the completions are so small (0.2 m of side) that cannot be distinguished. The blocks in the borders have a dimension of 20 m x 20 m x 10 m. The slice on the top is a view of the model from above (x,y plane is shown along with main well section), while the slice on the bottom is a view from the front (x,z plane is shown along with the four needles).

The representative element of a fishbone completion is the "sub": a 12 m main bore section with four needles (about 10 m each) having a 90° phasing. Therefore, the minimum distance between two consecutive needles is 12 m. In order to minimize their competing effect during hydrocarbon drainage, this distance is increased a little. In this chapter, only fishbone subs (composed by four needles) are studied, while Dreamliner subs (three needles) have a trajectory that is more difficult to be approximated with a Cartesian grid.

To make a more fair comparison between conventional and unconventional completions the reservoir model is further simplified by making inactive cells outside a volume of 300 m x 20 m (along main well direction) x 100 m (see Figure 6-3 and Figure 6-4). Therefore, only a 20 m open hole conventional well and a 20 m sub are modelled and compared in terms of hydrocarbon production.

With the LGR technique, the total number of cells is 2.8 million. If a uniform refinement with the smallest cell dimension was done, the computational grid would be composed by 75 million of cells. Therefore, LGR decreases of one order of magnitude the grid blocks, meaning that also the computational time is reduced at least by one order of magnitude.

In real formations, the reservoir volume is usually split amongst three phases – gas, oil and residual water – distributed according to their density (see 2.1). In this simplified model, the formation is saturated just by a single hydrocarbon phase (oil or dry gas, see the Appendix for their PVT tables). So, water-oil-contact and gas-oil-contact are moved to have a single phase in the domain. The bubble pressure of the oil is set lower than the bottom hole pressure in order to not have free gas in the reservoir. Finally, homogeneous rock properties (porosity and permeability) are considered. All these simplifications are done since the well productivity is usually referred to a single phase fluid. In fact, in case of multiphase flow, the productivity index is influenced by relative permeability curves and fluid properties (like solution gas contained in the oil) and therefore it will depend not only on the completion geometry. This work is focused on understanding the benefits of fishbone subs on the liquid or gas productivity, without considering the effects coming from a multiphase flow model. Below in Table 6-1, the parameters that fully characterize the system are reported.

Table 6-1: List of parameter employed in the simulations.

Reservoir block	300 m x 20 m x100 m
Reservoir top depth	4300 m
Reservoir bottom depth	4400 m
Well depth	4350 m
Porosity	0.1
Permeability	From 0.01 mD to 100 mD
Hydrocarbon saturation	1
Main well length	20 m
Well radius	0.09525 m
Fishbone length	10 m
Fishbone radius	0.01 m

Two assumptions are done when this model is considered: i) the relative benefit of the fishbone completions computed using the representative element can be scaled to real type installation where several subs are mounted with a regular spacing of 20 and ii) the entire surface of main wellbore and fishbone needles is available to flow without local impairment.

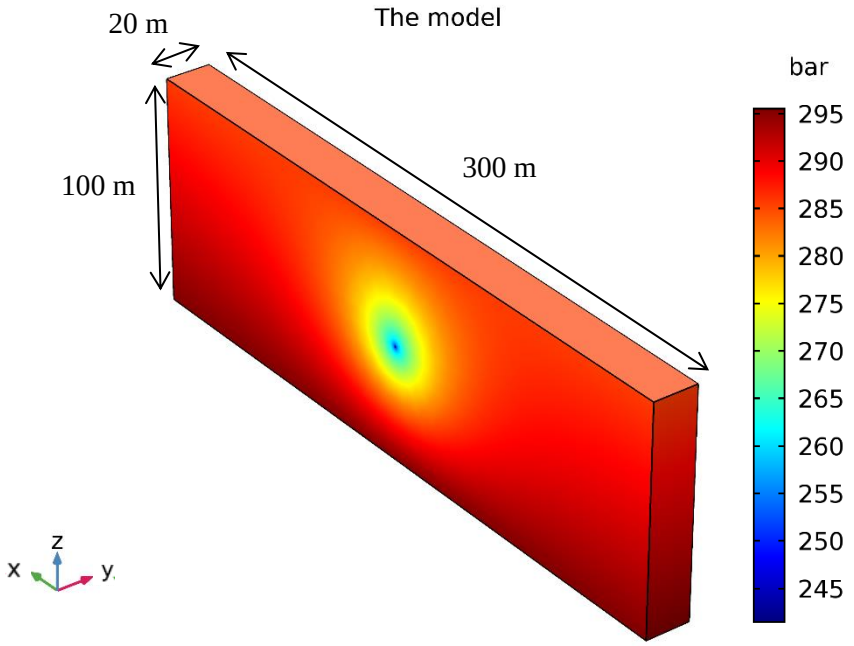

Figure 6-3: The figure shows the reservoir slice dimensions used in the simulations and the conventional well.

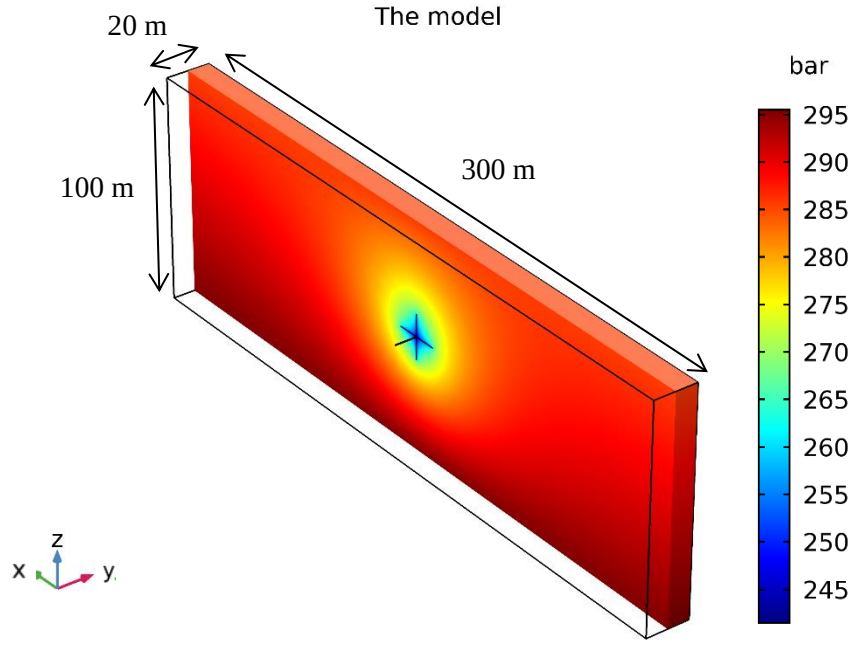

Figure 6-4: The figure shows the reservoir slice dimensions used in the simulations. Also the fishbone sub is visible.

6.2 Toward steady state productivity index

Formally, steady state conditions may be achieved by using proper Dirichlet's boundary conditions. In reservoir simulation, the typical way to set Dirichlet's boundary conditions consists in using very large pore volume at the reservoir borders where one may actually want to set constant pressure values. However, for an initial period, before the well pressure change reaches the boundary (see 2.3), fluids flow under transient conditions (infinite-acting reservoir) (Dake 1978). Once the pressure variation reaches the constant-pressure border, steady-state flow conditions establish.

Reservoir pressure is set to 300 bar at the reference depth of 4447 m, while the completions are producing at a constant bottom hole pressure of 250 bar (with respect to the reference depth).

In the following paragraphs, sensitivities on fluid types and reservoir permeability are shown; Dirichlet's boundary conditions influence is discussed; then, fishbone benefits are evaluated in case of sealed reservoir

The production increment of a fishbone sub with respect to a conventional well, thus the ratio of flow rates, will be called "**fishbone benefit**". While the ratio of cumulative production given by the two completions will be labelled as "**cumulative fishbone benefit**".

6.2.1 Single phase fluid, sensitivity on permeability

The first comparison between a fishbone sub and a conventional well section producing two different fluids - oil or dry gas - is done with several reservoir permeability. This parameter is changed from 0.01 mD to 100 mD to understand the potentiality of the fishbone completion in low and medium permeability formations. The large pore volume, used to simulate a Dirichlet's boundary condition, is assigned according to Figure 6-5.

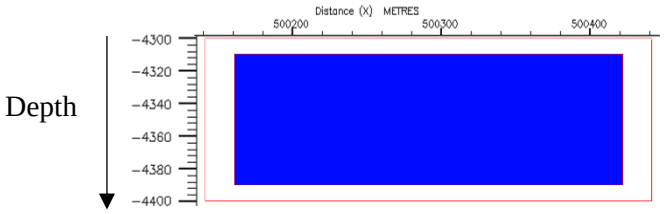

Figure 6-5: Reservoir slice that shows how the Dirichlet's boundary conditions are set on the reservoir border (outside the blue area).

Figure 6-7 and Figure 6-9 show the production rates respectively for an oil and a dry gas with various reservoir permeability. From these, it should be observed that:

- The initial transient period lasts more for low permeability formations and is further protracted with viscous fluids like oil. It represents the time that passes before the reservoir boundaries perceive the well effect.
- During steady state, the flow rate is proportional to formation permeability and fluid viscosity.

The results can be better visualized when the fishbone benefit $\left(\frac{Q_{fish}}{Q_{conv}}\right)$ is plotted versus time, as in Figure 6-8 for the oil and Figure 6-10 for the gas:

- In the transient period, the fishbone completion significantly produces more than the conventional well, in particular with a viscous fluid (e.g. in the first two months for k=0.01 mD and k=0.1 mD the oil production is more than doubled). The benefits with gas is still significant but much less than oil. The comparison between an oil and dry gas case is shown in Figure 6-11, where for an easier reading only low permeability cases are shown (the ones more affected by a long initial transient period). The production increment and anticipation rises if viscosity increases and permeability decreases (see Table 6-2).
- While during the transient, fluid and formation properties affect the relative increment, during steady state the fishbone benefit converges to the same value, no matter the fluid or rock type. Here, the fishbone completion produces about 1.75 times the rate of a conventional well, introducing an important improvement.
- If the benefit in steady state flow is the same for different cases, with low permeability reservoirs and viscous fluids, the production during the transient is further anticipated and boosted.

The effect of needles on reservoir pressure can be understood from Figure 6-6. Here, the fishbone sub depletes the reservoir at a significantly higher distances than a conventional well.

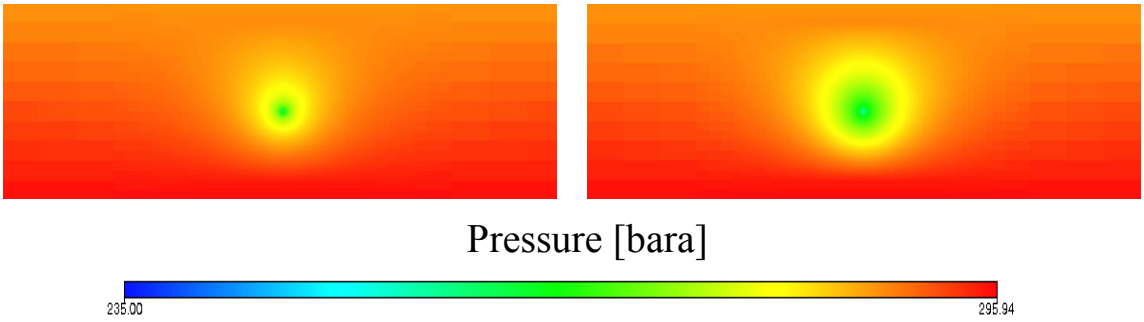

Figure 6-6: The figures compare the drainage area of a conventional well (on the left) and of a fishbone sub (on the right) in an oil reservoir. The needles significantly increase the drainage area, justifying the flow rate increment of 1.75 in steady state conditions. On the right chart, needles are not visible as in Figure 6-1 since the slice is taken at a distance of 10 m.

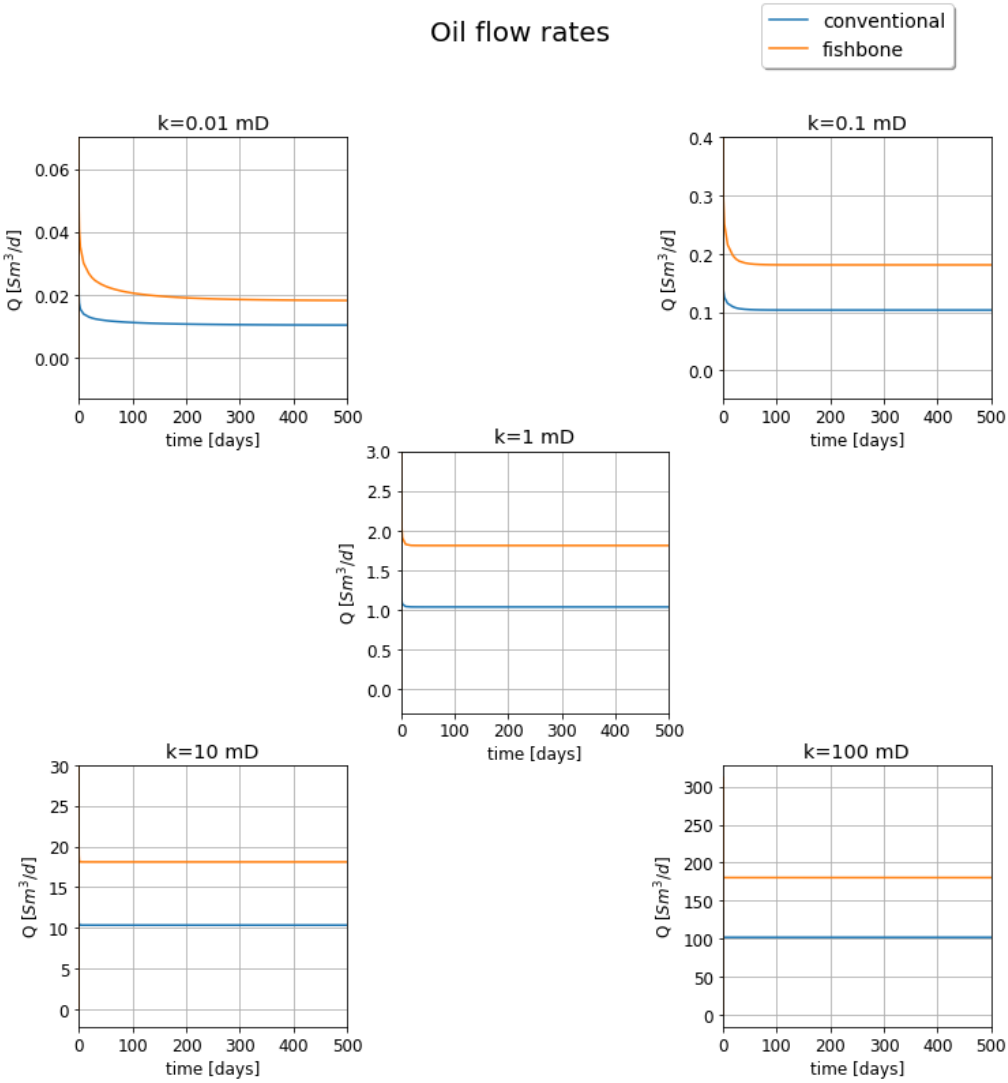

Figure 6-7: Oil flow rates for a fishbone completion (orange) and a conventional well (blue). The reservoir permeability is varied from 0.01 mD to 100 mD.

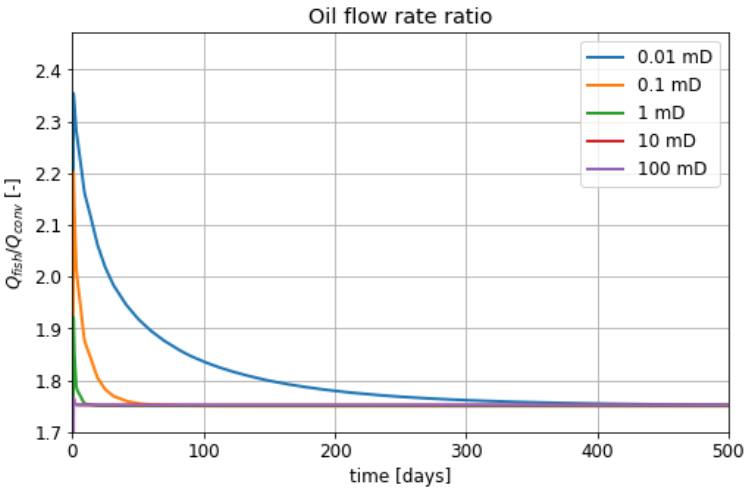

Figure 6-8: Fishbone benefit in an oil reservoir with permeability varied from 0.01 mD to 100 mD.

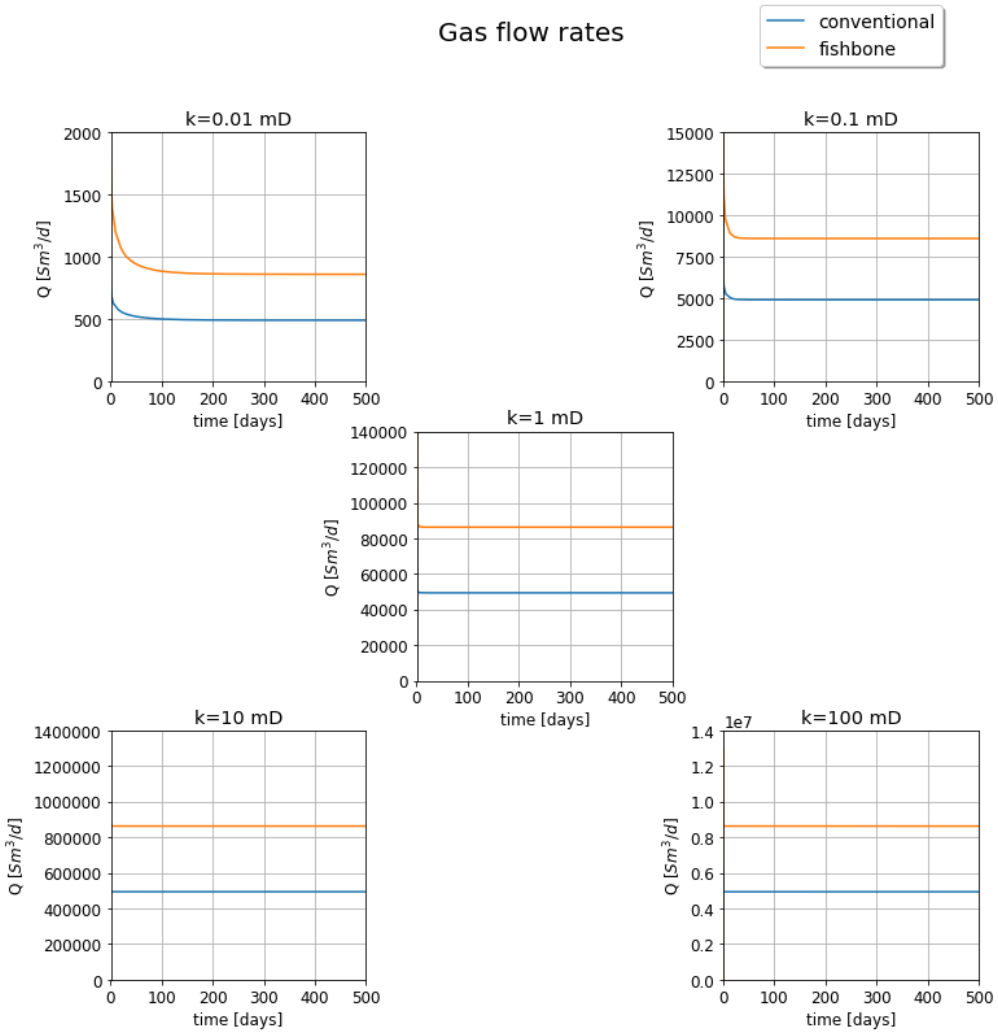

Figure 6-9: Gas flow rates for a fishbone completion (orange) and a conventional well (blue). The reservoir permeability is varied from 0.01 mD to 100 mD.

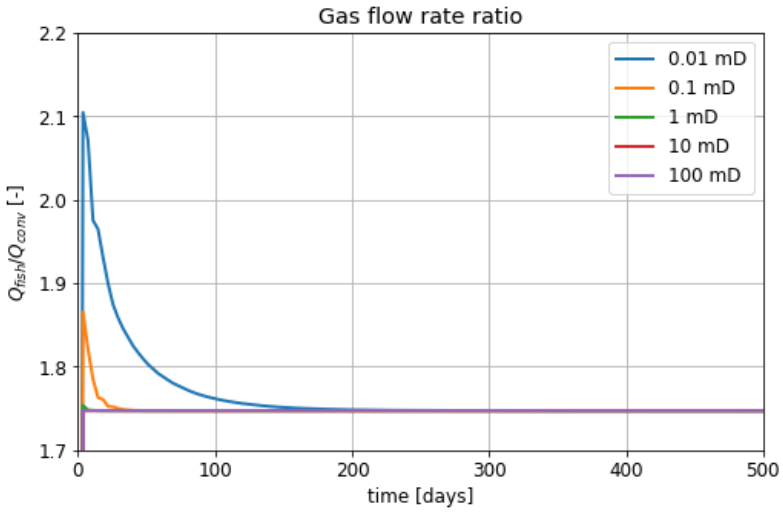

Figure 6-10: Fishbone benefit in a gas reservoir with permeability varied from 0.01 mD to 100 mD.

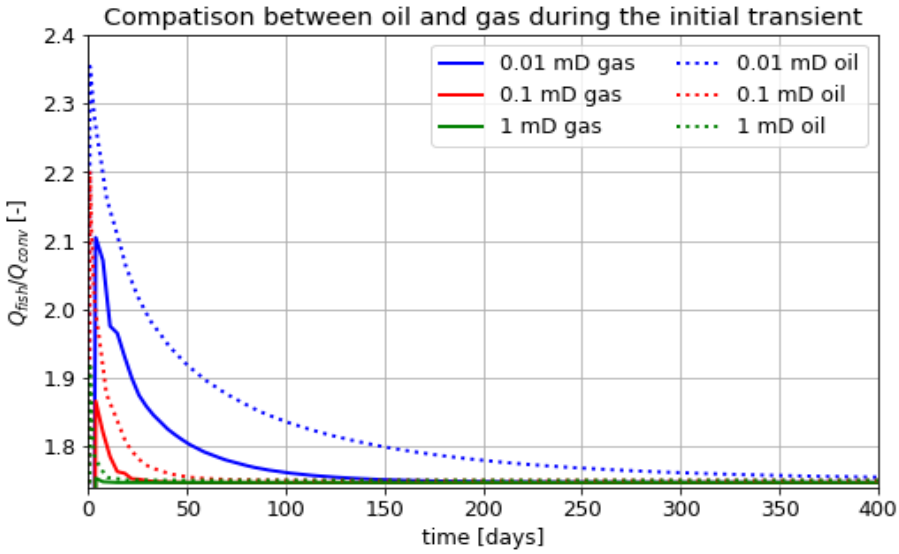

Figure 6-11: Fishbone benefit for oil and gas cases during the initial transient period (only low permeability formations are shown).

Table 6-2: Cumulative fishbone benefit at the end of the initial transient period for low permeability formations.

k [mD]	Oil	Gas
1	1.783	1.757
0.1	1.800	1.765
0.01	1.824	1.806

6.2.2 Sensitivity on boundary conditions

Dirichlet's boundary conditions can be defined at different distances from the well. In this section the effect of fishbone performance and benefit estimates with respect to boundary condition locations are evaluated. Results achieved in the previous paragraph for an oil case are here compared with the ones obtained using a closer boundary condition.

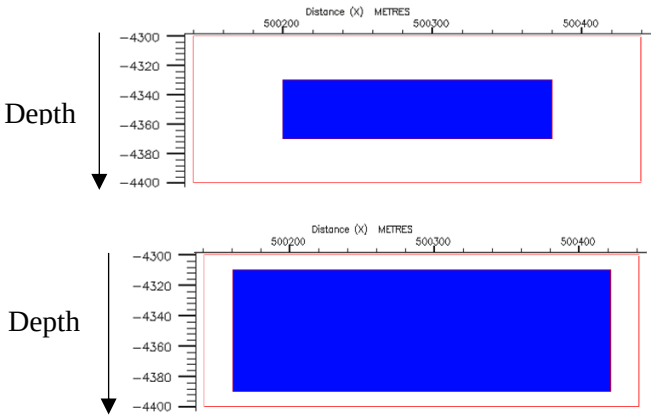

Figure 6-12: On the top a closer Dirichlet's boundary condition. The original pore volume is shown in blue. On the bottom, boundary is far away from the well (as in 6.2.1), which is placed in the center of the slice.

A nearer Dirichlet's boundary means that the reservoir pressure is sustained also in zones closed to the well. The boundary does not change its initial pressure, only the zones with original pore volume (blue part in Figure 6-12) are affected by a pressure reduction. Vertical needles result to be immersed in zone at high pressure (since they are closer to the boundary with respect to the main well). This situation is enhanced once a constant pressure is set closer to the completion, resulting in a higher fishbone benefit.

Results are shown in Figure 6-13, where with a closer boundary the needle production is more significant, giving a benefit higher than 90% during steady state. The opposite happens with a faraway boundary condition (as in Figure 6-14 and in chapter 6.2.1), where the benefit in the transient period is less significant (75% of increase). In this case, also needles contact zones with low pressure since the boundary is far, therefore their benefit is reduced.

The Dirichlet's condition can approximate the behavior of a reservoir where the aquifer or the gas cap provide a significant pressure support. The closer the Dirichlet's boundary, the higher the support.

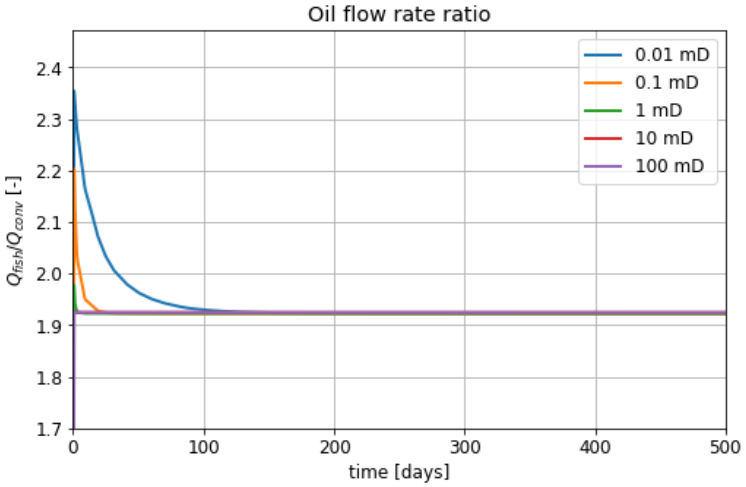

Figure 6-13: Fishbone benefit for a close boundary (see Figure 6-12).

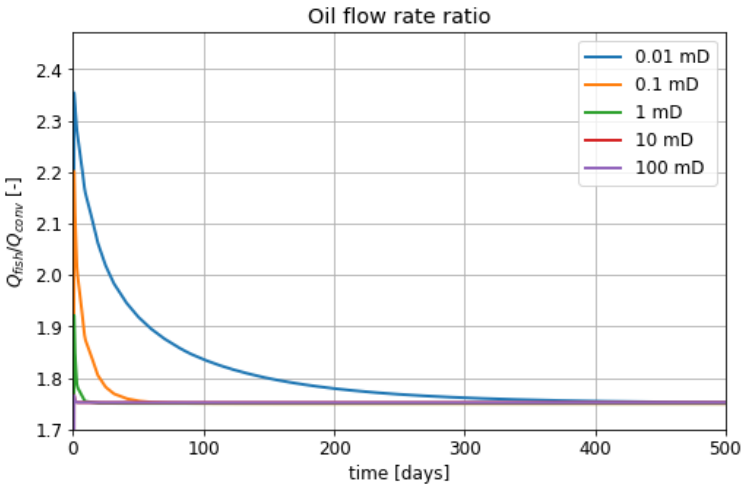

Figure 6-14: Fishbone benefit for a distant boundary (see Figure 6-12).

6.2.3 Fishbone in a layered reservoir

Broadly speaking, reservoirs consist of thin mineralized layers staked one at the top of the others. Communication across layers may be loose or even absent when shale or anidrite provide total vertical sealing. In this case, horizontal or slanted wells may be penalized. If vertical wells are not a choice because of formation tightness, fishbone may offer an upside giving the possibility to contact many layers altogether from a horizontal well. Thus, the potentiality of a fishbone sub with respect to a conventional well is here investigated in such formations.

The reservoir is assumed to be composed by three sealed layers. Two impermeable barriers are placed above and below the main horizontal well, meaning that no flow can pass from one layer to the other in absence of stimulation (see Figure 6-15). The horizontal well drains only the central one, while

the vertical needles, by-passing non-permeable zones, reach also the bottom and upper layers, enabling the production also from these.

The needles increase the drainage radius in the middle layer, but also improve vertical communication contacting layers not producible with a simple horizontal well. Only the fishbone completion allows the entire reservoir production. Figure 6-16 and Figure 6-17 show the ratio of cumulative production respectively for an oil and dry gas case. While for a leaky reservoir (layers perfectly communicate) both conventional well and fishbone sub reach steady state, resulting in a fixed cumulative production ratio (about 1.76 both for oil and dry gas), in a sealed reservoir, once the main bore has depleted the central layer (see Figure 6-15), it starts to produce less. On the contrary, the vertical needles keep draining the top and bottom layer. This results in an increasing cumulative fishbone benefit. Since it takes more time for the oil to flow with respect to the dry gas, the cumulative oil ratio increment is in delay with respect to the gas case, however after 500 days both for oil and gas it is closed to 4.5.

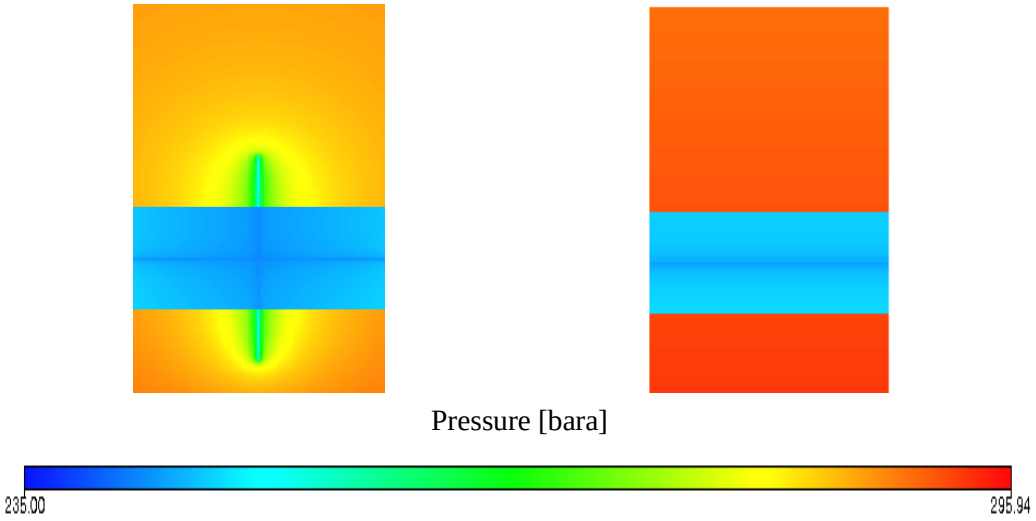

Figure 6-15: Comparison of a layered reservoir depleted by a fishbone sub (on the left) and a conventional well (on the right). Vertical needles allow to contact and produce also the top and bottom layers.

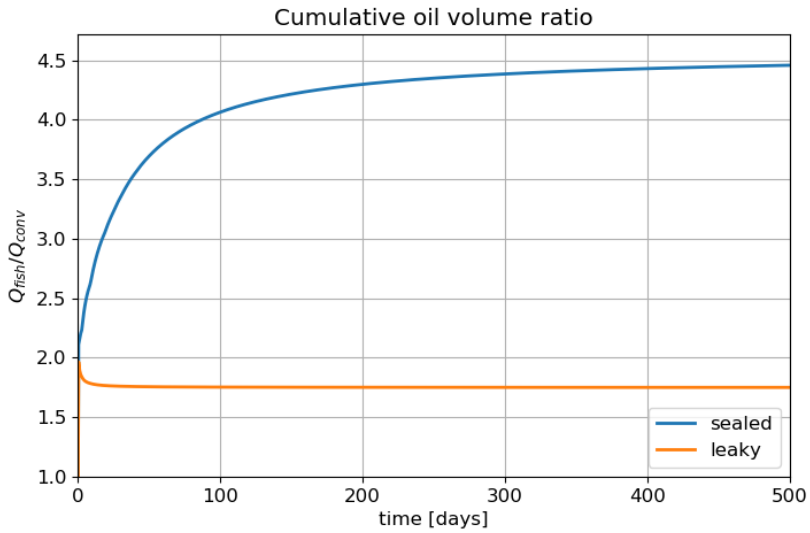

Figure 6-16: Cumulative fishbone benefit in a leaky and in a sealed oil reservoir.

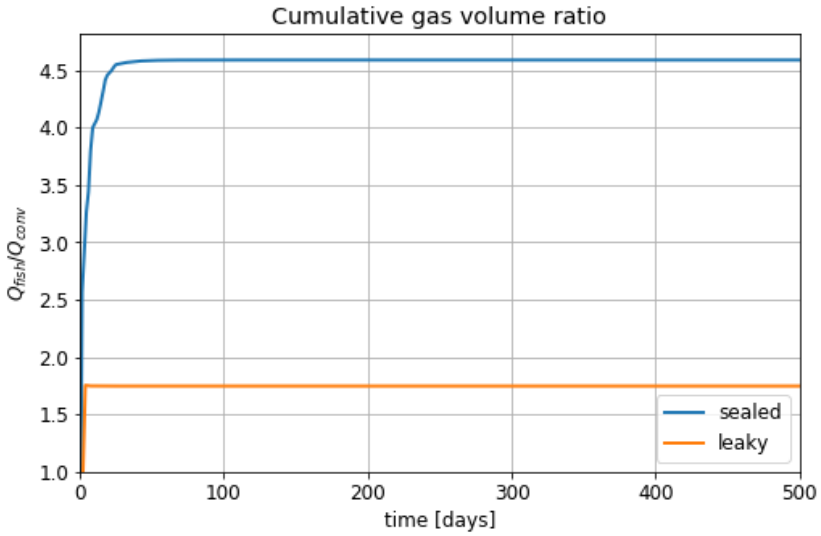

Figure 6-17: Cumulative fishbone benefit in a leaky and in a sealed gas reservoir.

6.3 Depletion for primary recovery

Different results can be obtained with respect to section 6.2.1 if no Dirichlet's boundary conditions are assigned. Instead, a Neumann's condition is set to the reservoir borders. The formation will be depleted (meaning that the reservoir pressure tends to well pressure) and steady state flow will not be reached. This situation represents the primary hydrocarbon recovery resulting only from fluid expansions (Dake 1978) which is significantly influenced by fluid and rock compressibility. The ultimate recovery factor can be expressed as:

- for an undersaturated oil:

$$URF = 1 - \frac{B_{o,1}}{B_{o,2}}(1 + c_r \Delta p) \quad (6\text{-}1)$$

- for a dry gas:

$$URF = 1 - \frac{B_{g,1}}{B_{g,2}}(1 + c_r \Delta p) \quad (6\text{-}2)$$

The ultimate primary recovery will be drastically different. In particular, the recovery factor due to oil expansion and rock compaction is just 0.4%, while for the gas case is 17% (Dake 1978). This values are extremely low, however during reservoir production other supplementary recoveries are usually exploited (as gas cap expansion, aquifer support, fluid injections…).

Figure 6-18 shows the different cumulative productions of a fishbone sub and of a conventional well. Only an oil case with reservoir permeability of 1 mD is shown. On the left hand side, steady state flow is considered (as is 6.2.1) leading to straight (diverging) cumulative productions. On the right hand side, without the Dirichlet's boundary, a limited amount of hydrocarbon can be recovered, thus the important parameter is production anticipation. While for steady state flow, both a production anticipation and an increased final recovery is obtained, the same is not always valid during primary recovery. Also a conventional well can deplete all the block if a sufficient long time is considered. However, it should be noticed that the concession for a field is usually assigned to the operator for a limited amount of years. Therefore, it can happen that a company has to leave the field since the contract expires, even if the reservoir is not fully depleted (up to the maximum primary recovery factor). Thus, production anticipation is always desired.

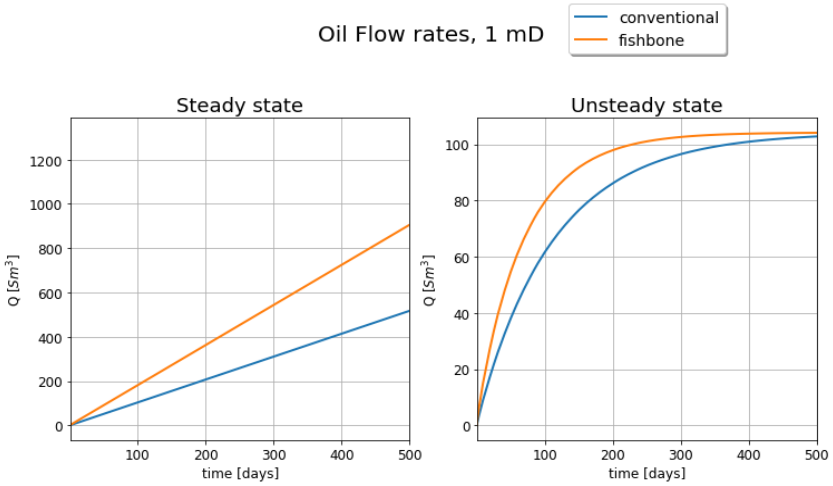

Figure 6-18: Steady state and non-steady state cumulative productions.

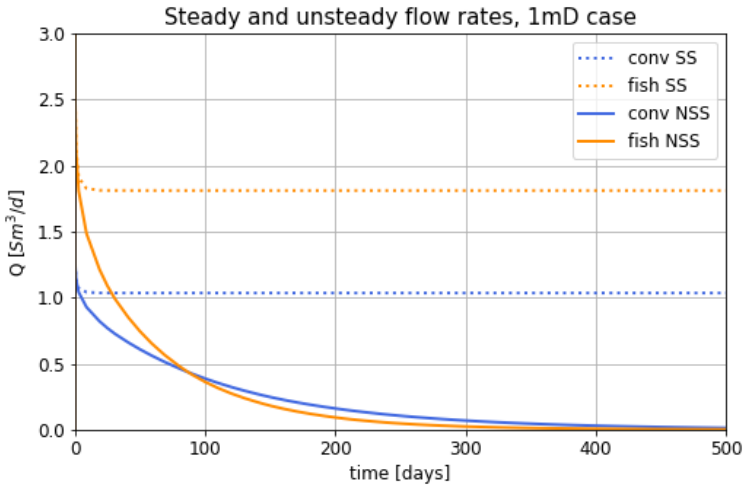

Figure 6-19: Steady state and non-steady state production rates.

The reservoir primary recovery is simulated for different rock permeability. Figure 6-20 and Figure 6-21 show respectively the cumulative productions during the first 500 days for an oil and a dry gas case:

- For high permeability (10 mD and 100 mD) both fishbone sub and conventional well fully deplete the block in few days. The needle effect on production anticipation is extremely low.
- For low permeability cases (0.01 mD, 0.1 mD) fishbone sub anticipates the production but it also has a significantly higher final recovery (e.g. for 0.01 mD oil and gas cases, the final production after 500 days is almost doubled with respect to a conventional well).
- With a reservoir permeability of 1 mD, both the completions reach the ultimate recovery. However, the fishbone sub leads to an anticipation of the final production of almost 200 days.
- The production anticipation is more significant for high-viscosity fluid as oil with respect to dry gas.

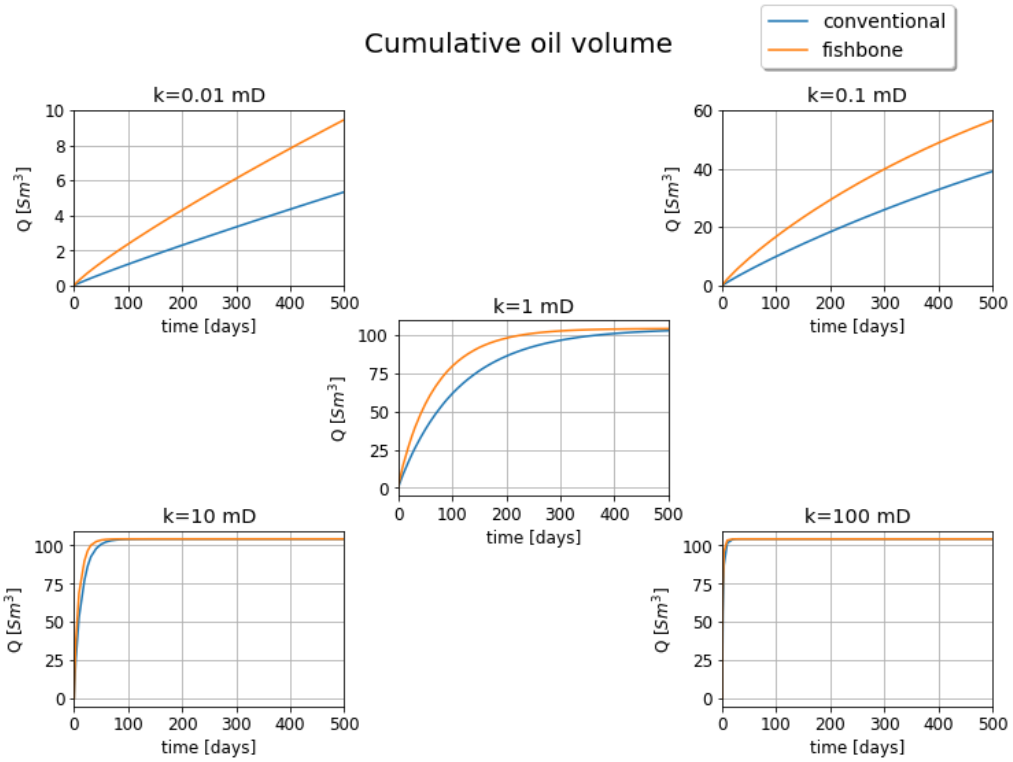

Figure 6-20: Cumulative oil productions for a fishbone sub and a conventional well. The reservoir permeability is varied from 0.01 mD to 100 mD. Note that the y-axis is not the same for all the cases.

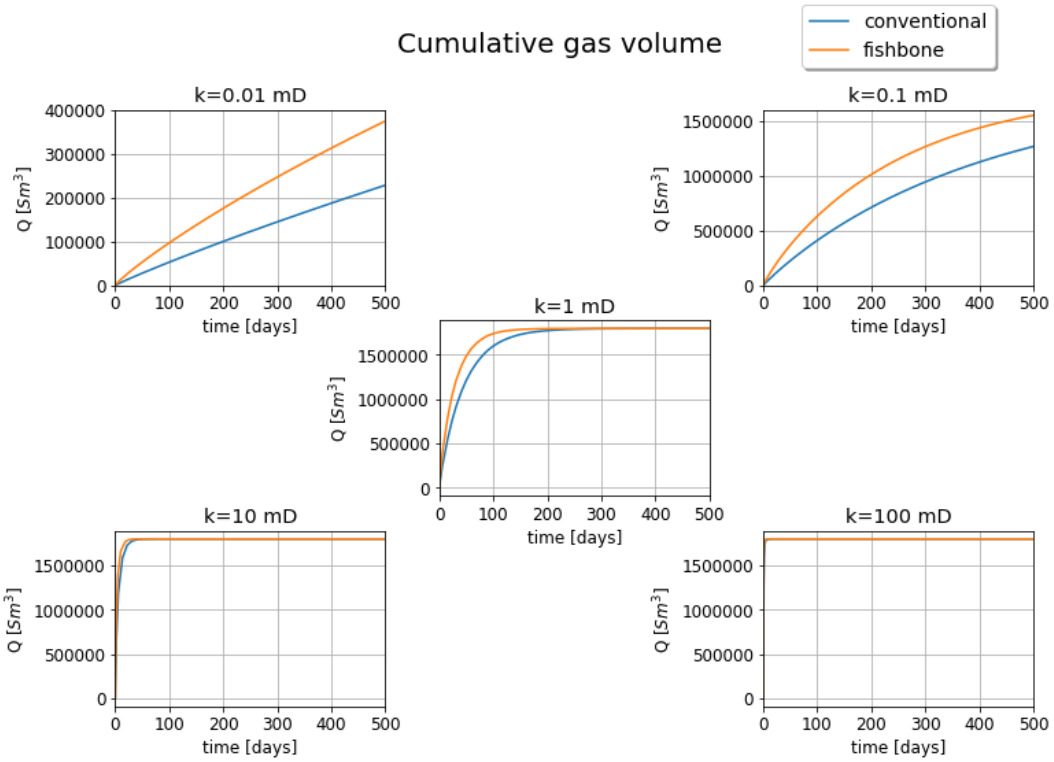

Figure 6-21: Cumulative gas productions for a fishbone sub and a conventional well. The reservoir is filled with oil and permeability is varied from 0.01 mD to 100 mD. Note that the y-axis is not the same for all the cases.

Table 6-3 summarizes the benefit of the fishbone sub on cumulative production after 500 days. Only low permeability cases are shown (a 0.001 mD case is added). In a 0.001 mD formation, the cumulative production is doubled after 500 days, showing how fishbone technology has high performances in unconventional resources.

Table 6-3: Cumulative fishbone benefit after 500 days of production through primary recovery in low permeability formations.

k [mD]	Oil	Gas
0.1	1.44	1.22
0.01	1.77	1.64
0.001	2.04	1.91

6.4 Semi steady state flow

Semi steady state flow, as described in 2.3, takes place when the well produces at a constant rate decreasing its bottom hole pressure and a Neumann's condition is assigned on reservoir boundary.

A production well can be controlled in term of bottom hole pressure or produced flow rate. In chapters 6.2 and 6.3, the bottom hole pressure is kept constant, however it is interesting to see what happens when a fishbone sub and a conventional well are both producing at a constant rate (e.g. 1 Sm^3/d) of oil. The reservoir permeability is fixed at 1 mD and Neumann's conditions are set on the boundary.

Figure 6-22 shows the declining well pressure in order to sustain a constant production of 1 Sm^3/d. It should be noticed how the minimum bottom hole pressure allowable is set to 100 bar. This value derives approximately from the condition that must be respected in order for the fluid to reach surface in absence of artificial lifting (see 2.3). From Figure 6-22 it can be notice how the conventional well pressure is much lower (20 bar) than the fishbone pressure to sustain the same fixed flow rate. Below the minimum bottom hole pressure the well is usually closed or artificial lifting has to be done. Therefore, the conventional well stops to produce at a fixed rates several days before the fishbone sub (about 50 days). However, from Figure 6-23 it can be seen how the software allows the two wells to produce also when their pressure is 100 bar. In this case, the completions are producing at a constant bottom hole pressure (100 bar) with a decreasing rate, where the fishbone sub produces more than the conventional well.

Well pressure is crucial not only for guarantee flow till the surface. In fact, at higher drawdowns ($p_{res} - p_{well}$) more problems arise in the reservoir as sand production or water/gas coning.

Moreover, once in the reservoir the pressure goes below the oil bubble pressure, gas liberates, reducing the liquid hydrocarbons (more valuable) production.

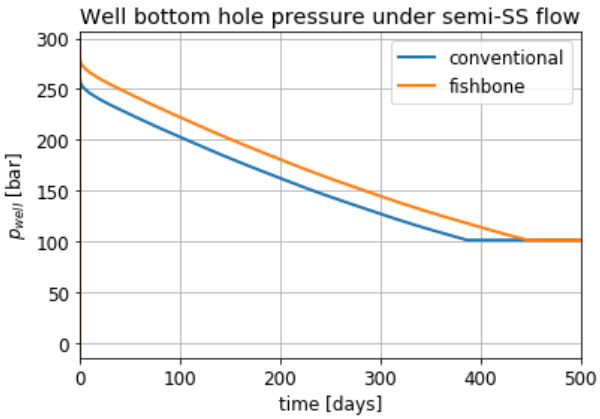

Figure 6-22: Well bottom hole pressure versus time for a fishbone sub and a conventional well producing at constant rate. The minimum bottom hole pressure is set to 100 bar. During semi-steady state, the conventional well produces with a pressure 20 bar lower that the fishbone sub.

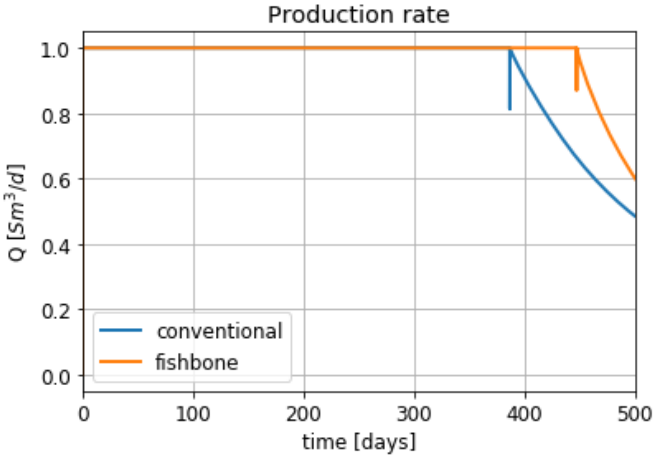

Figure 6-23: Oil production rate pressure versus time for a fishbone sub and a conventional well. The two completions produce at constant rate until the well pressure is above 100 bar, then the well control is changed. The strange behavior between constant production and declining production comes from the switch of the well constraint.

During semi steady state flow, the productivity index can be computed as:

$$PI_{SSS} = \frac{Q}{p_{res} - p_{well}} \left[\frac{Sm^3}{d\ bar}\right] \tag{6-3}$$

Where p_{res} is the average reservoir pressure. According to eq. (6-3) the fishbone sub gives a semi steady state PI of $0.034 \left[\frac{Sm^3}{d\ bar}\right]$, while the conventional well only of $0.020 \left[\frac{Sm^3}{d\ bar}\right]$.

7 The Embedded Discrete Fracture Model

Needles can be modelled as discrete fractures adopting the Embedded Discrete Fracture Model. Thus, they are seen as equivalent high-permeable channels departing from the main wellbore. As done for long fractures in the classic EDFM developed by (Cavalcante, et al. 2015), needles are explicitly modelled as auxiliary grid blocks added to the main grid (see 5.1.2). At each of the new cells, properties like conductivity and pore volume (which is almost negligible) are assigned. The flow from fracture to fracture (or better, from auxiliary cell to auxiliary cell) and the one from matrix to fracture (or from matrix to auxiliary cell) are described by two transmissibility terms.

The methodology implemented is discussed in 7.1. In section 7.2 a grid sensitivity analysis is done in order to find a suitable grid block dimension able to model the completions with accuracy. Then, sensitivity through the initial transient period and in steady state conditions are done on fluid types and reservoir permeability (7.3.1), on boundary condition locations (7.3.2) and for a layered reservoir (7.3.3). Section 7.4 reports the cumulative fishbone benefit during depletion for primary recovery, while section 7.5 discusses semi steady state flow.

7.1 The customization of the Petrel plug-in

The EDFM methodology is employed in Eni using a work-flow implemented in Petrel geomodelling package throughout dedicated plug-ins, named “EDFM Builder” and “EDFM Flowsim”. Basically, these plug-ins take as input data the structure of a CPG grid, including permeability, and the geometry of a set of fractures approximated as very thin parallelepipeds (with thickness corresponding to fracture aperture and length/width to fracture length/width). This information is included in a standard file format used in the oil industry for fracture sets definition. The idea behind the implementation of fishbone completions in the EDFM framework is based on the assimilation of needles to fractures.

In particular, a needle with length *L* and radius r, see Figure 7-1, can be substituted with fracture characterized by a length *L*, aperture *a* and width *w*.

The cross-section area (A_{cs}) open to flow between two consecutive fracture segments should be equivalent to the cross-sectional area of a needle:

$$A_{cs} = \pi r_{fb}^2 \tag{7-1}$$

While the area open to flow from matrix to fracture (A_{mf}), should have the same value of the needle lateral surface:

$$A_{mf} = 2\pi r_{fb} L \tag{7-2}$$

A_{cs} and A_{mf} can be expressed also as functions of the fracture geometry:

$$A_{cs} = \text{width} \cdot \text{aperture} = w \cdot a \tag{7-3}$$

$$A_{mf} = \text{width} \cdot \text{lenght} = w \cdot L \tag{7-4}$$

Since these two areas must be equal to the ones of a needle, the fracture parameters used as input in a Python code (to generate the fracture file) can be expressed as functions of the fishbone radius. Considering the length of two needles equals to the fracture length:

$$A_{mf} = 2\pi r_{fb} L = wL \rightarrow w = 2\pi r_{fb} \tag{7-5}$$

$$A_{cs} = \pi r_{fb}^2 = wa \rightarrow a = \frac{r_{fb}}{2} \tag{7-6}$$

With a Python code two numerical fractures are created, a vertical and a horizontal one. These depart normally from the main horizontal well and are the substitutes of the four needles since they are characterized by an equivalent geometry in term of height and fracture aperture, as shown in Figure 7-1:

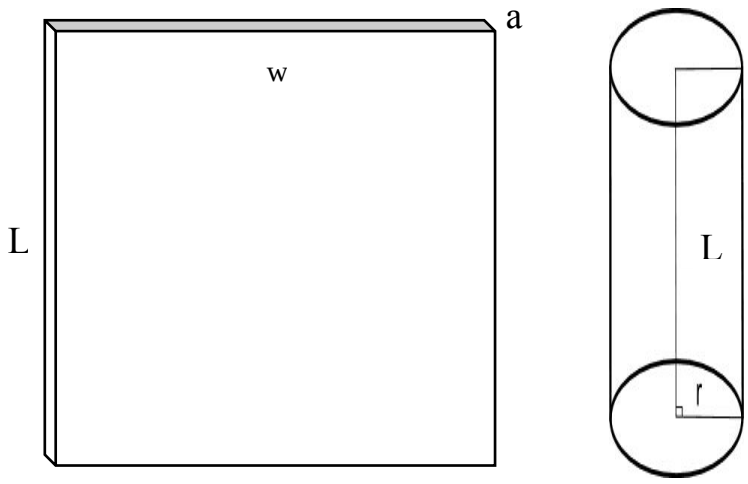

Figure 7-1: On the left side the geometrical parameters that fully define a fracture, on the right the ones for the needles.

Fracture are then defined by means of two transmissibility terms, which describe the flow towards and along them:

- the flow from fracture to fracture should represent the stream in the fishbone annulus, thus the transmissibility is calculated by the software as:

$$T_{ff} = \frac{A_{cs} k_{fb}}{< d >_{ff}} \tag{7-7}$$

where k_{fb} is the fracture permeability and $< d >_{ff}$ is the distance between the centers of two adjacent fracture sections. Since the fracture is a high conductivity channel, its permeability is extremely high (10^7 mD). Therefore, it approximates a short pipe where pressure drops are negligible.

- the flow from the matrix cell towards a fracture segment, which has to be equivalent to the one from matrix towards laterals is described by the following term:

$$T_{mf} = \frac{A_{mf} k_m}{< d >_{mf}} \tag{7-8}$$

where k_m is the average permeability of the matrix and $< d >_{mf}$ is the average distance between the center of a matrix block and a fracture segment.

The matrix to fracture transmissibility, according to (Cavalcante, et al. 2015), should be equivalent to the connection factor computed with the Peaceman's equation, which for a fracture oriented in the vertical direction is:

$$T_{cf} = \frac{2\pi \left(k_{x,m} k_{y,m}\right)^{0.5} \Delta z_{fb}}{\ln\left(\frac{r_o}{r_{fb}}\right)} \tag{7-9}$$

And for one in the horizontal direction:

$$T_{cf} = \frac{2\pi \left(k_{z,m} k_{y,m}\right)^{0.5} \Delta x_{fb}}{\ln\left(\frac{r_o}{r_{fb}}\right)} \tag{7-10}$$

Where $k_{z,m}$, $k_{y,m}$, $k_{y,m}$ are the matrix permeability in X,Y,Z directions, r_o is the Peaceman's radius and Δz_{fb} and Δx_{fb} are the penetration lengths in the vertical and horizontal directions of a lateral.

Matrix to fracture transmissibility (T_{mf}) generated by the Petrel plug-in (that employs the standard EDFM) underestimates the correct values derived from Peaceman's equation (T_{cf}), since it is dealing with an equivalent fracture instead of a well (needle). This difference can be highlighted with a ratio:

$$\frac{T_{cf}}{T_{mf}} = \left(\frac{k_{z,m}}{k_{x,m}}\right)^{0.5} \frac{< d >_{mf}}{r_{fb} \ln\left(\frac{r_o}{r_w}\right)} \tag{7-11}$$

Since $< d >_{mf}$ in a hexahedral grid where needles are centered inside a block with $\Delta x = \Delta y$, is in the order of $\frac{\Delta x}{4}$, the ratio in (7-11) depends on grid resolution and it results to be much higher than one. Hence, an underestimation is made if T_{mf} is set to be the transmissibility between matrix and fracture in the simulation.

To solve the problem, this parameter is substituted with one based on Peaceman's model. Thus, a simulation on the same model but with two wells having the same geometry and bottom hole pressure of fishbone laterals are run. From the output of this simulation, the Peaceman's connections between matrix and wells are picked and substituted to the wrong values of matrix to fracture transmissibility. Finally, with a new set of corrected NNCs, the real simulations with main well and needles modelled as modified fractures are run.

Following EDFM literature (Miao, et al. 2018), the fishbone implementation, differently from the methodology discussed in chapter 6, is not intended for very high resolution grids. Typically, people use EDFM for computational efficiency with respect to high resolution grid implemented ad hoc around fracture geometry. The same logic can be used for the purpose of this work. In the next section, however, a sensitivity analysis on grid resolution of the results achieved using EDFM is presented with the aim to confirm what is generally accepted in the literature for fracture modelling.

7.2 Sensitivity analysis on grid resolution

The sensitivity analysis is performed using five grids, with increasing resolution. In particular, the focus is on lateral resolution, since vertical resolution is constrained by well data resolution, which can be metric, while lateral spacing is constrained only by well distances in most of the cases. Then, in the sensitivity analysis, cell thickness is set constant to one meter, which is a typical spacing in many reservoir studies, while lateral grid resolution is sequentially increased:15x15, 45x45, 75x75, 135x135 and 255x255 cells. These numbers are set to be odd on purpose so that the well completions can be placed at the centre of the model. The completions and the reservoir geometry considered in this chapter are the same as the ones used in chapter 6 (see Figure 6-3 and Figure 6-4). Table 7-1 reports the relation between cell spacing and cell numbers in X and Y.

Table 7-1: Number of cells in X- and Y- directions with the corresponding block sizes used in the grid sensitivity.

Cell number	X and Y dimension [m]
15x15	20
45x45	6.67
75x75	4
135x135	2.22
255x255	1.18

Figure 7-2 illustrates how the flow rates converge as the grids are refined. The difference between a coarse grid (i.e. the one called “15x15”) and fine grid (like “135x135” and “255x255”) is more evident for a gas case respect to the oil. This can be justified by the fact that the well index is based on a linear inflow performance. A linear correlation is suitable for liquids, while for gas is a good approximation only if the pressure gradient across a cell is small. Non linearity in pressure profiles characterizes the gas case, therefore with big cells the linear approximation error is more evident.

The fishbone benefits at different grid dimensions are reported in Figure 7-3 for an oil case and in Figure 7-4 for a gas. Increasing main grid refinement, as for the rates, also in this case a convergence can be noted (see Figure 7-5). In particular, the grids 75x75, 135x135 and 255x255 give practically the same results in terms of fishbone benefit. This means that the model with 75x75 cells in the X and Y direction (and 100 cells along Z) is sufficiently accurate to model fishbone laterals. More refined and time-consuming grids are not necessary. Therefore, the grid “75x75” is chosen for the upcoming sensitivities along this chapter. This grid is affected by an error of 0.5% with respect to more refined grids, that from an engineering point of view can be accepted.

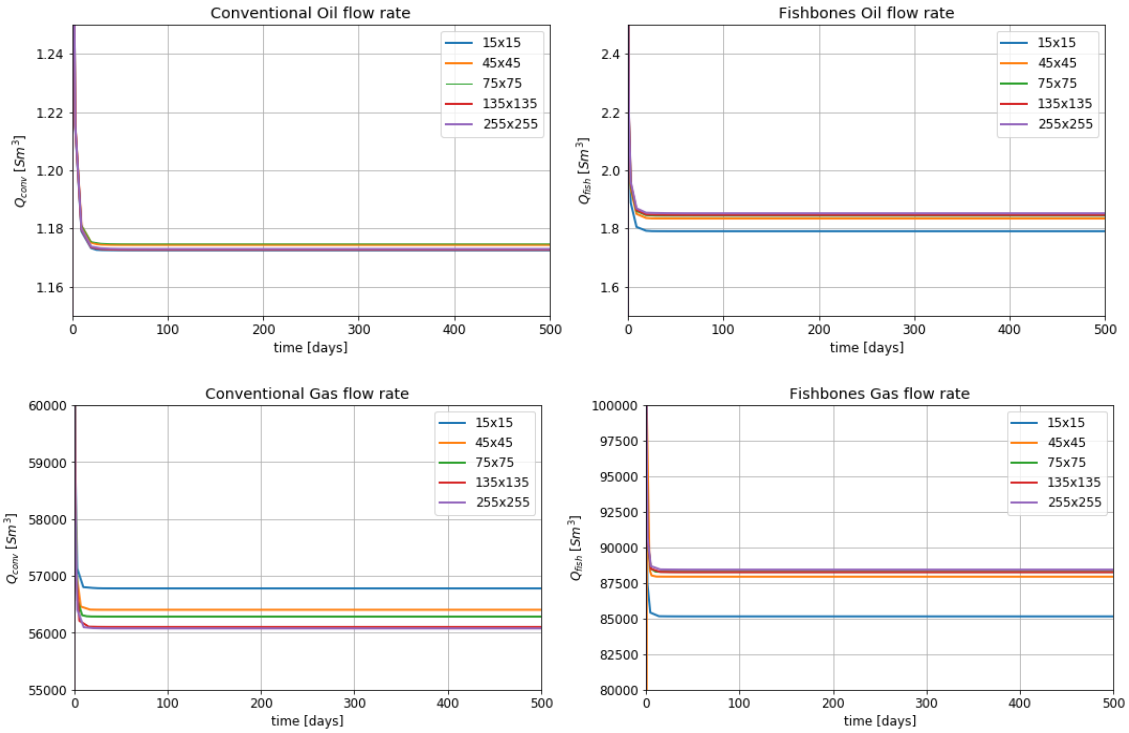

Figure 7-2: Flow rate convergence for a conventional well and a fishbone sub increasing the number of blocks. Both an oil case and a dry gas are shown.

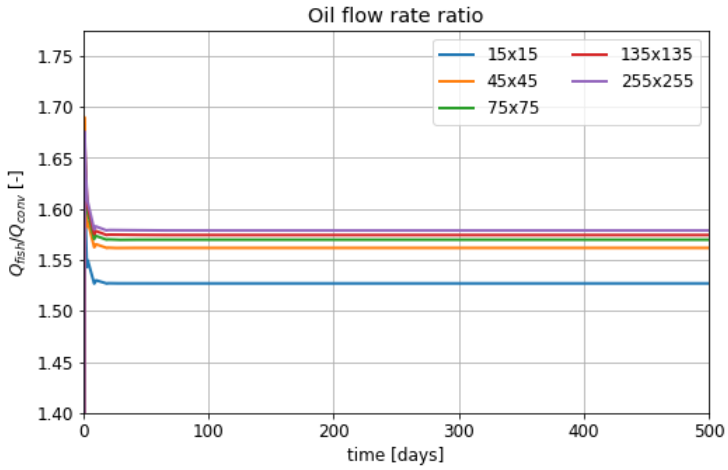

Figure 7-3: Fishbone benefit for an oil case. Increasing the cell number (or equivalently the main grid refinement), the results converge towards the same value.

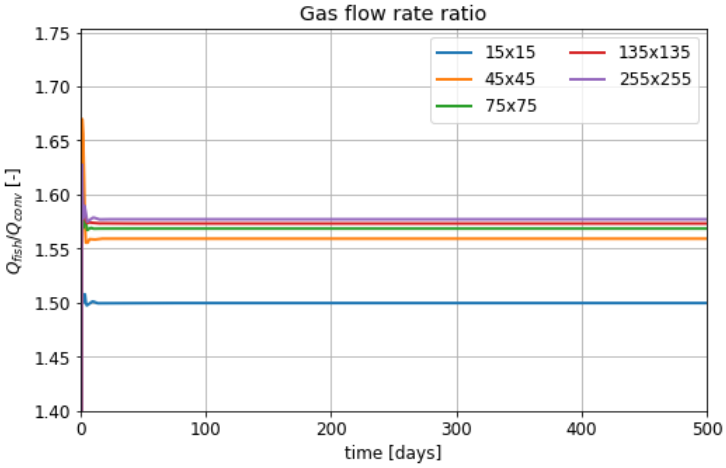

Figure 7-4: Fishbone benefit for a gas case. Increasing the cell number, the results converge towards the same value.

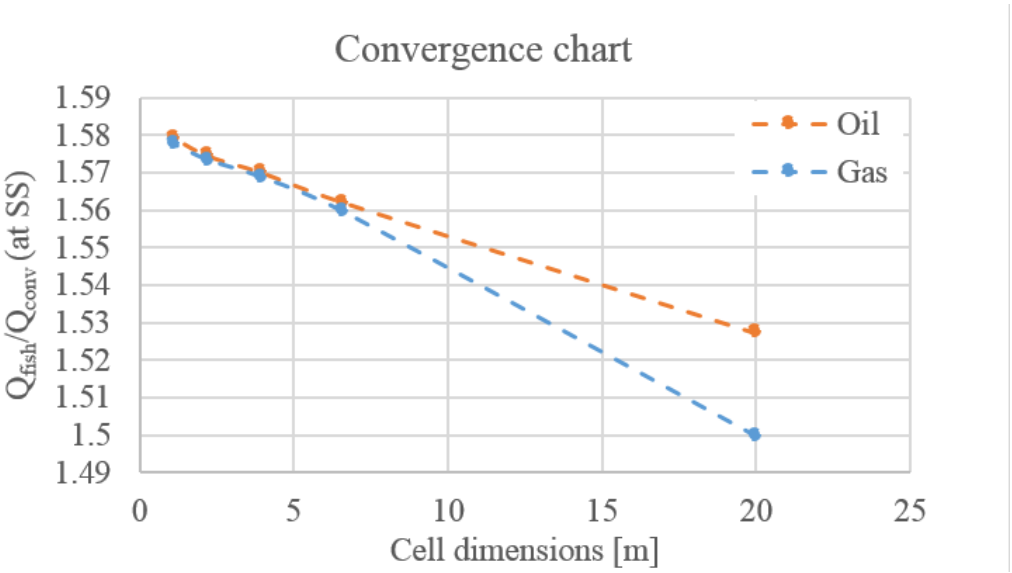

Figure 7-5: Convergence chart of steady state fishbone benefit reducing horizontal cell dimensions. Both oil and gas cases are shown.

7.3 Toward steady state productivity index

As in chapter 6.2, steady state conditions are achieved by using proper Dirichlet's boundary conditions. In particular, in reservoir simulation these are set using very large pore volume at the reservoir borders.

In this section, sensitivities on fluid types and permeability are analyzed; boundary condition influence is discussed; then, fishbone benefits are evaluated in case of sealed reservoir.

7.3.1 Single phase fluid, sensitivity on permeability

Sensitivity on reservoir permeability is done here for an oil and dry gas case. The Dirichlet's boundary conditions are assigned as in chapter 6.2.1 (see Figure 6-5).

In Figure 7-6 and Figure 7-8 the production rates for an oil and a dry gas are shown. It should be observed that:

- The initial transient period lasts more for low permeability formations and viscous fluids.
- During steady state, the flow rate is proportional to permeability and fluid viscosity.

The fishbone benefit $\left(\frac{Q_{fish}}{Q_{conv}}\right)$ is shown in Figure 7-7 for the oil and in Figure 7-9 for the gas:

- During the transient period, the fishbone production is significantly greater than the conventional well. The graphical comparison between an oil and dry gas case is shown in Figure 7-10, while Table 7-2 reports the cumulative fishbone benefit at the end of the transient for low permeability cases. The production increment and anticipation rises if viscosity increases and permeability decreases.
- During steady state the fishbone benefit converges to the same value, no matter the fluid or rock type. Here, the fishbone completion produces about 1.57 times the rate of a conventional well.

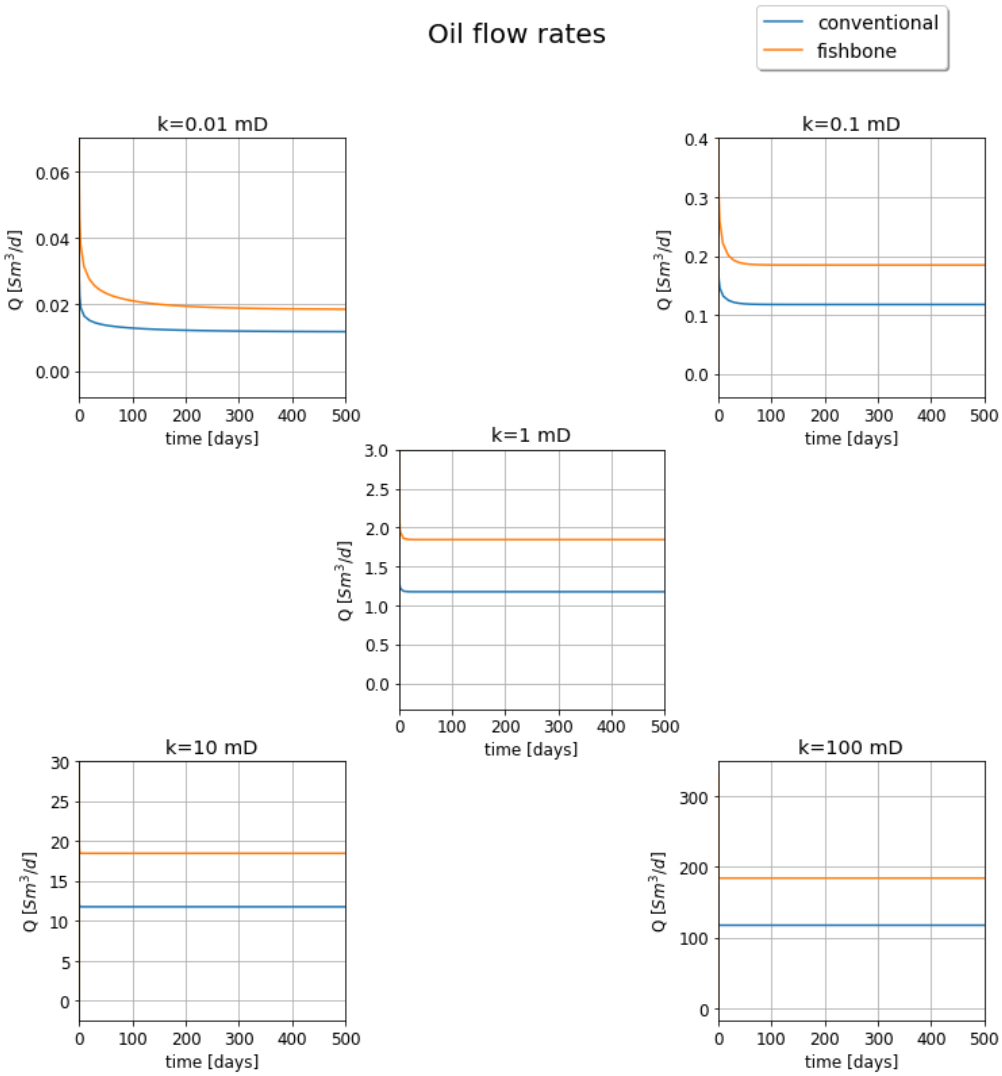

Figure 7-6: Oil flow rates for a fishbone completion (orange) and a conventional well (blue). The reservoir permeability is varied from 0.01 mD to 100 mD.

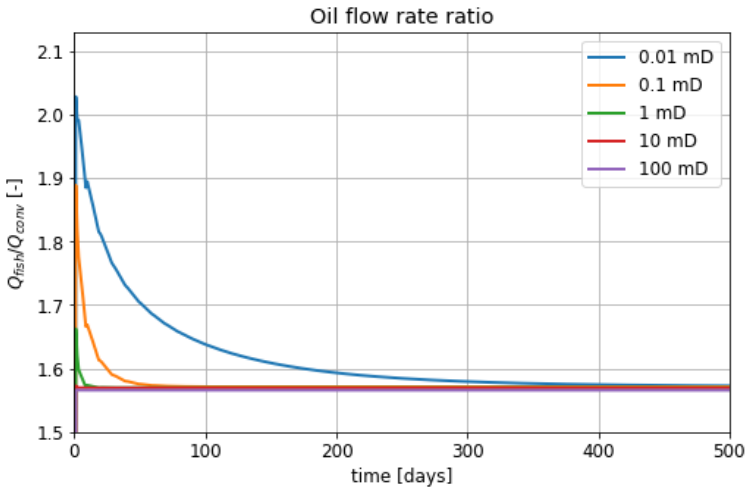

Figure 7-7: Fishbone benefit in an oil reservoir with permeability varied from 0.01 mD to 100 mD.

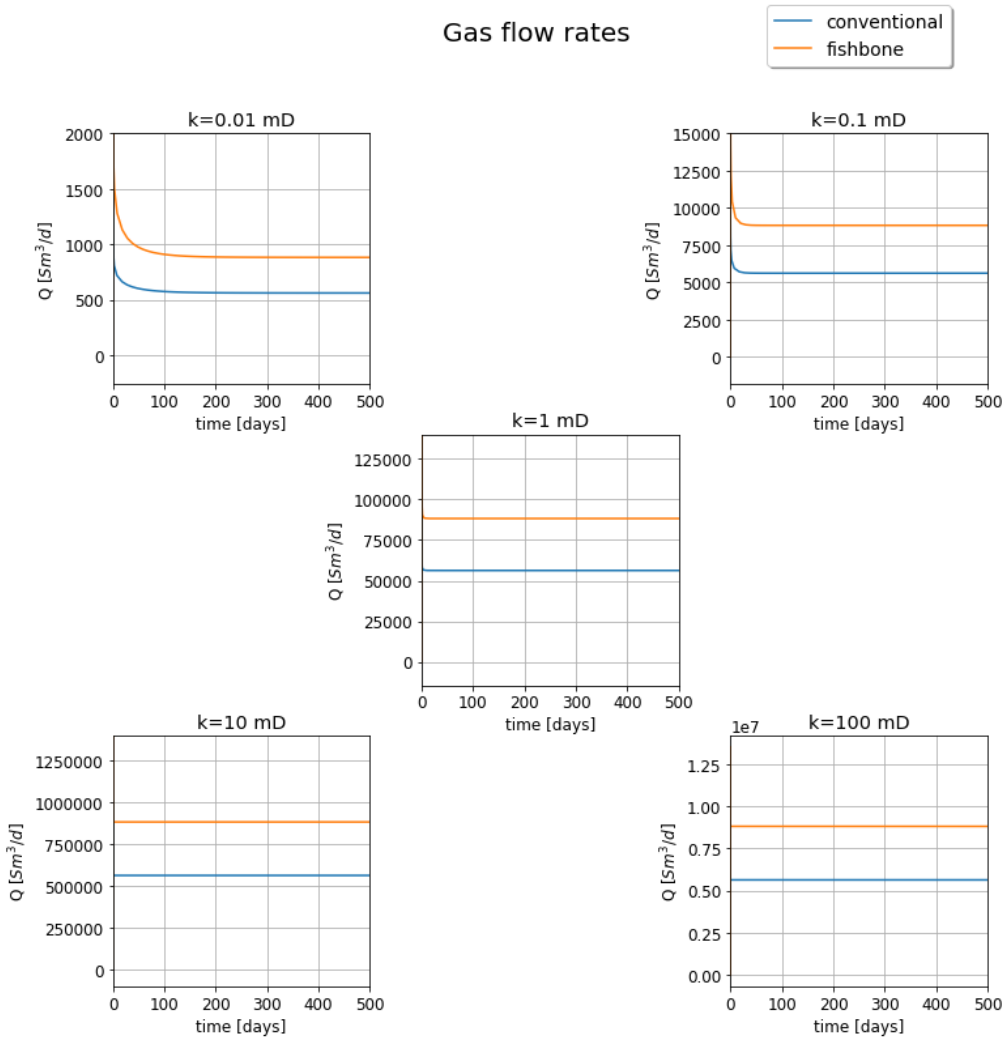

Figure 7-8: Gas flow rates for a fishbone completion (orange) and a conventional well (blue). The reservoir permeability is varied from 0.01 mD to 100 mD.

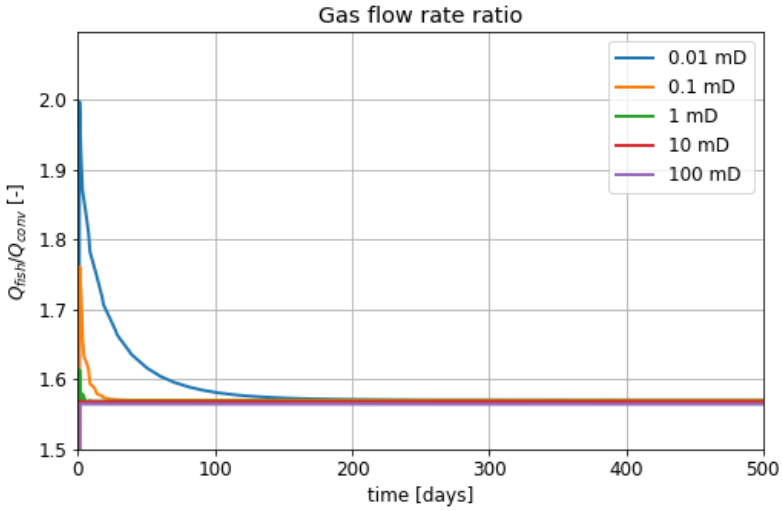

Figure 7-9: Fishbone benefit in a gas reservoir with permeability varied from 0.01 mD to 100 mD

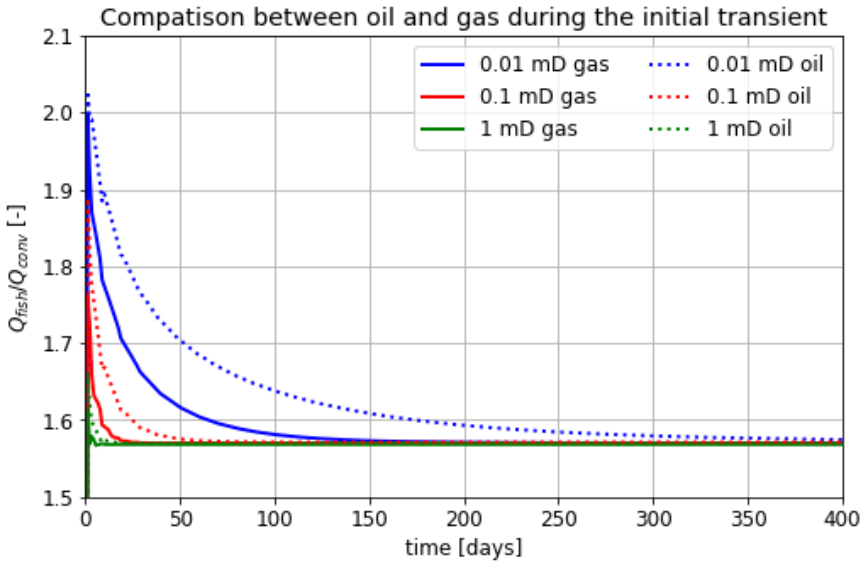

Figure 7-10: Fishbone benefit for oil and gas cases during the initial transient period (only low permeability formations are shown).

Table 7-2: Cumulative fishbone benefit at the end of the initial transient period.

k [mD]	Oil	Gas
1	1.594	1.584
0.1	1.611	1.603
0.01	1.624	1.612

7.3.2 Sensitivity on boundary conditions

Dirichlet's boundary distance from the well affects the production of the two completions and therefore the relative benefit. Results achieved in the previous paragraph for an oil case are here compared with the ones obtained with a closer boundary (see Figure 6-12 for clarification).

With a closer boundary, vertical needles result to be near zones at high pressure, leading to a higher productivity of the fishbone sub. Figure 7-11 shows that a closer Dirichlet's boundary significantly improves the fishbone benefit, resulting in a benefit higher than 75% during steady state. For a remote boundary condition (as in Figure 6-14 and in chapter 7.3.1), the benefit is lower (just 57% of increase). Moreover, the initial transient period, where the production increment is more significant, changes its length once the Dirichlet's condition is placed in a different position.

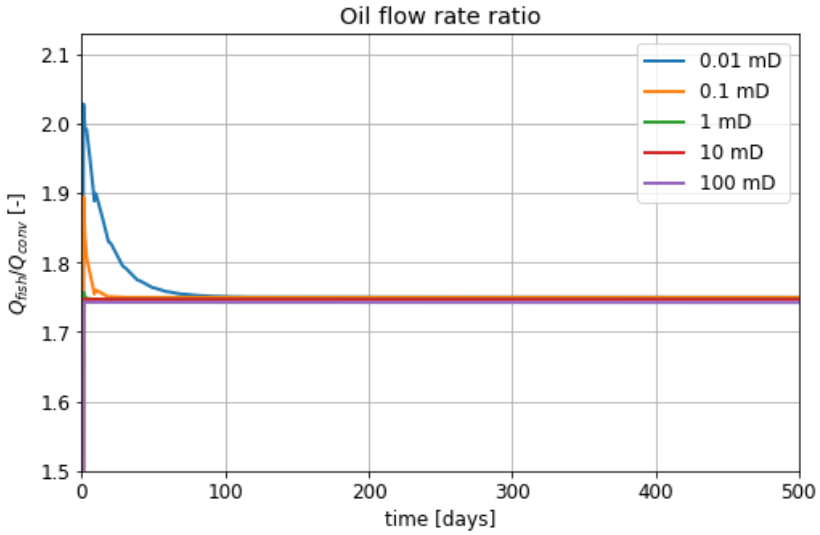

Figure 7-11: Fishbone benefit in an oil reservoir with close boundary.

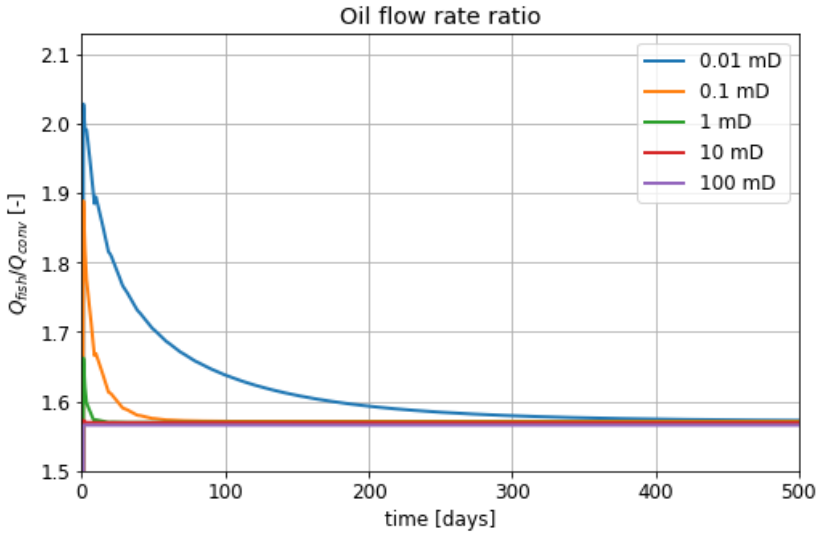

Figure 7-12: Fishbone benefit in an oil reservoir with distant boundary.

7.3.3 Fishbone in a layered reservoir

A layered reservoir system is here considered. It should be noticed that due to different grid dimensions, the impermeable barriers used in this section are different respect to the ones used in 6.2.3. While in the LGR case, the small cells allowed to simulate a thin barrier of 0.2 m, here its thickness is 1 m according to vertical cell dimension. Therefore, the effect of vertical needles is slightly reduced since a smaller part of them is in contact with the top and bottom layers. The horizontal well can drain only the central one, while the vertical needles allows the entire reservoir production (see Figure 7-15).

Figure 7-13 and Figure 7-14 show the cumulative fishbone benefits respectively for an oil and dry gas case. In the leaky reservoir, both conventional well and fishbone sub reach steady state, therefore the cumulative production increment is constant and equal to 1.57 both for oil and dry gas. For a sealed reservoir, since the simple horizontal well depletes only the central layer, it significantly produces less. On the contrary, the vertical needles drain also the top and bottom layers. After 500 days the oil production has not reached steady state, therefore the fishbone benefit keeps increasing. However, for both oil and dry gas, it is close to 3.7.

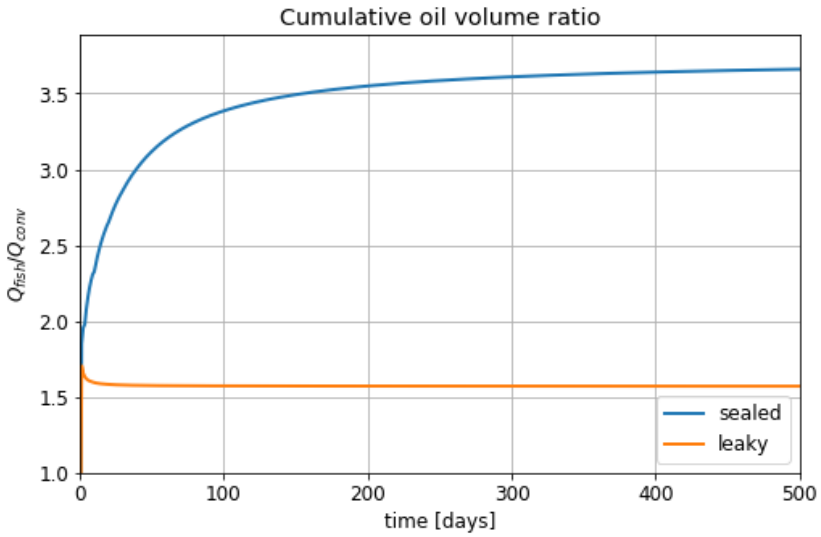

Figure 7-13: Cumulative fishbone benefit for a leaky and a sealed oil reservoir.

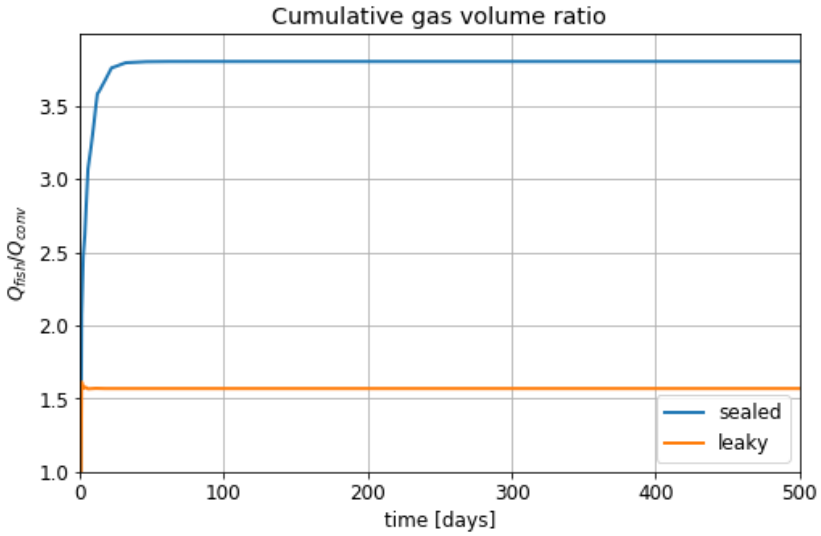

Figure 7-14: Cumulative fishbone benefit for a leaky and a sealed gas reservoir.

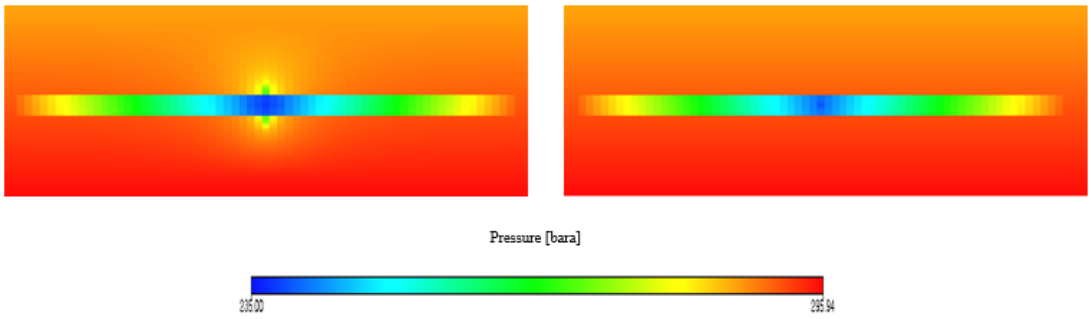

Figure 7-15: Comparison of a layered reservoir depleted by a fishbone sub (on the left) and by a conventional well (on the right). Vertical needles allow to contact and produce also the top and bottom layers.

7.4 Depletion for primary recovery

Depletion for primary recovery is driven only by fluid expansion and rock compaction. It is simulated with a Neumann's condition at the reservoir borders. The formation will be depleted and steady state flow will not be reached.

The reservoir primary recovery is analyzed for different rock permeability. Figure 7-16 and Figure 7-17 show respectively the cumulative productions during the first 500 days for an oil and a dry gas case:

- For high permeability (10 mD and 100 mD) both the completion reach the ultimate recovery. The needle effect on production anticipation is extremely low.
- For low permeability cases (0.001 mD, 0.01 mD and 0.1 mD) fishbone sub anticipates the production but it also has a significantly higher recovery after 500 days (see Table 7-3).
- For 1 mD, both the completions reach the ultimate recovery. However, the fishbone sub leads to an anticipation of the final production in the order of 200 days.

Table 7-3 shows how the cumulative fishbone benefit after 500 days is extremely high in unconventional resources.

Table 7-3: Cumulative fishbone benefit after 500 days of production through primary recovery in low permeability formations.

k [mD]	Oil	Gas
0.1	1.336	1.163
0.01	1.591	1.488
0.001	2.024	1.839

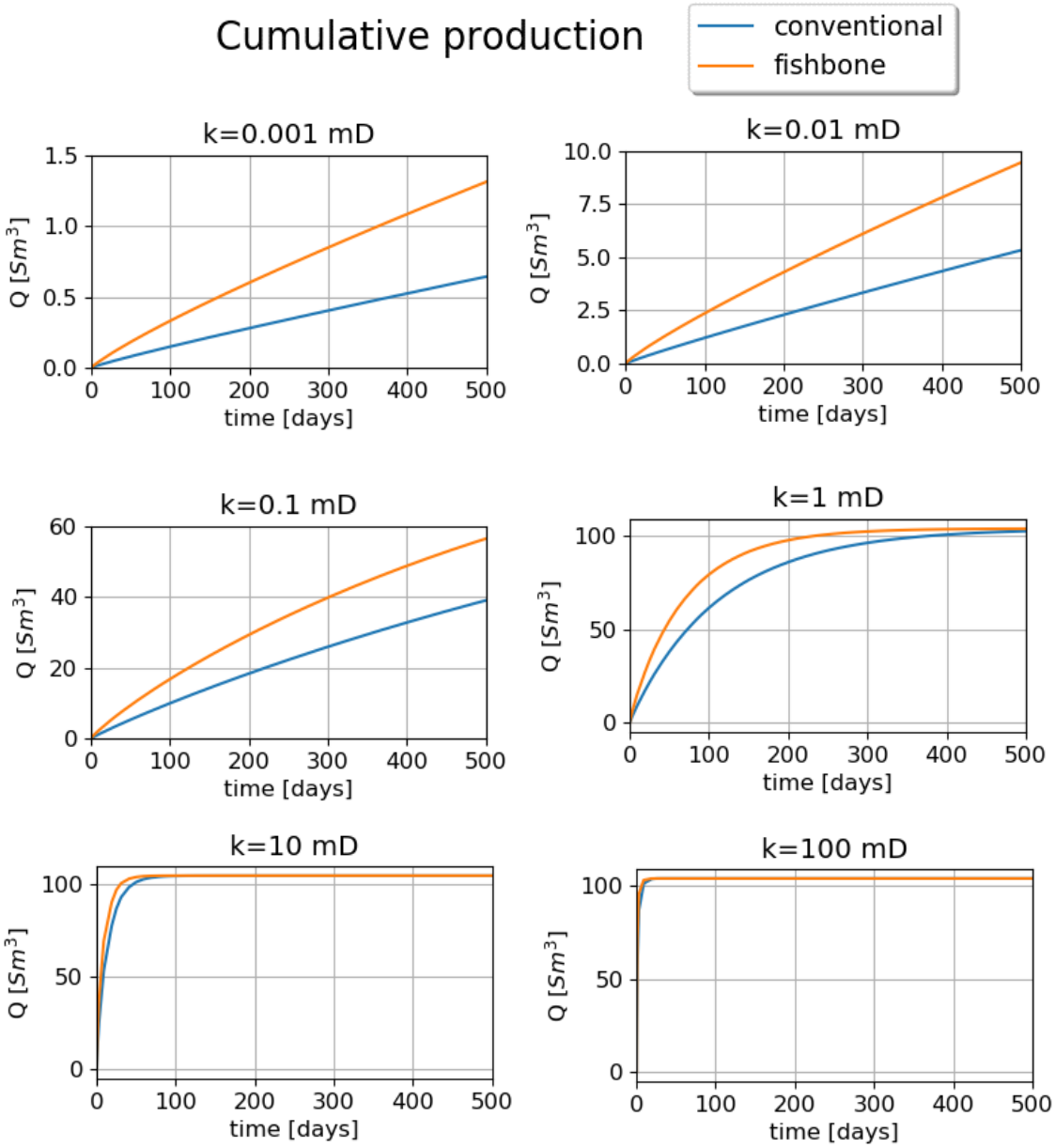

Figure 7-16: Cumulative oil productions for a fishbone sub and a conventional well section. The reservoir permeability is varied from 0.001 mD to 100 mD. Note that the y-axis is not the same for all the cases.

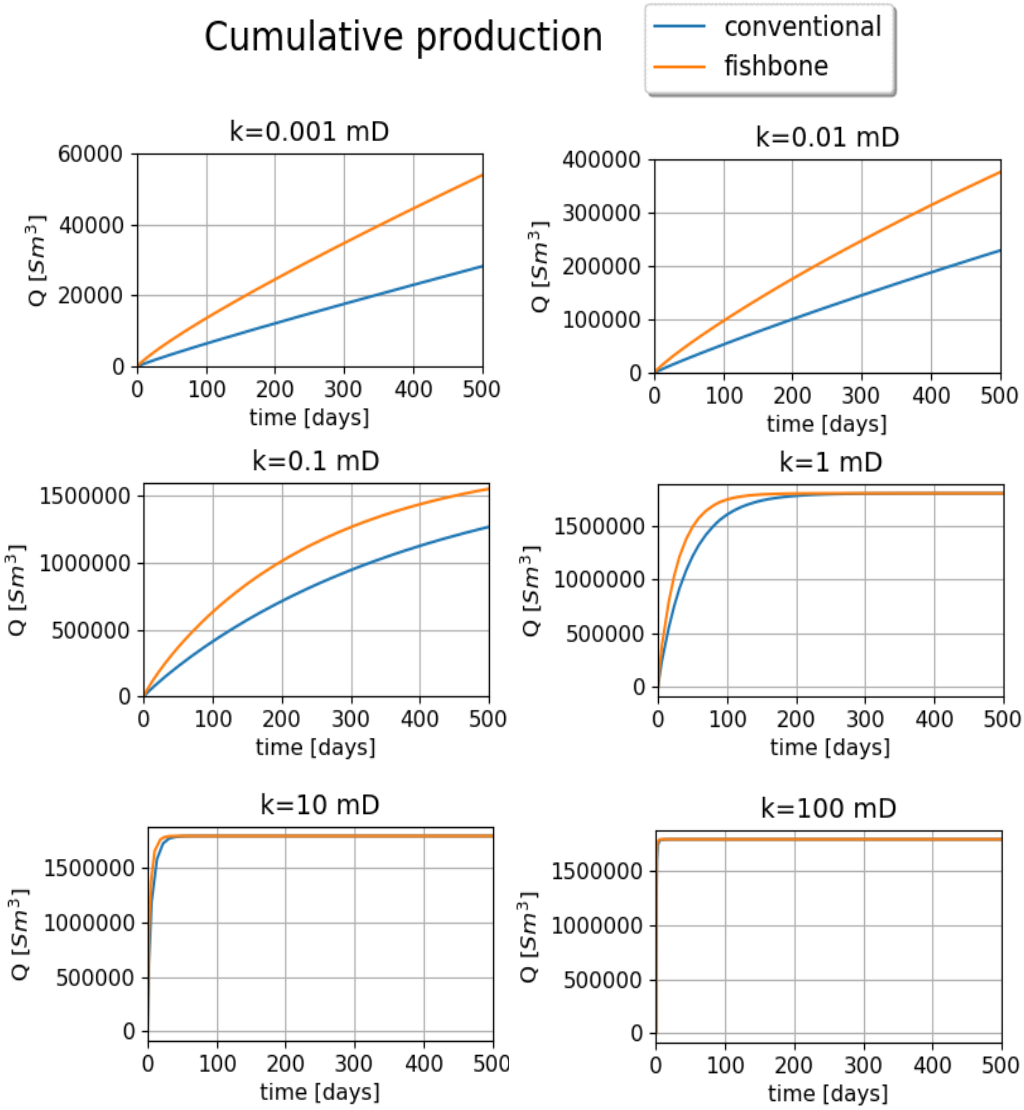

Figure 7-17: Cumulative gas productions for a fishbone sub and a conventional well section. The reservoir permeability is varied from 0.001 mD to 100 mD. Note that the y-axis is not the same for all the cases.

7.5 Semi steady state flow

Semi steady state flow takes place when the well produces at a constant rate decreasing its bottom hole pressure and a Neumann's condition is assigned on reservoir boundary.

Both the completions produce at a constant rate of 1 Sm^3/d of oil. The reservoir permeability is set to 1 mD.

Figure 7-18 shows the declining well pressure in order to sustain a constant production of 1 Sm^3/d. The conventional well produces the fixed flow rate with a bottom hole pressure lower than the

fishbone sub (about 15 bar). Below the minimum allowed bottom hole pressure the well is usually closed, thus the conventional well stops to produce at constant rate 50 days before the fishbone sub. However, Figure 7-19 show how the wells still produce when they reach 100 bar. Here, to keep the bottom hole pressure constant, the production rate decreases, with the fishbone sub producing more than the conventional well.

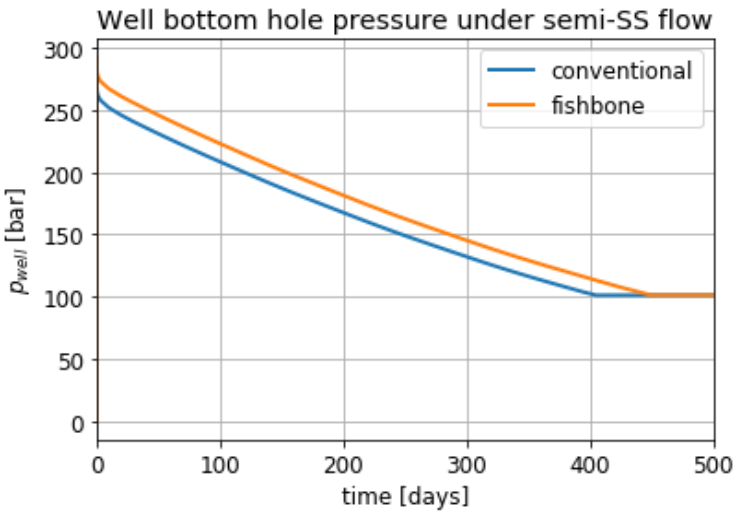

Figure 7-18: Well bottom hole pressure versus time for a fishbone sub and a conventional well producing at constant rate. The minimum bottom hole pressure is set to 100 bar. During semi-steady state, the conventional well produces with a pressure 15 bar lower that the fishbone sub.

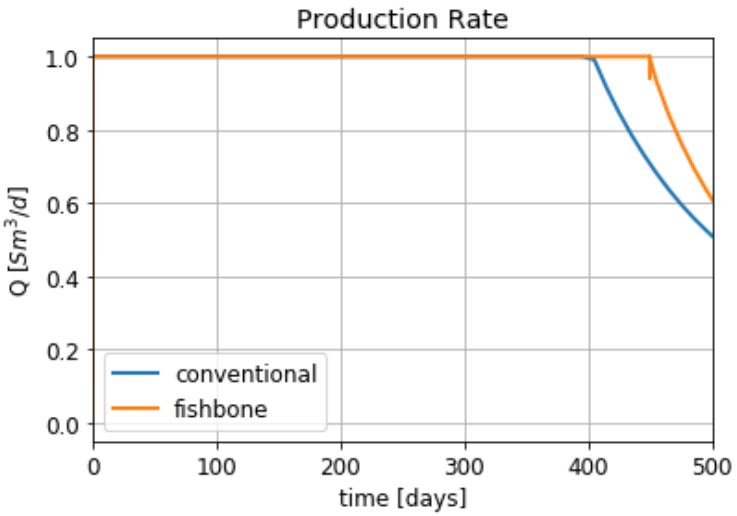

Figure 7-19: Oil production rate pressure versus time for a fishbone sub and a conventional well. The two completions produce at constant rate until the well pressure is above 100 bar, then the well control is changed

During semi steady state flow, the productivity index can be computed according to equation (6-3). The PI at various reservoir permeability are reported in Table 7-4. It can be noticed how the ratio between the PI of a fishbone sub and a conventional well is not influenced by permeability.

Table 7-4: Semi steady state productivity indexes at different reservoir permeability.

k [mD]	PI (Fishbone) [Sm3/d/bar]	PI (Conventional) [Sm3/d/bar]	RATIO
0.1	0.009	0.006	1.503
1	0.035	0.023	1.507
10	0.341	0.227	1.505

7.6 Discussion about the differences between High Resolution Grid (HRG) and EDFM results

Looking at chapter 6 and 7, a discrepancy can be seen between the results coming from the HRG approach and the EDFM approach.

Considering steady state flow, a comparison is performed on a dry gas case. In detail, in Figure 7-20 the results of the grid resolution sensitivity done with the EDFM approach (respectively named according to the grid) are compared with the results of the other methodology (labelled LGR) in terms of conventional well and fishbone completion flow rates, and fishbone benefit.

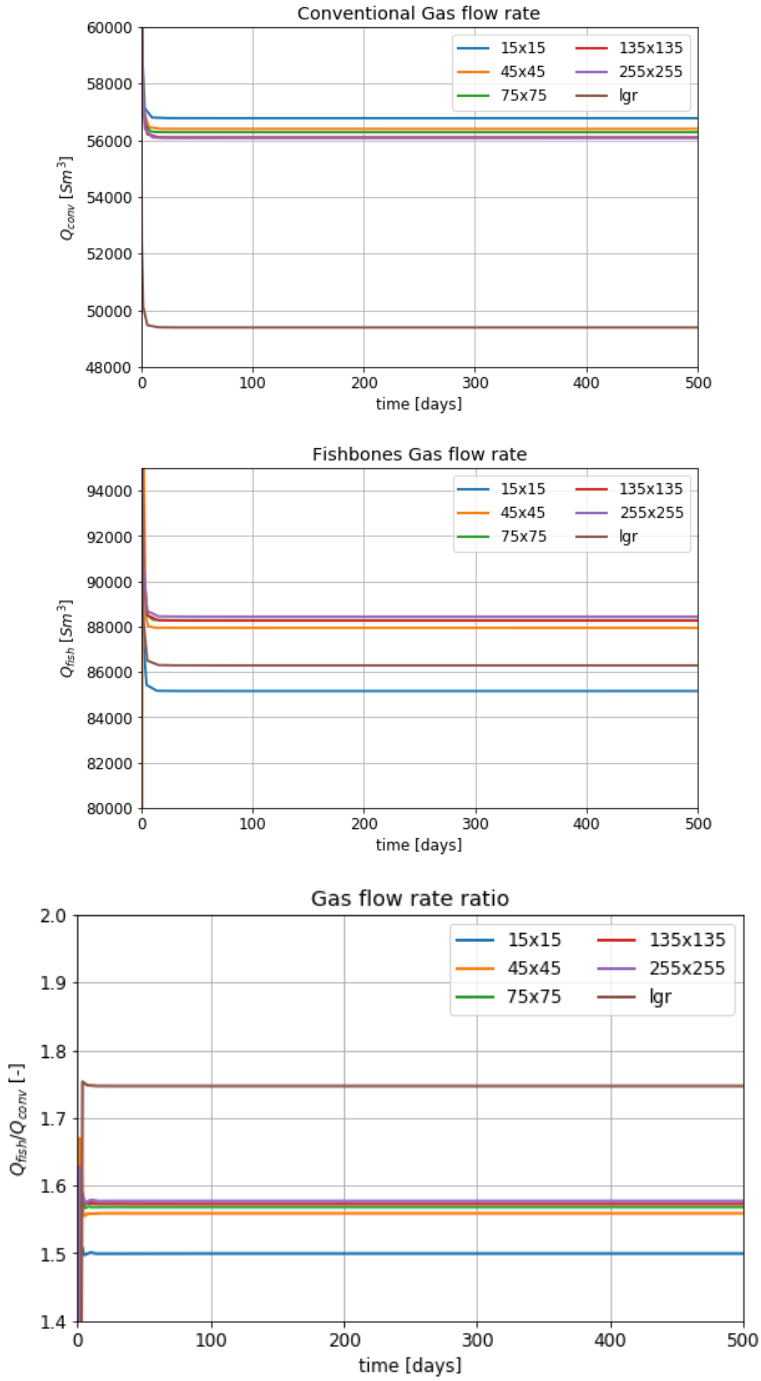

Figure 7-20: Comparison between EDFM and HRG results for a gas case.

While for the EDFM cases a clear convergence can be noticed (see also Figure 7-5), the HRG results are out of trend. Similar behavior is observed for the oil cases.

In chapter 8, the analysis performed with COMSOL will allow to deeper investigate the expected behaviour and to eventually identify the more coherent solution.

8 Modelling fishbone completion using conformal mesh

Oil & Gas industry adopts finite volume reservoir simulators based on CPG grids: computational atoms are hexahedral cells, and mass conservation equations are discretized on a cell basis. The finite volume framework ensures local mass conservation for multi-phase flow and abrupt permeability change across cell borders. In the previous chapters the CPG gridding frameworks are stretched as much as possible using very high resolution grids to capture the pressure gradient near small entities like fishbone laterals. In this chapter, the target of the work is to move away from the finite volume framework giving the possibility to use detailed grids where boundaries can also conform to fishbone completion geometry. This means moving to finite element technology, where a higher grid flexibility can be used. The Finite Element Method (FEM) is widely employed for many problems, in particular where the underling partial differential equations are elliptic or parabolic (see (Quarteroni, et al. 2006). On the contrary, FEM is not well suited for multiphase problems where equation coefficients (e.g. permeability) may change abruptly: local mass conservation constraints are not used in most of the standard implementations and this may lead to unacceptable mass losses in multiphase flow conditions. In this chapter, the deviation from the more comfortable finite volume framework can be accepted because the reference problem is single phase.

In this work, for practical reasons the COMSOL Multiphysics implementation of the FEM is used. COMSOL implementation of the FEM is integrated with sophisticated gridding capabilities which ease the construction of mesh conforming to the completion geometry (see Figure 5-5). It is worth noticing that what has been done here highlights only a small part of the capabilities of the software. As far as model equations are concerned, COMSOL provides the user with a large set of fundamental equations, from single phase mass conservation to general Navier-Stokes type systems or force balance equations arising in mechanical and geotechnical problems. All these equations can be combined by properly defining their domains and the boundary conditions amongst them. In this work, the equations selected are mass conservation equation for a single phase fluid combined with Darcy's law. In particular for steady state problems the model equations are:

$$\nabla \cdot (\rho \boldsymbol{v}) = Q_m, \tag{8-1}$$

$$\boldsymbol{v} = -\frac{k}{\mu}(\nabla p - \rho \boldsymbol{g}), \tag{8-2}$$

while for unsteady state problems the following equations are used:

$$\frac{\partial}{\partial t}(\phi\rho) + \nabla \cdot (\rho \boldsymbol{v}) = Q_m, \tag{8-3}$$

$$\boldsymbol{v} = -\frac{k}{\mu}(\nabla p - \rho \boldsymbol{g}), \tag{8-4}$$

Where Q_m $\left[\frac{kg}{m^2 s}\right]$ is a mass source/sink.

The boundary conditions of the system are usually assigned in terms of pressure or flow rate:

- To simulate reservoir or well pressure, the following Dirichlet's condition are applied to surfaces:

$$p = p_{well} \quad and \quad p = p_{res} \tag{8-5}$$

- Alternatively a known flow rates $\left(Q_0 \left[\frac{kg}{m^2 s}\right]\right)$ or a normal velocity (v_0) across a surface are assigned as:

$$-\boldsymbol{n} \cdot \rho \boldsymbol{v} = Q_0 \quad or \quad -\boldsymbol{n} \cdot \rho \boldsymbol{v} = \rho v_0 \tag{8-6}$$

  Where $\boldsymbol{n}$ is the vector orthogonal to the surface.

The fluid is defined by means of density and dynamic viscosity, while the porous medium by permeability and porosity. Notably, for steady state problems, ρ and μ are constant, while for unsteady state problems $\rho = \rho(p)$ and $\mu = \mu(p)$.

8.1 An insight on FEM in COMSOL

A wide set of FEM implementations are available in COMSOL, however it is outside the scope of this work to provide a review of all the implementations. Rather, the focus is on Galerkin implementation for steady state or unsteady state single phase flow problems in porous media. Then, the independent variables are pressure and material properties, that for fluid and rock are at most function of pressure. If the computational domain is discretized using conformal elements and N_{nodes} is the number of nodes $\{x_j\}_{j=1,..,N_{nodes}}$ of the grid, the solution can be sought in the space V generated by the linear combination of a set of basis functions $\{\psi_i(x)\}_{i=1,..N_v}$, where N_v is the number of variables. The general requirement for these functions is to be zero only for a small subset of elements. The simplest set $\{\psi_i(x)\}_{i=1,..N_v}$ consists of linear functions subject to the conditions that $\psi_i(x_j) = \delta_{ij}$ and in this case $N_v = N_{nodes}$ while the mesh consist of linear elements. An example of a 2D mesh consisting of linear triangles is shown in Figure 8-1.

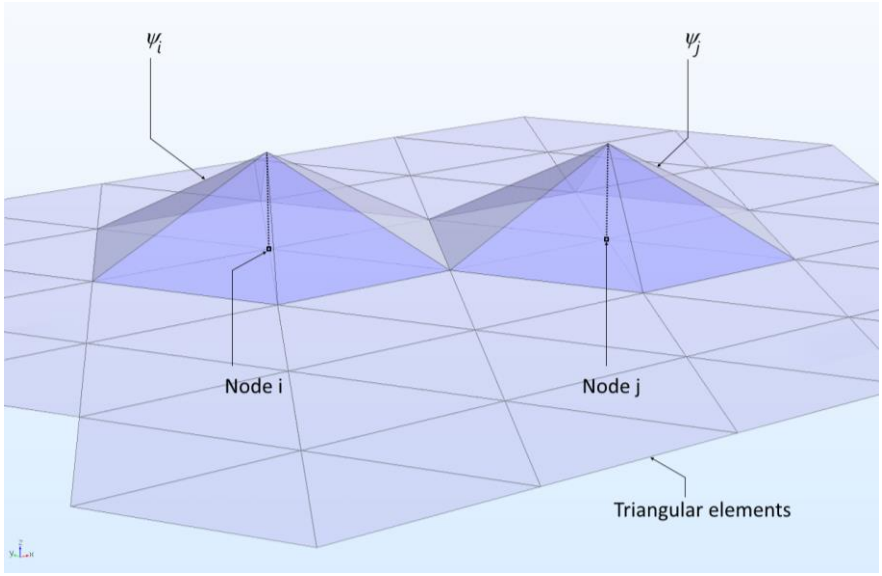

Figure 8-1: A 2D finite element mesh consisting of triangular linear elements. Basis functions for two representative nodes are included. Source: (https://www.comsol.it/multiphysics/finite-element-method#second)

The complexity of the basis functions set is related to the accuracy of the definition of the pressure p, which can be approximated in that space as:

$$p = \sum_{i=1}^{N_v} p_i \psi_i(x), \tag{8-7}$$

Using linear elements $N_v = N_{nodes}$, while quadratic elements lead to a more complex approximation. Figure 8-2 shows a quadratic tetrahedron, highlighting the actual points, each of them associated with a basis function ψ. These basis functions are quadratic functions and the condition $\psi_i(x_j) = \delta_{ij}$ still holds for a set of points $\{x_j\}_{j=1,..,N_v}$ consisting of vertices and edge midpoints.

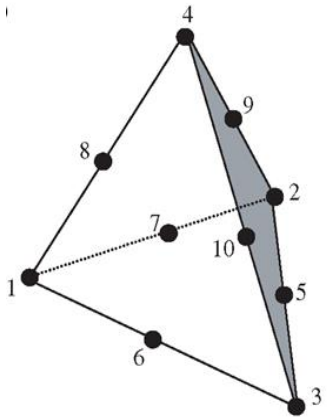

Figure 8-2: A quadratic tetrahedron element; nodes 1 to 4 are mesh vertices, while nodes 5 to 10 are midpoints.

The coefficients in the finite element discretization, eq.(8-7), can be computed assuming that the original PDE holds in a weak - integral - sense for a set of test functions W.

$$\int_{\Omega} \nabla \cdot \frac{k}{\mu} \nabla p \, v d^3x = -\int_{\Omega} \frac{Q_m}{\rho} v d^3x \tag{8-8}$$

Where v is a generic test function $\in$ W, Ω is the computational domain, gravity is neglected and density ρ is constant. Using Gauss-Green identity the previous equation can be written as:

$$\int_{\Omega} \frac{k}{\mu} \nabla p \cdot \nabla v d^3x - \int_{\partial\Omega} \left(\frac{k}{\mu} p\right) \nabla v \cdot \mathbf{n} ds = -\int_{\Omega} \frac{Q_m}{\rho} v d^3x \tag{8-9}$$

Where s is the surface on which integrate. In the previous equation, the second integral at the left hand side runs along the boundary of the domain, which eases to set Dirichlet's boundary conditions.

The simplest and most used choice for the test functions is W=V (test functions and basis functions coincide). Then for equation (8-9) to hold it is enough that it holds for

$$\int_{\Omega} \frac{k}{\mu} \sum_{i=1}^{N_v} p_i \nabla \psi_i(x) \cdot \nabla \psi_j d^3x = -\int_{\Omega} \frac{Q_m}{\rho} \psi_j d^3x, \quad j = 1,..N_p, \tag{8-10}$$

Because of the locality of the support for the basis functions, the previous equation can lead to a linear system for the coefficients $\boldsymbol{p} = (p_1, \ldots, p_{N_p})^T$,

$$\boldsymbol{A}\boldsymbol{p} = \boldsymbol{b} \tag{8-11}$$

Where the coefficients of the square matrix $\boldsymbol{A}$ are computed as:

$$A_{ij} = \int_{\Omega} \frac{k}{\mu} \nabla \psi_i(x) \nabla \psi_j d^3x,$$

The integral is actually computed only on the intersections between the supports of the two functions ψ_i and ψ_j, while $\boldsymbol{b}$ is the right hand side vector which accounts for both source terms and boundary conditions. Notably, thanks to the local support of the basis functions, $\boldsymbol{A}$ is a sparse matrix.

Moving from steady state to unsteady state problems leads to time integration. In the time integration, COMSOL automatically switches from different time-marching schemes, including a fully implicit method similar to the one used in reservoir simulation. Time is usually spent most in the solution of linear systems arising from FEM discretization or corresponding linearization. In this the default choice for the solution of the linear systems (a direct method) is replaced by an iterative solution, namely the multi-grid method, which is the best choice for linear systems arising from the discretization of steady state or unsteady state problems like in equations (8-1), (8-2) and (8-3), (8-4).

8.2 Mesh system

COMSOL can mesh 3D domains with prisms, tetrahedrons, pyramids and hexahedrons. In this work, the element of choice is the tetrahedron because with this element is very easy to approximate complex geometries, including fishbone subs. An automatic gridding process can be guided by the user throughout the following process parameters:

- Maximum element size - h_{max} - upper limit to element dimensions.
- Minimum element size - h_{min} -lower limit to element dimensions.
- Maximum element growth rate - G_{max} - maximum size difference between two adjacent mesh elements.
- Curvature factor - γ - how big a mesh element can be along a curved boundary.
- Resolution of narrow regions - λ - defines the number of layers of mesh elements in narrow regions, the higher the better.

Adjusting one or more of these parameters allows to build a customized mesh, specific to the model and physics needs. Later, sensitivities on mesh quality will be done employing some of the predefined sizes. As an example, Figure 8-3 shows how a well of 0.19 m of diameter is meshed when tetrahedron dimensions are changed.

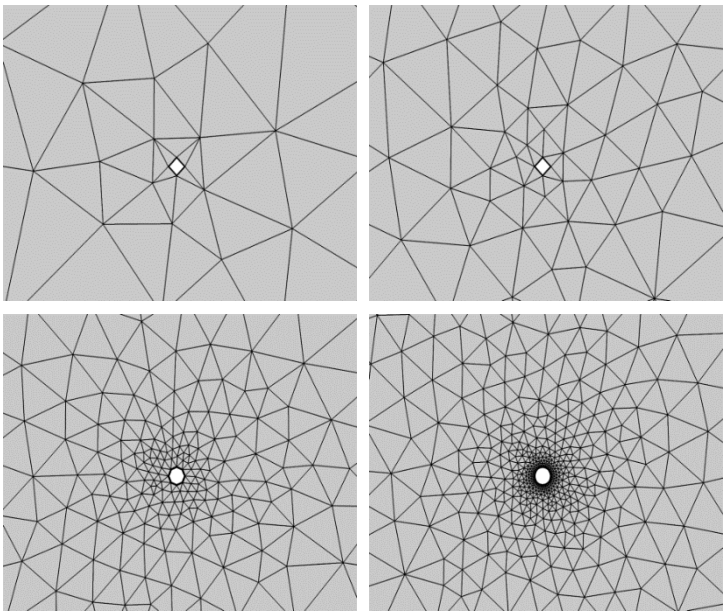

Figure 8-3: A 0.19 m well diameter meshed with a *"Coarse", "Normal, "Finer"* and *"Extremely Fine*" quality. Only the last two steps accurately model the completion. The images report only a slice of the 3D mesh.

8.3 Analytical comparisons under steady state flow

COMSOL Multiphysics is not commonly used for reservoir simulations. This work is one of the first applications of this modelling package inside Eni, hence it is worth providing some evidences that the actual implementations developed here are also consistent with fundamental solutions for fluid flow in porous media. The results of this analysis provide robustness to the overall workflow, with the possibility to use COMSOL as a litmus test to identify and sort out inconsistencies found between the approaches of chapter 6 and 7.

8.3.1 Cylindrical reservoir

In order to have an analytical solution as benchmark, a cylindrical reservoir is first analyzed. The results obtained by the software will be compared to known solutions, in order to confirm the goodness of the mesh and of the solver configurations.

The conditions under which the simulations in this section are performed can be summarized in the following points:

- Steady state,
- Radial flow toward the well due to full penetration of the cylindrical reservoir,
- No vertical pressure gradient (no gravity force),
- Axial-symmetric problem,
- No fluid flow coming from cylinder bases (homogeneous Newman's boundary conditions),
- Homogeneous, uncompressible fluid,

Under these assumptions, the Laplace's equation in radial coordinates is valid in the reservoir (Muskat 1937):

$$\frac{1}{r}\frac{\partial}{\partial r}\left(r\frac{\partial p}{\partial r}\right) = 0 \tag{8-12}$$

Using the following the following Dirichlet's boundary conditions:

$$\begin{cases} p = p_w & for\ r = r_w \\ p = p_{res} & for\ r = r_e \end{cases} \tag{8-13}$$

Integrating eq. (8-13) and substituting the boundary conditions to find the integration constants, the following pressure distribution is obtained:

$$p = p_w + \frac{p_e - p_w}{\ln\left(\frac{r_e}{r_w}\right)} \ln\left(\frac{r}{r_w}\right) \tag{8-14}$$

Inflow velocity can be computed using Darcy's law:

$$v = -\frac{k}{\mu}\frac{dp}{dr} = -\frac{k}{\mu r}\frac{p_e - p_w}{\ln\left(\frac{r_e}{r_w}\right)} \tag{8-15}$$

The mass flow rate produced is then evaluated integrating the radial velocity on the well lateral surface:

$$m = -\rho_f h \int_0^{2\pi} r v_r d\theta = \rho_f \frac{2\pi K h}{\mu} \frac{(P_e - P_w)}{\log\left(\frac{r_e}{r_w}\right)} \tag{8-16}$$

Eq. (8-16) is known as Muskat's equation. It provides a verified result that can be use as reference for the solutions coming from the software.

The parameters used in the following analysis are shown in Table 8-1 below:

Table 8-1: Parameter that fully describe the system.

Fluid density	1000 kg/m^3
Dynamic viscosity	0.214 Pa·s
Porosity	0.1
Rock permeability	1 mD
Well pressure	250 bar
Reservoir pressure (on cylinder lateral surface)	300 bar
Well radius	0.09525 m
Reservoir radius	5 m
Well length	10 m
Reservoir height	10 m

Applying Muskat's equation, the obtained mass flow rate during steady state is:

$$m = 3.658 \cdot 10^{-1} \left[\frac{g}{s}\right]$$

8.3.1.1 Uniform mesh

The mesh has significant impacts on the results. COMSOL gives the possibility to choose the mesh size close to the well and far from it. In this section, a sensitivity on uniform grid refinement in all

the reservoir volume is done. Understanding the errors associated to different degree of refinements is the target of this paragraph.

Three uniform refinements, namely *"Coarser", "Normal"* and *"Finer"* are employed (see Table 8-2 for their mesh parameters).

Table 8-2: Parameters for three predefined mesh qualities.

	"Coarser"	*"Normal"*	*"Finer"*
$h_{max\ [m]}$	9.5	5	1.05
$h_{min\ [m]}$	2	0.9	0.1
G_{max}	1.7	1.5	1.1
γ	0.8	0.6	0.4
λ	0.3	0.5	0.9

Table 8-3 reports the numbers of generated mesh elements and the relative errors on mass flow rates with respect to Muskat's solution, defined as: $error\% = \frac{sol_{COMSOL} - sol_{Muskat}}{sol_{Muskat}} \times 100\%$.

COMSOL provides in the results many flow rates as the number of Dirichlet's conditions applied. Since in the model the well and the reservoir pressures are set, two flow rates are computed. The one coming from the reservoir boundary will be called "inflow rate" while the one entering the well "outflow rate".

Table 8-3: Results obtained with uniform meshes. COMSOL gives two flow rates, one entering in the well and one departing from reservoir boundaries, therefore two errors are reported. The number of meshing element is linked to run time.

Mesh quality	*"Coarser"*	*"Normal"*	*"Finer"*
n° mesh elements	1.83E+04	7.06E+04	1.40E+06
Error % (outflow rate)	19.30%	9.50%	0.55%
Error % (inflow rate)	0.57%	0.17%	0.03%

Some considerations can be done looking at these results:

- *"Coarser"* mesh is not suitable for this model, the few amount of tetrahedrons leads to significant error (up to 19%). However, it is interesting to notice how the inflow rate, that for the assumptions made (steady state conditions) should be equal to outflow rate, is very close to the analytical solution (0.6% of relative error).
- Increasing the mesh quality to *"Normal"* is not enough for a correct estimation of the flow rate. The time increases a little (in the order of tens of seconds), but the error is still significant (about 9%) excluding inflow rate.

- The further mesh improvement *"Finer"* allows predicting the analytical flow rate, both the inflow and outflow. The run time is less than one minute, which can be accepted.

  It is worth noticing that the large errors in the outflow rates seen for low quality mesh (see Table 8-3) are related to the accuracy in the approximation of the boundary, where Dirichelet's conditions are prescribed: using a low-resolution grid leads to very rough estimates of the wellbore cylinder (see Figure 8-3).

8.3.1.2 Non-uniform mesh

COMSOL can implement non-uniform meshing employing a variable resolution algorithm to change the average element dimension in the computational domain. This can be seen as a finite element counterpart of the local grid refinement option available in reservoir simulators. Three non-uniform meshes are selected for the sensitivity analysis: *"Normal-Finer", "Fine-Extra Fine"* and *"Finer-Extremely Fine"*. Basically, the mesh has different quality close to the well and far from it, the range of quality parameters can be seen in Table 8-4.

Table 8-4: Non-uniform mesh parameters.

	"Normal Finer"	*"Fine Extra Fine"*	*"Finer Extremely Fine"*
h_{max}	1.05-5	0.65-1.5	0.37-1.05
h_{min}	0.1-0.9	0.04-0.3	0.005-0.1
G_{max}	1.1-1.5	1.08-1.11	1.05-1.1
γ	0.4-0.6	0.3-0.5	0.2-0.4
λ	0.5-0.9	0.8-0.95	0.9-1

Mesh elements and relative errors are reported in Table 8-5.

Table 8-5: Results coming from a non-uniform mesh.

Mesh quality	*"Normal Finer"*	*"Fine Extra Fine"*	*"Finer Extremely Fine"*
n° mesh elements	6.77E+05	1.34E+06	3.68E+06
Error % (outflow rate)	0.60%	0.32%	19.30%
Error % (inflow rate)	0.09%	0.06%	0.57%

- The *"Normal-Finer"* quality seems perfect for meshing 3D wells. Few mesh elements and flow rates close to the analytical solution.

- *"Fine-Extra Fine"* quality improves a little the excellent results already found with the previous mesh, however run time increases a lot (about 10 minutes) and it does not counterbalance the low error reduction in flow rates estimation.
- The final step *"Finer-Extremely Fine"* leads to computational problems. The high number of meshing elements generates instabilities on the predefined linear solver. Therefore a weird solution is reached. This suggest that the solver configuration should be changed when dealing with a complex mesh, for instance switching from a direct solver to an iterative one (see 8.1).

According to the results obtained in this section and in the previous one, the uniform *"Finer"* mesh is selected for the next studies.

8.3.1.3 Sensitivity on well radius

Until now, a main bore radius, in the order of 10 cm, was considered. However, fishbone subs consist of tiny needles with a radius of 0.5-1 cm. To understand if COMSOL can mesh a so small element and capture the pressure gradient around it, sensitivities on the main well radius are done. The mesh during this analysis is set to *"Finer"* in the entire domain. Figure 8-4 reports the results of this comparison in terms of COMSOL inflow/outflow rates and Muskat's solution. Inflow rates accurately replicate the analytical solution. However, the outflow follows the analytical values only for radii bigger than 5 cm, thus a small radius (in the order of needle radius) is not modelled with accuracy with this kind of mesh (the uniform *"Finer"*). Since for small radii the two flow rates computed by COMSOL differ, it means that the gradient nearby the well is badly approximated.

Then, to check the mesh refinement impact, several tetrahedral dimensions were employed. After some simulations, a good compromise between error and run time is found. Adopting a predefined *"Fine"* mesh and customizing the minimum element size of a tetrahedron (set to 0.001 m), Muskat's solution is accurately matched (error below 1.5% and 0.12%, see Figure 8-5) by both the two flow rates computed by the software. Even if this second mesh is more refined than the previous one close to the completions, run time decreases from 4-7' for the uniform *"Finer"* to 15"-1' for this customized mesh. This is justified by the lower meshing elements, from 1.5 million to 1 million. When the mesh is customized, small tetrahedrons are employed only where necessary (as in the LGR).

With this sensitivity, one can understand which is the most important parameter of a mesh when dealing with small objects: the minimum element size. Its reduction allows to mesh with accuracy small domains but at the same time huge regions will be modelled with bigger tetrahedrons. This is

crucial in particular for complex and vast geometries, since this method keeps low the number of elements that models the domain without losing accuracy.

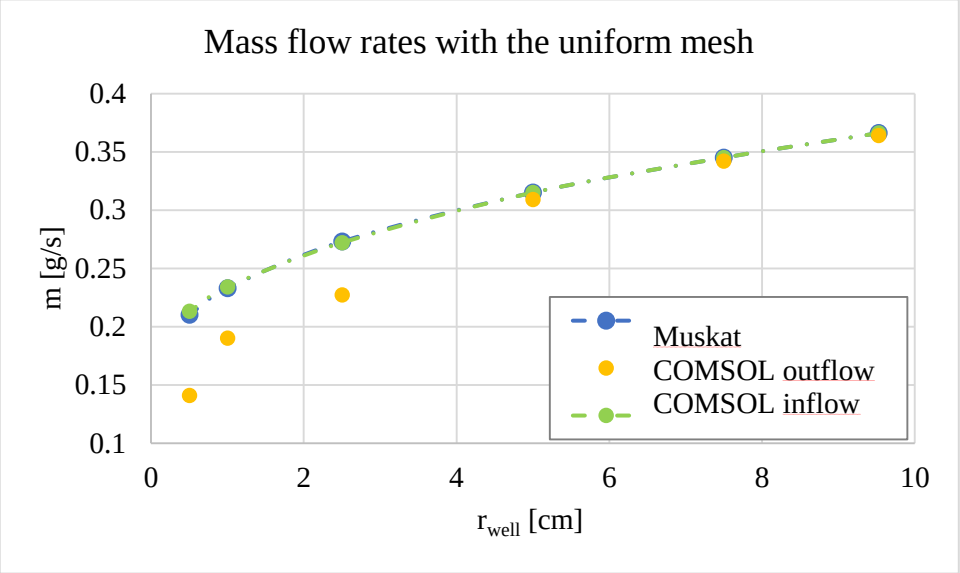

Figure 8-4: Mass flow rates of the analytical solution and the ones computed by COMSOL with a uniform "*Finer*" mesh.

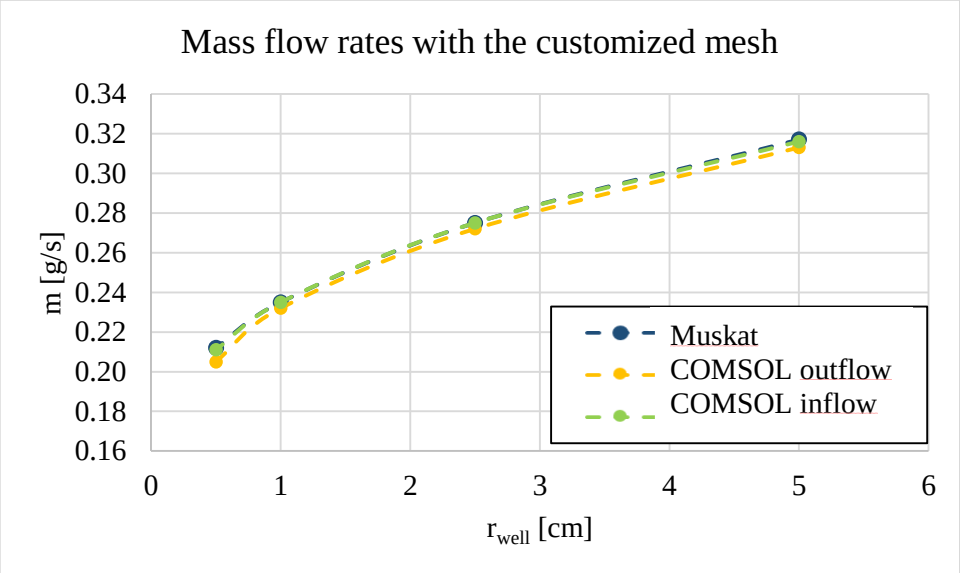

Figure 8-5: Mass flow rates of the analytical solution and the ones computed by COMSOL with a customized "*Fine*" mesh.

8.3.1.4 Sensitivity on well partial penetration

Differently from a long main well, fishbone needles partially penetrate reservoir blocks. This generates a spherical flow towards the later tips. An analytical solution for steady-state homogenous single phase flow towards a well partially perforating a cylindrical reservoir is available (eq. (8-17) and (8-18)) (Muskat 1937).

The flow rate reduction due to the partial perforation is lumped in a positive skin factor S_{pp}. The flow rate of a vertical well can be then computed as:

$$Q_i = (p_e - p_w)\frac{2\pi k_h h}{\mu_i B_i \left[\ln\left(\frac{r_e}{r_w}\right) + S_{pp}\right]} \tag{8-17}$$

$$S_{pp} = \frac{1-\tilde{h}}{\tilde{h}}\ln\left(\frac{4h}{r_w}\right) - \frac{1}{2\tilde{h}}\ln\left[\frac{\Gamma(0.875\tilde{h})\Gamma(0.125\tilde{h})}{\Gamma(1-0.875\tilde{h})\Gamma(1-0.125\tilde{h})}\right] \tag{8-18}$$

Where:

- S_{pp} is the skin due to partial perforation, $S_{pp} = 0$ for a fully perforating well,
- $\tilde{h} = \frac{h_p}{h}$ is the ratio between vertical well length and reservoir thickness,
- Γ is the gamma function, defined as: $\Gamma(n) = \int_0^\infty x^{n-1}\, e^{-x} dx$.

Notably, solution in eq. (8-18) holds only if $0.05 \leq \tilde{h} \leq 0.99$.

According to eq. (8-17), the ratio between flow rates of a partial perforating and a fully perforating well, simplifing the common terms is given by:

$$\frac{Q_{o,PartialPerf}}{Q_{o,FullPerf}} = \frac{\ln\left(\frac{r_e}{r_w}\right)}{\ln\left(\frac{r_e}{r_w}\right) + S_{pp}} \tag{8-19}$$

The reservoir under investigation for this analysis is a cylinder with external radius ($r_e = 600\ ft$) and variable thickness: $0\ ft \leq \tilde{h} \leq 200\ ft$. The well radius r_w is set to be 0.5 ft.

Below in Figure 8-6, the production capacities of a partially perforating well over production capacity of a completely perforating well $\left(\frac{Q_{PartPerf}}{Q_{FullPerf}}\right)$ is sketched versus the formation thickness. The colored dots are the results computed by COMSOL employing a uniform "*Finer*" mesh. On the background (black-dashed lines) there are the analytical solutions proposed by (Muskat 1937) according to eq.(8-18) and (8-19). Four ranges of perforations are investigated (10, 25, 50 and 75% of the reservoir thickness).

For formation thicknesses higher than 40 ft (about 12 m), COMSOL accurately follows the analytical benchmark. For lower values, and thus disk-shaped formations, there is a higher difference. Again, this is due to a not enough accurate mesh, in particular the minimum element size of tetrahedrons is not customized and reduced to low values for this analysis.

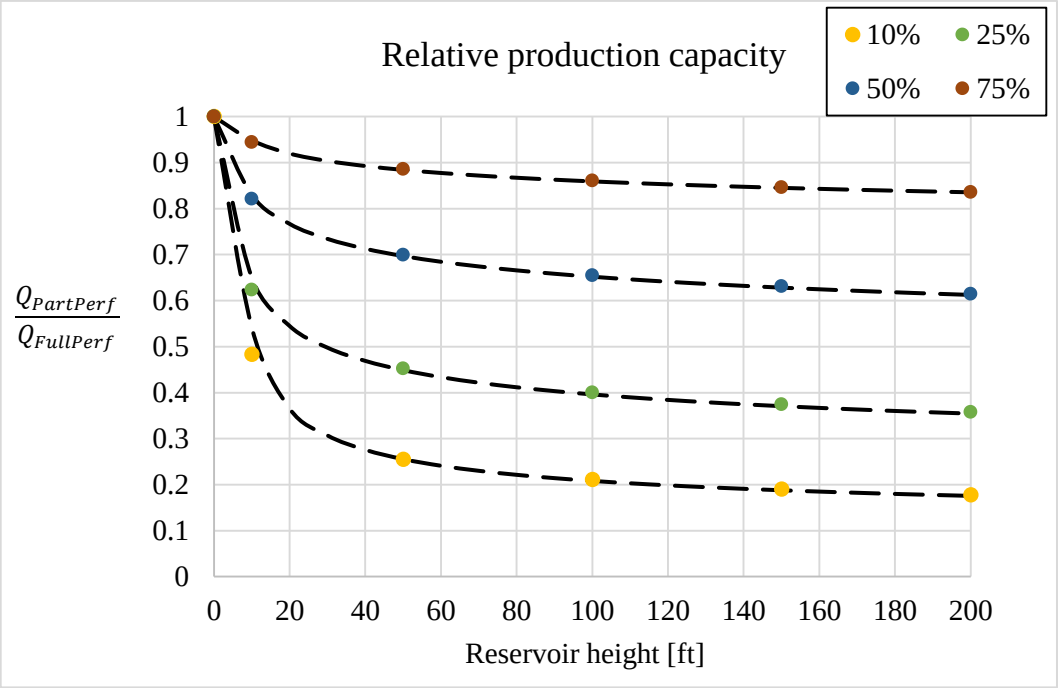

Figure 8-6: Relative production capacity between a partial perforating well and one fully perforating a reservoir. The comparison is between the analytical solution (dashed lines) and COMSOL results (colored dots).

8.3.2 Parallelepiped reservoir

In section 8.3.1 only cylindrical reservoirs were modelled in COMSOL. However, formations are usually discretized with hexahedral blocks/cells in reservoir simulation. Thus, in this section, the attention is on this kind of geometry by using available analytical/semi-analytical solutions as benchmarks for COMSOL simulations.

8.3.2.1 Full penetration: long horizontal well

For parallelepiped and isotropic reservoirs, fully penetrated by a horizontal well, it exits an equation for deriving the steady state productivity index, from which one can compute the mass flow rate (Borisov 1954):

$$m = \rho_{fluid}(p_r - p_w)\frac{4\pi kh}{\mu_o B_o\left[\pi\frac{x_e}{L_w} + 2\frac{h}{L_w}\left(\ln\frac{h}{2\pi r_w} + S\right)\right]} \quad (8\text{-}20)$$

where: x_e is the half reservoir length (distance from well and reservoir boundaries), h the reservoir thickness, L_w the well length and p_r the average reservoir pressure.

The main assumption under which this equation is valid, is that the late radial convergence in a small area around the well has a marginal impact on the average reservoir pressure. Thus, it is assumed

that the reservoir pressure corresponds to the local pressure in the half way between the well and the reservoir boundaries $\left(\frac{x_e}{2}\right)$, according to Figure 8-7.

The mesh quality is set to *"Finer"* and the minimum element size is customized to 0.001 m. The reservoir dimensions are: 40 m, 40 m, 10 m (X,Y,Z). The well length 40 m and its radius 0.095 m. No skin factors are assumed. Well pressure is 250 bar, while a constant Dirichlet's boundary of 300 bar is set to the two vertical reservoir surfaces parallel to the well. The analytical solution gives a mass flow rate of:

$$m = 6.3949 \cdot 10^{-1} \quad \left[\frac{g}{s}\right]$$

The two flow rates computed by COMSOL have an error lower than 0.30%, meaning that the customized mesh is able to model with accuracy also non axial-symmetric problems.

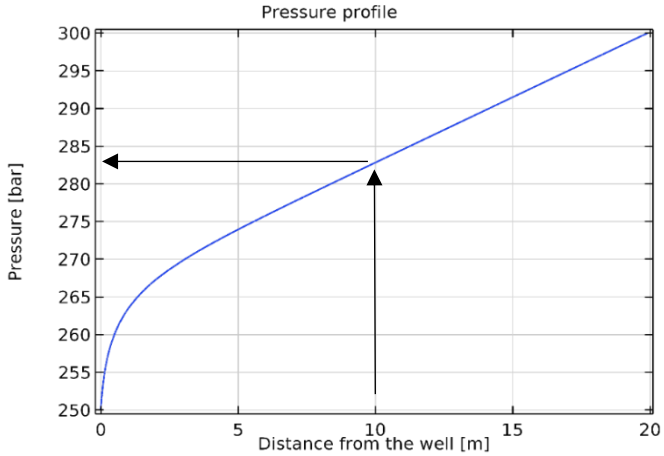

Figure 8-7: The average reservoir pressure is assumed to be at the half way between the well and the reservoir boundaries.

8.3.2.2 Partial penetration: short horizontal well

The partial perforation case can be compared with the formula of "short horizontal wells", based on the mathematical solution for a line source in a two-dimensional space. The equation is an approximation of the solution for long horizontal wells (eq. (8-20)). Elliptic pressure lines around the well are present as shown in Figure 8-8.

For an isotropic reservoir that can be approximated by an equivalent radius $A = \pi r_e^2$, the mass flow rate is given by (Borisov 1954):

$$m = \rho_{fluid}(p_r - p_w)\frac{2\pi kh}{\mu_o B_o\left[\ln\left(\frac{4\pi x_e}{L_w}\right) + \frac{h}{L_w}\left(\ln\frac{h}{2\pi r_w} + s\right)\right]} \quad (8\text{-}21)$$

The reservoir geometry is the same as the previous point while the well is centered in the domain, with a length reduced to 20 m. Dirichlet's conditions (p=300 bar) are applied to the four vertical surfaces of the reservoir.

The approximated analytical solution gives a value of:

$$m = 4.970 \cdot 10^{-1} \quad \left[\frac{g}{s}\right]$$

COMSOL provides a value of $m = 5.044 \cdot 10^{-1}\left[\frac{g}{s}\right]$. The difference respect to the analytical solution is 1.49%. This can be attributed not only to the mesh quality but also to the approximations done when the analytical solution is derived. However, this error is extremely low from a practical point of view.

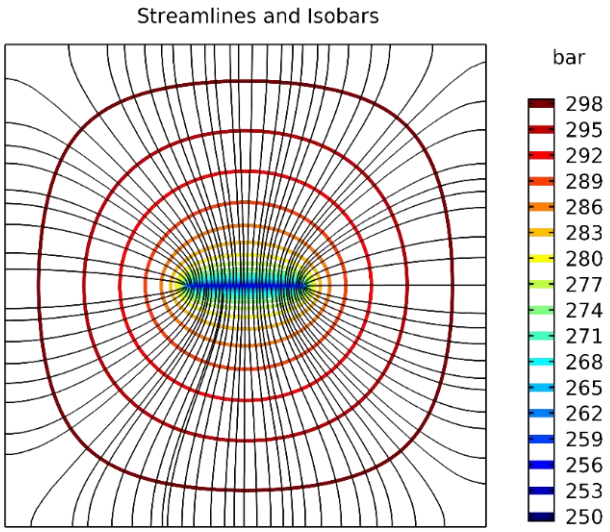

Figure 8-8: Elliptic isobars around the well and related streamlines.

8.4 Sensitivity analysis for steady state flow

In the first sections of this chapter, the sensitivity of the results to the grid resolution has been evaluated. The work led to the conclusion that the *"Finer"* grid -see Table 8-2 - with a customized h_{min} of 1 mm provides enough accurate results in comparisons with various analytical solutions. This grid is labelled as Reference from now on and all COMSOL simulations discussed hereafter are run using the quoted grid unless otherwise stated.

In section 8.4.1 some sensitivities on reservoir parameters are done. Formations are usually characterized by permeability heterogeneity (between vertical and horizontal) and the well is likely to be surrounded by a damaged zone due to mud filtration. This last situation cannot be modelled with CPG grid of the common reservoir simulator due to the radiality of the problem. Then, the Dirichlet's boundary condition effect on production is investigated.

In section 8.4.2 the attention is on fishbone sub geometry. In particular, the production is affected by needle inclination, sub type (Dreamliner or Fishbones), needle radius and length. While the first parameter (the kind of sub) depends on the formation to be completed, the needle configurations (radius and length) is under the operator control. Finally, sub spacing impact on fishbone benefit is analysed.

8.4.1 Sensitivity on reservoir parameters

8.4.1.1 Permeability anisotropy

Reservoirs are usually characterized by heterogeneity. In particular, according to depositional processes, the porous medium is composed by several layers, and this leads to vertical/horizontal permeability anisotropy. Usually the ratio $\frac{K_v}{K_h}$ is less than one, and often it can be much less. Then, a horizontal well can be less and less effective if the ratio $\frac{K_v}{K_h}$ is lower and lower. Therefore, it is interesting to see the benefit that the vertical needles of a fishbone completion can give in those cases. Vertical permeability is varied from 1 mD to 0.001 mD, while the horizontal one is fixed to 1 mD. Figure 8-9 shows how in an homogeneous medium of 1 mD the fishbone benefit at steady state is 1.58, while in case of $\frac{K_v}{K_h} = 0.1$, a common value, it is around 1.94. For extreme permeability contrast, $\frac{K_v}{K_h} < 0.01$, the benefit in even higher.

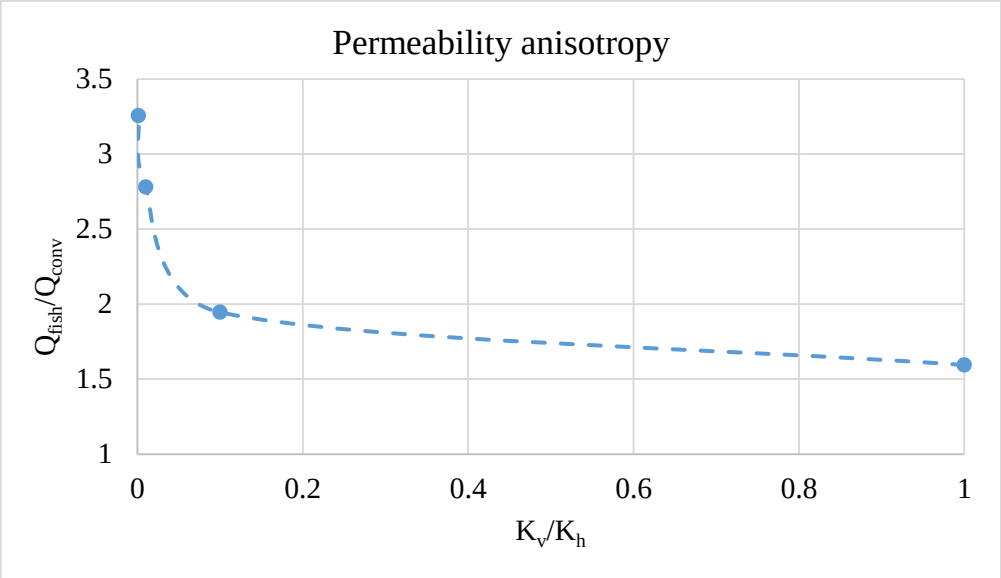

Figure 8-9: Fishbone benefit varying permeability anisotropy.

During the upcoming sensitivities, a base case will be always reported. For this case, homogeneous permeability (1 mD) is considered, while the fishbone sub has needles of 10 m long, with a radius of 1 cm. The fishbone benefit in the base case is 1.58.

8.4.1.2 Invasion zone

Following the works of (LR Senergy 10/06/2015) and (Szanyi, et al. 2017), the analysis of the impact of near wellbore formation damage is done in the following section. During drilling, the permeability in the main bore vicinity is altered by mud invasion due to pressure overbalance. For what concerns the needles, since they are created with a jet or with a drilling sequence that does not require pressure overbalance, formation damage is not generated. Therefore, needles can be seen as an alternative to gun perforations for removing the skin due to damage.

The reservoir permeability is 1 mD, while the altered zone has a permeability of 0.3 mD. The ratio of these numbers is deduced from the data used by (LR Senergy 10/06/2015). The thickness of the invasion zone is changed according to realistic values in order to find a trend for the fishbone benefit.

Table 8-6 shows the invasion zone thicknesses and the relative skin factor due to damage computed according to Hawkins' equation (4-17) at page 38. The fishbone benefit goes from 1.58 (base case), without damage, to 2.59 for an equivalent damage skin of 5.24.

Table 8-6: Fishbone benefit with various invasion zones thicknesses or equivalently damage skin factor

Invasion thickness [cm]	S [-]	Q_{fish}/Q_{conv}
0	0.00	1.58
30	2.68	2.20
60	4.29	2.44
90	5.24	2.59

Figure 8-10 shows how fishbone completed wells are less affected by big invasion zones since needles by-pass them. In fact, the flow rate trend at various invasion thicknesses is almost horizontal. On the contrary, just a thin altered zone drastically reduces the production of a conventional well. The drainage area of a conventional completion is contained inside the damage zone (see Figure 8-11), resulting in a lower reduction of the local reservoir pressure. This means that the pressure difference available from reservoir to the well is dissipated to cross this low permeable zone (see Figure 4-8). Instead, needles increase the drainage radius, since reservoir pressure is reduced also far from the well.

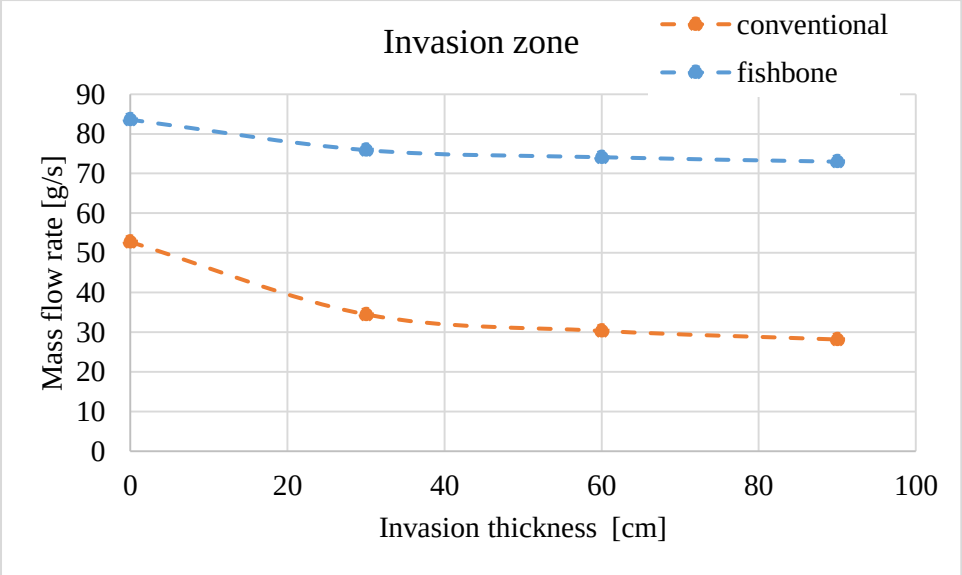

Figure 8-10: Flow rates of a fishbone sub and a conventional well at different invasion thicknesses.

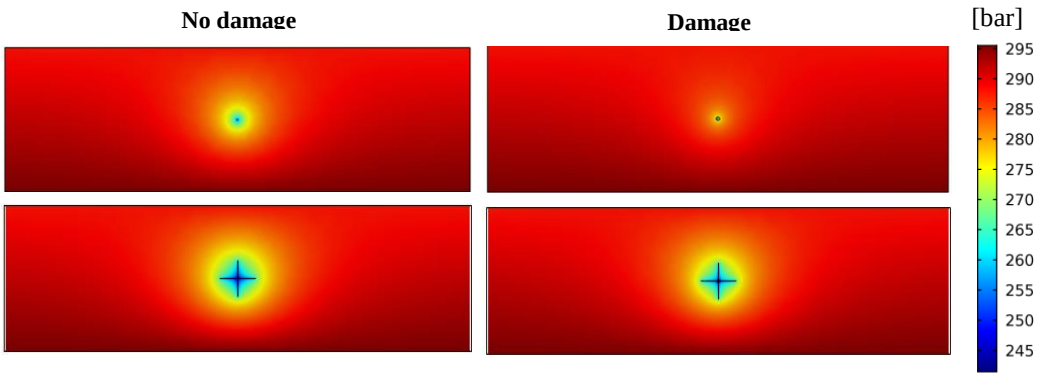

Figure 8-11: Field pressure, on the left no damage, on the right 0.9 m of invasion thickness. On the top a conventional well and on the bottom a fishbone sub.

8.4.1.3 Reservoir boundary condition distance

As seen in section 6.2.2 and 7.3.2, the distance between the Dirichlet's boundary and the well affects the fishbone benefit during steady state flow. This situation is further investigated with COMSOL; since the software allows to easily shaping new reservoir geometries it is possible to perform the sensitivity on a wider range with respect to the high resolution grid and EDFM approaches.

Dirichlet's conditions are set at the top, at the bottom and on the two vertical faces of the reservoir parallel to the well path. The reservoir thickness (H_{res}) is varied from 20 m (the tips of the vertical needle touch the boundary) to 400 m, while the other dimensions are kept constant (see Figure 8-12). For all the cases, the well pressure is set to 241.5 bar while the Dirichlet's conditions on the reservoir boundaries are set imposing a constant gradient. As can be seen in Figure 8-13, when the reservoir top/bottom touch the needle tips, the fishbone benefit is drastically enhanced. While for far Dirichlet's conditions, the production increment mildly depends on the distance (the benefit keeps constant to 1.49).

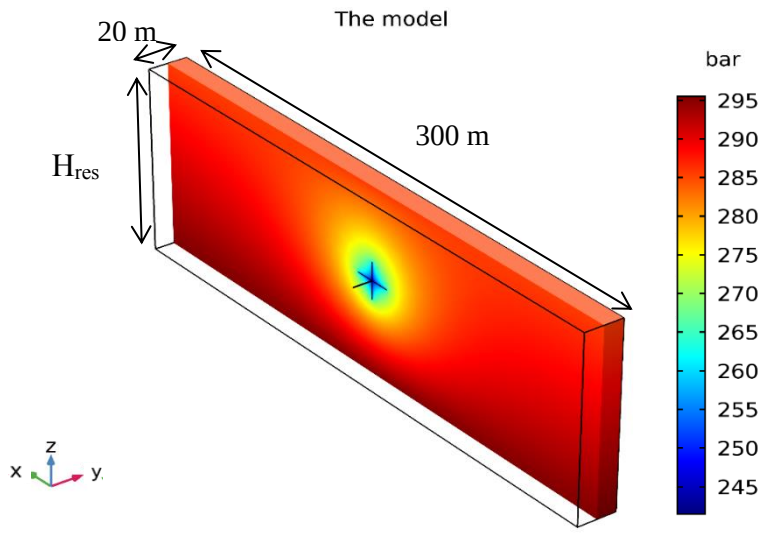

Figure 8-12: Reservoir model, lateral dimensions are fixed while reservoir height is varied.

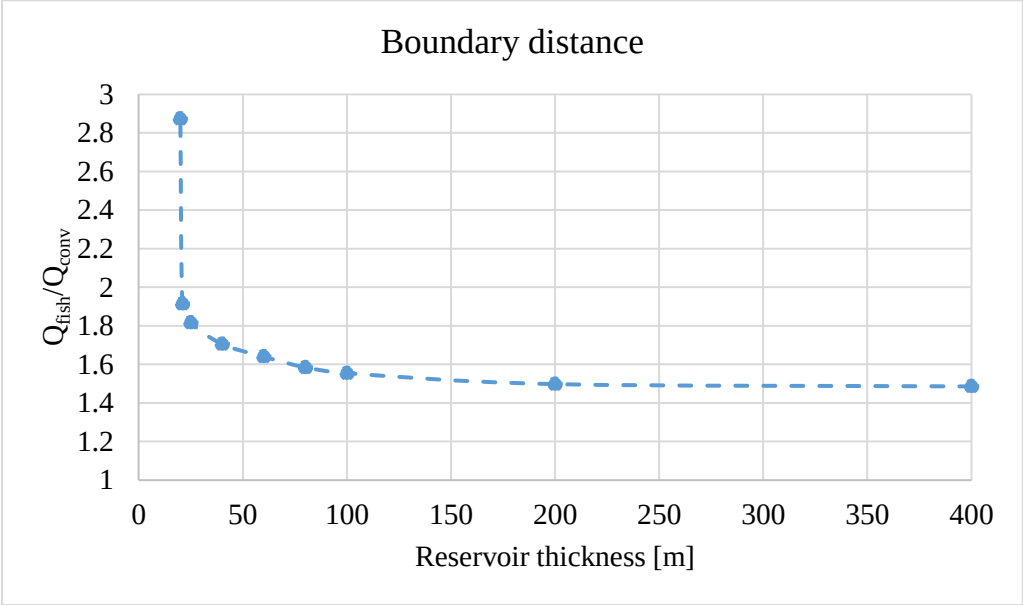

Figure 8-13: Fishbone benefit with several reservoir thicknesses.

8.4.2 Sensitivity on fishbone completion geometry

After analysing the impact of reservoir configurations on the production, sensitivities on needle geometry are done. Parameters as needle inclination, number of needles per sub, needle radius/length and sub spacing are analysed. These are all the aspects that the operator can modify to find the best configuration.

The aim is to find practical correlations able to describe a geometric skin factor that lumps the fishbone benefit.

When the flow rate produced by a conventional well and by a fishbone sub are known, a skin factor can be computed:

$$\frac{q_{Fishbones}}{q_{conventional}} = \frac{\ln\left(\frac{r_e}{r_w}\right)}{\ln\left(\frac{r_e}{r_w}\right) + S} \tag{8-22}$$

Where r_w is the conventional well radius, and r_e the drainage radius that can be approximated as:

$$r_e = \sqrt{\frac{A_{drainage}}{\pi}} \tag{8-23}$$

From eq. (8-22), the geometric skin is easily computed, starting from the flow rates of COMSOL:

$$S = \ln\left(\frac{r_e}{r_w}\right)\left(\frac{q_{conventional}}{q_{fishbone}} - 1\right) \tag{8-24}$$

This can be applied to a simple conventional well in full field reservoir simulations. The fishbone benefit can be lumped into the geometric skin factor. Without the need of modelling the real geometry of a fishbone sub.

8.4.2.1 Inclined needles

Needles were previously modelled as small channels departing perpendicularly from the main bore. In reality, from laboratory test it was seen that they exit with an angle of 40°, building 10° every meter and reaching 90° at the tip (as in Figure 8-14).

Modelling the variable angle requires the use of a CAD program. This more realistic shape of the needles is drawn with a sweep extrusion. The aim is to understand the differences of this geometry with respect to orthogonal needles.

Table 8-7 shows that the sub with the needles exiting at 40° produces only 1% less than the sub with orthogonal needles. Therefore, their benefits with respect to a conventional well are extremely close (1.57 vs 1.58). Since the variable angle requires a time consuming CAD procedure to be built and gives results close to the classical sub, it can be assumed that negligible approximations are done if one does not consider this specific shape, considering also that the real exiting angle is not known with accuracy.

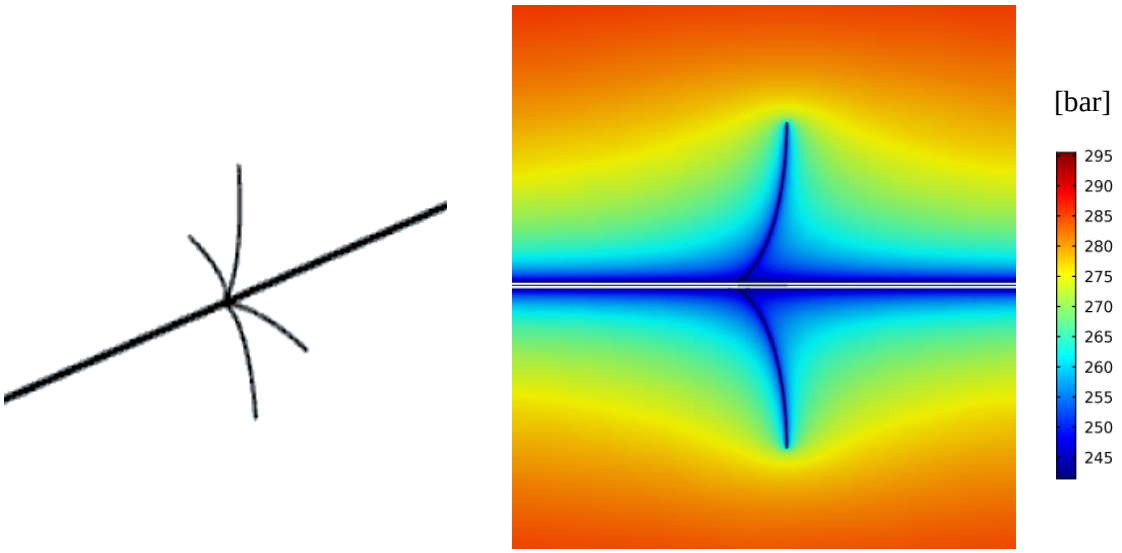

Figure 8-14: Fishbone sub with needles exiting with a 40° angle reaching 90° at the tip.

Table 8-7: Benefit of a sub with needles exiting at 40° or 90° with respect to a conventional well.

Well type	**Mass flow rate [g/s]**	**Increment respect to conventional well**
Conventional	52.74	-
Needles at 90°	83.36	1.58
Needles at 40°	82.63	1.57

8.4.2.2 Dreamliner vs Fishbones

A Dreamliner is characterised by three needles per sub instead of four (see 3.1.1 and 3.1.2). The installation of this completion or the Fishbone one depends on the formation type - sandstone instead of carbonates - and it is not an operator choice. Dreamliner geometry (needles with 120° phasing) is hardly captured by the Cartesian grids of reservoir simulators, therefore its benefit is here investigated.

From Figure 8-15 it is difficult to see differences in field pressure reduction between a Dreamliner and a fishbone sub. However, Table 8-8 shows how the fishbone sub leads to a benefit with respect to a conventional well of 1.58, while the Dreamliner stops at 1.47.

For a homogeneous permeability reservoir, simulations done with different needle orientations with respect to the main bore show that the rotation angle has a negligible impact on production enhancement. While the same cannot be said in case of high permeability heterogeneity.

Table 8-8: Fishbone sub and Dreamliner relative increment with respect to a conventional well.

Well type	Mass flow rate [g/s]	Increment respect to conventional well
Conventional	52.74	-
Fishbones	83.36	1.58
Dreamliner	77.56	1.47

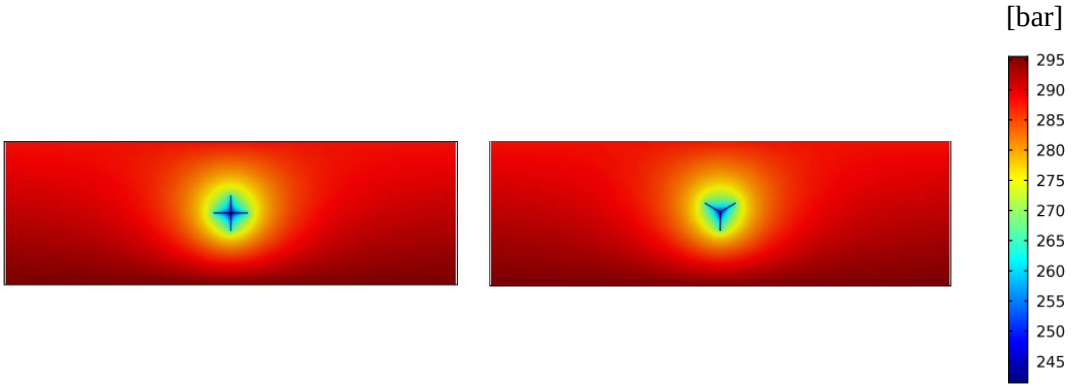

Figure 8-15: Field pressure in case of depletion with a fishbone sub and a Dreamliner.

8.4.2.3 Sensitivity on needle radius

Needle radius can vary according to the technology used for perforating the rock, jetting or drilling. Thus, a sensitivity on this parameter is done to assess its impact on the production. The radius is changed from 0.5 cm to 3 cm, covering all the possible range of needle radii (Freyer, et al. 2011).

Figure 8-16 shows the production increment of the sub with respect to the conventional well. The base case, 1 cm of needle radius, gives an increment of 58%, while the extreme cases, 0.5 cm and 3 cm, provide respectively 55% and 68% of benefit. Therefore, needle radius has a mild influence on production increment.

Table 8-9:Fishbone benefit at various needle radii and the corresponding geometric skin factor.

Needle radius [cm]	Q_{fish}/Q_{conv}	S
0.5	1.54	-2.35
1	1.58	-2.49
2	1.64	-2.64
3	1.68	-2.74

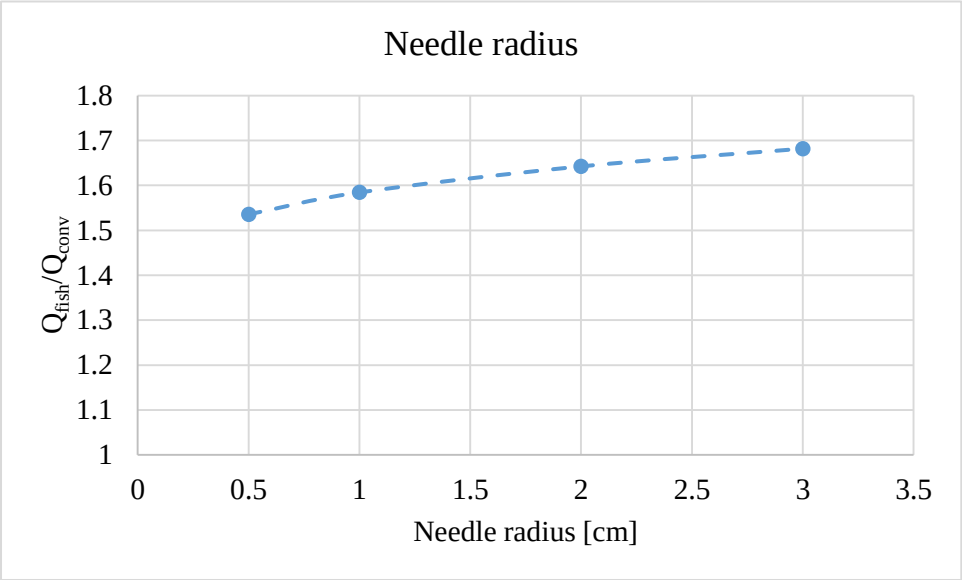

Figure 8-16: Fishbone benefit changing the needle radius.

8.4.2.4 Needle length

According to the different technology or operator will, needle length can vary a lot. This section is focused on homogeneous reservoir, drilled by a main well and a sub of four needles.

Needle length is varied from 8 m to 20 m with a 2 m stepping. For these values, the increment respect to a conventional well go from 43% to 136% (see Table 8-10).

From Figure 8-17 it can be seen that there is almost a linear trend between fishbone benefit and needle length. As expected, this parameter has a large impact on production improvement.

Table 8-10: Fishbone benefit at various needle length and corresponding geometric skin factors.

Needle length [m]	Q_{fish}/Q_{conv}	S
8	1.44	-2.06
10	1.58	-2.49
12	1.73	-2.85
14	1.88	-3.17
16	2.04	-3.44
18	2.20	-3.68
20	2.37	-3.90

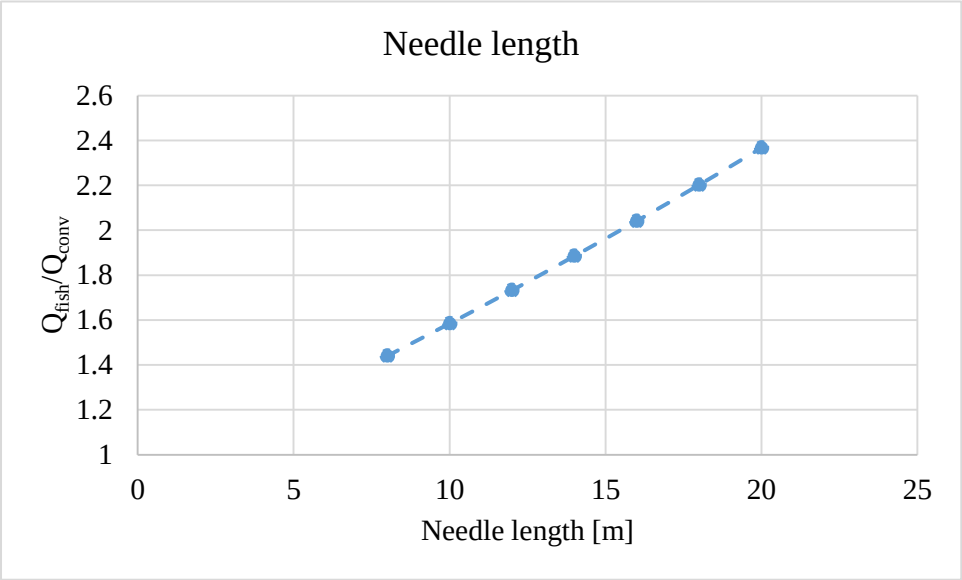

Figure 8-17: Fishbone benefit changing needle length.

8.4.2.5 Fishbone sub density

During the analysis of the fishbone performance, along chapters 6, 7 and section 8.4, the sub distance has been set to 20 m. This is a realistic value, since the minimum physical distance is 12 m and subs too close interfere with each other's. On the other side, a well completed with subs at too high distances (i.e. 50-100 m) has a reduced performance, meaning that its production is slightly higher than a conventional well.

To understand the production capacity of a well completed with fishbone subs at varying distance and the competing effect of needles, a new reservoir geometry is analyzed. Instead of the 20 m reservoir slice (see Figure 6-3) a 100 m length along the Y direction is considered. At the same time, the conventional well and the main bore of the fishbone completion are extended to 100 m long. The sub distance is varied adding one sub at a time (i.e. only 1 sub is for 100 m of relative distance, 2 subs for 50 m, and so on), see Figure 8-18 for a clarification.

Figure 8-19 reports the ratio of flow rates between a fishbone completed well and a conventional one. Sub distance is simulated for cases ranging between 10 m and 100 m. However, the lower limit is 12 m, where the fishbone benefit is 1.84. When a sub is placed every 100 m, the production increment is only 1.13.

Figure 8-20 shows how the production from the needles of a single sub is reduced due to the presence of the adjacent ones at various distances. The sub spaced by 100 m is considered the reference since it does not perceive the presence of other subs. Therefore, the chart reports the efficiency of the sub

with respect to the reference one once the distance is varied. If for spacing bigger than 20 m, the efficiency keeps high (above 90%), for high sub density it sharply decreases to 75%.

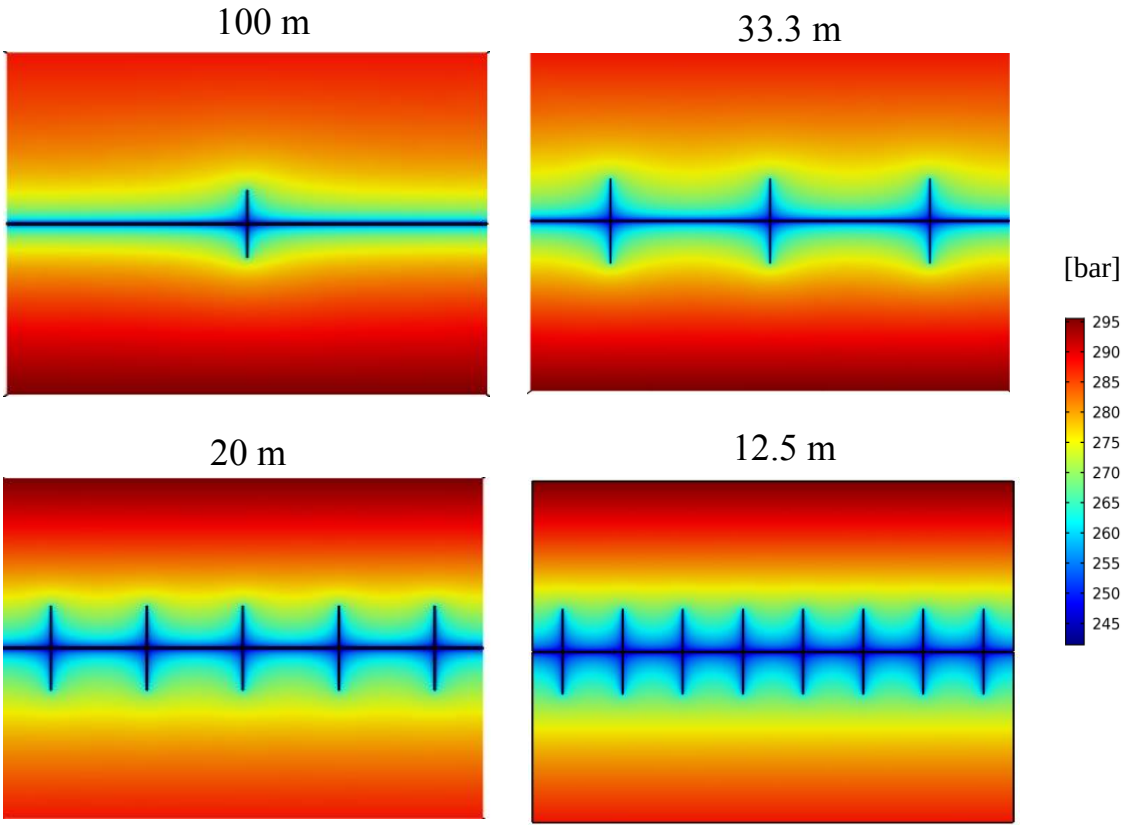

Figure 8-18: The 100 m main bore with increasing number of subs. The distance between them decreases as reported in the labels.

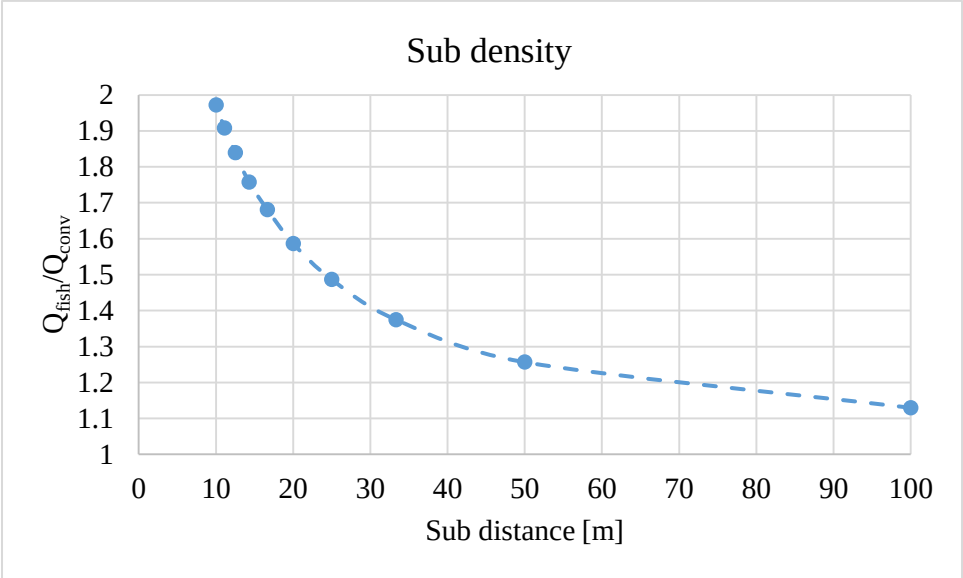

Figure 8-19: Fishbone benefit at various sub distances.

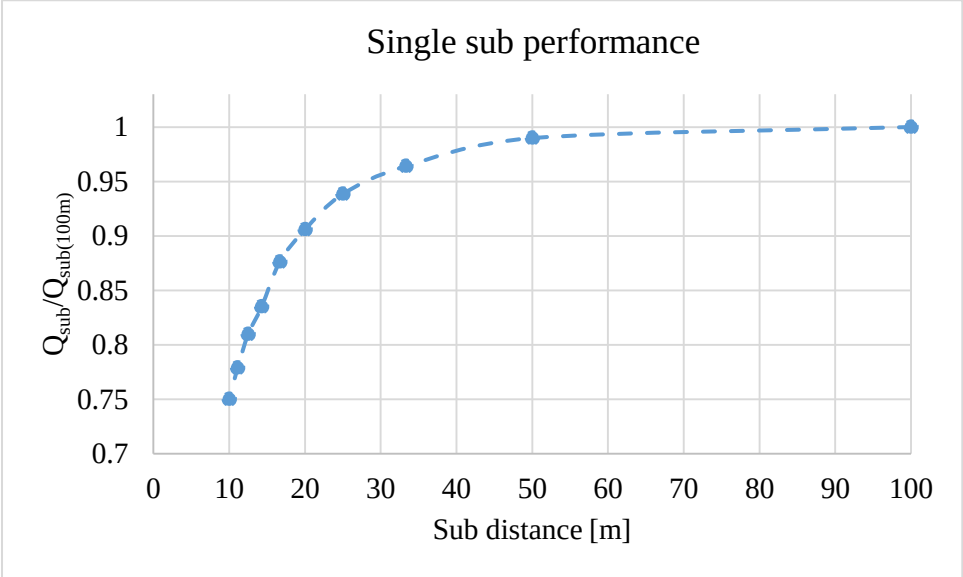

Figure 8-20: Relative production of needles at various distance with respect to a reference case of 100 m distance.

9 Discussion of the results and application on a real field

As seen in section 7.6, discrepancies in flow rate estimations are present between the two reservoir modelling methodologies. Now, the results obtained in chapter 8 with a conformal mesh, provide a supplementary term of comparison. In particular, considering an identical model (same reservoir dimensions, Dirichlet's conditions and fluid properties), fishbone benefit evaluated with the three methodologies during steady state condition is shown in Table 9-1.

Table 9-1: Steady state fishbone benefit evaluated with the three methodologies.

Methodology	Fishbone benefit (Q_{fish}/Q_{conv})
High Resolution Grid (HRG)	1.75
EDFM (75x75 cells)	1.57
EDFM (135x135 cells)	1.575
EDFM (255x255 cells)	1.58
COMSOL	1.58

The results obtained with the EDFM (chapter 7) and COMSOL (chapter 8) during steady state are practically the same, while the HRG methodology overestimates the fishbone benefit. Moreover, if the EDFM case is run with a more refined grid, as the 255x255 (about 1.2 m of cell side), the fishbone benefit during steady state converges to the same value found in COMSOL (see also Figure 7-5).

The fishbone benefit overestimation done by the high resolution finite volume simulations is systematic. In fact, what said for a homogeneous reservoir during steady state flow can be seen also for a layered reservoir, for primary recovery, during semi steady state or when Dirichlet's conditions are placed at different distances.

Hence, results provided by the three methods suggest that the HRG approach is not suitable for the modelling of fishbone completions and deeper investigations of this methodology are required. For this reason, a simple test has been performed on a homogeneous reservoir consisting of a flat layer. The reservoir domain is 300x80x1 m^3, discretized in cells having dimensions of 0.2x0.2x1 m^3. Steady state flow is imposed by applying Dirichlet's boundary conditions. Just a conventional well, completed along Z (and thus 1 m long), is modelled according to the high resolution grid approach, hence by means of an arbitrary high well index. Since the well coincides with the cell, the flow

towards the well is equivalent to the flow from adjacent cells to the completed cell (see Figure 9-1). The same problem is simulated by means of the EDFM approach on a much coarse grid (with gridblocks having dimensions of 4x4x1 m3). For this simple case, the approach reduces to the application of the Peaceman's model for the main bore. Results are available also for a coherent COMSOL simulation, which shows agreement with the EDFM modeling.

Differently, also in this simulation, the high resolution grid approach provides an underestimated well production. The main difference in the well modeling lies in the flow path assumed towards the well. While the high resolution grid implies a cell-to-cell flow in a 5-cell stencil (central cell and cells 2, 4, 5, 7 in Figure 9-1), Peaceman's model assumes radial flow inside the completed cell (see Figure 9-12). Hence, the hypothesis is that the absence of radiality leads to the underestimation of the flow rate produced by the main bore.

To support this assumption, a simple test was performed in order to increase the radiality of the flow towards the well in the high resolution grid. By means of non-neighbouring-connections a 9-cells stencil flow path is implemented. As a result, the well production becomes much more in agreement with the EDFM and COMSOL values.

This result supports the conclusion that the high resolution grid methodology explored in this work is not suitable for the modeling of wells because it does prevent radial flow, while EDFM approach is suitable for both conventional and fishbone modeling.

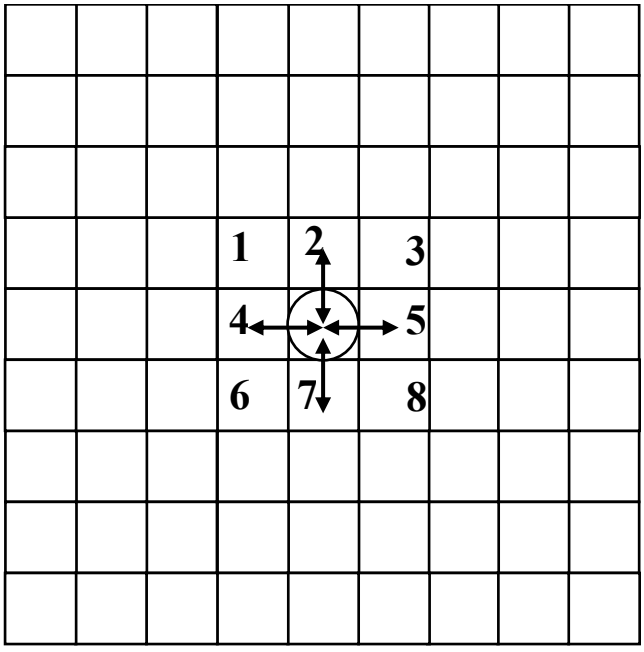

Figure 9-1: Flow toward a well having the diameter equal to the grid size (as in the HRG cases).

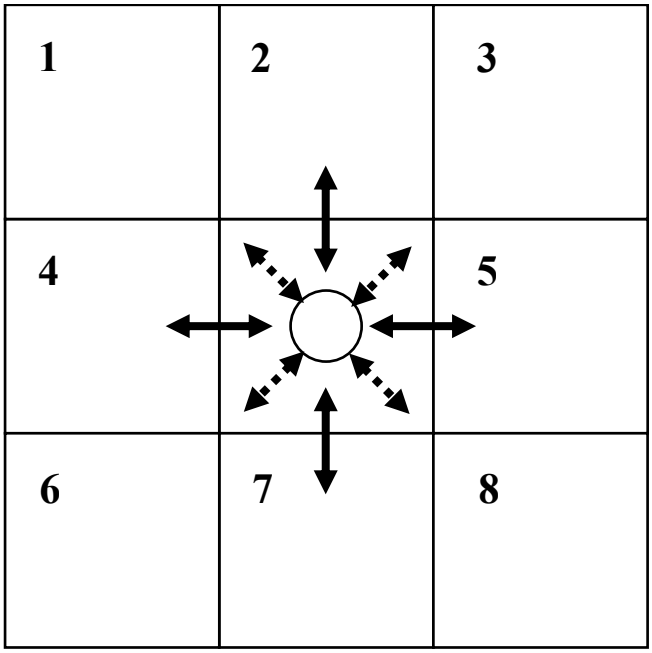

Figure 9-2: Flow between adjacent cells and toward a well having the diameter much smaller than the grid size (as in the EDFM cases).

9.1 Real field

In this section, a "proof-of-concept" of the EDFM modelling solution for a fishbone completion in finite-volume models is provided by applying the methodology to a real case.

The field selected for this test, called in this work "Field A", was identified by Eni's reservoir engineers as a candidate for the application of fishbone technology for some criticalities highlighted during the definition of the development strategy. The field is a gas reservoir located around 100 km offshore, classified as high-pressure (792 bar) high-temperature (150°C) (HPHT) with high CO_2 content (5% molar fraction c.a.). The average gas saturation is 0.72, while water fills the rest of the pore volume according to petrophysics of the porous media. Field depth ranges between 4242 m and 4450 m below sea bottom, and operations are run in 400 m water depth. In the Appendix, Table A6 shows the properties of the dry gas. These properties were also employed in the previous sensitivities, the only difference here is the gas density, which is 0.919 kg/Sm^3 (at surface conditions).

The proposed development plan includes 4 deep subsea wells with long horizontal sections. According to preliminary simulations, the production wells would need five stages of hydraulic fracturing and a horizontal section between 1000 and 1700m to produce commercial volumes.

However, the hydraulic fracturing on HPHT subsea wells is an extremely risky operation. Therefore, Eni is investigating different development scenarios, and fishbone technology was proposed as a possible alternative solution. From a modelling point of view however, no methodologies were so far available for evaluating the benefits of this completion.

The EDFM fishbone modelling solution described in chapter 7, is considered a suitable approach to be used for the study of Field A, and in general for cases where real reservoir geometry and real well configurations increase the complexity of the grid and of the completion definition with respect to the simple ones used for the development of the modelling workflow.

Field A reservoir model is composed by 102x300x148 cells, with homogenous grid block areal dimensions (100 m x 100 m) and variable vertical resolutions (from 1 to 5 m). The reservoir is characterized by strong vertical heterogeneity and by the presence of low-permeability layers. In order to test the actual applicability of the EDFM fishbone modelling approach, one of the five proposed wells of Field A is considered, labelled W-1. A sector model with a volume of 3 km x 1 km x 100 m is designed around W-1, so that heterogeneity and original grid characteristics are preserved while limiting the domain dimensions.

The conventional and fishbone completion productivities are compared with the assumption of wells produced under BHP constraint (set to 250 bar) without bounds on rates. This type of simulation is usually labelled as potential simulation, because the target is to establish the potential of the reservoir upon which facility can be developed. The current BHP value is a reasonable estimate for the abandonment pressure expected for that reservoir according to the asset team. The fishbone completed well is modelled by assuming 51 subs with a spacing of 20 m (see Figure 9-3). Following the EDFM methodology developed in chapter 7, by using a Python script, fishbone needles are "converted" into fracture planes having properties (length, aperture and height) resembling needle geometry. The fractures are then imported in Petrel and used by the EDFM plug-ins in order to define the EDFM simulation case, based on the geometry and properties of the sector. Matrix-fracture transmissibility are then corrected as discussed in section 7.1.

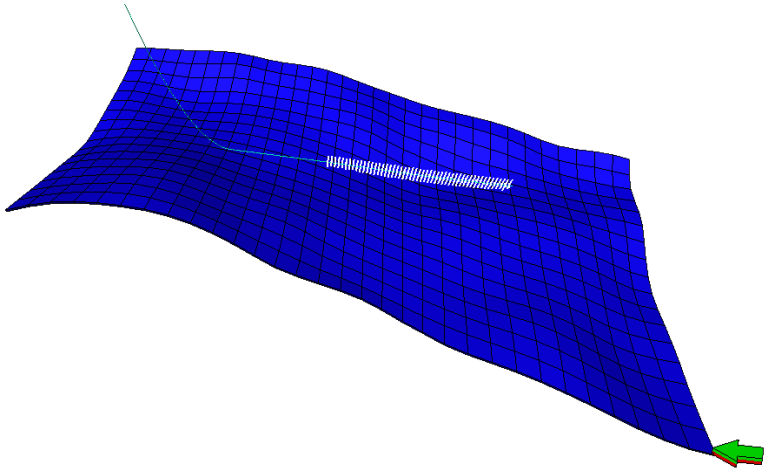

Figure 9-3: The image shows the sector model, the well W-1 and fishbone subs. It highlights that the grid is almost orthogonal to the well path (along J direction).

To begin with, average properties of the sector region are considered for a homogenous case. Then, real heterogeneous properties are used. In the following paragraphs, the results in terms of cumulative gas productions are presented for the various situations. In all the cases, results for different grid refinements are shown. In detail, the original grid refinement is compared with a 3x3x3 refined grid (X,Y and Z cell dimensions are reduced by a factor 3) (REF3 case) and then with a 9x9x3 refined grid (REF9 case).

9.1.1 Homogenous case

The petrophysical properties used are shown in Table 9-2:

Table 9-2: Petrophyscal properties for the homogeneous case. In the first column the simulator jargon is used to label the property.

PERMX	X- permeability	0.6 mD
PERMY	Y- permeability	0.6 mD
PERMZ	Z- permeability	0.06 mD
PORO	Porosity	0.11
NTG	Net-to-gross ratio	0.56

The net-to-gross ratio is used in sandstone formations to account for the presence of shaly interbeds which reduce the volume of sand and the pore volume available for flow. Net-to-gross zero means that the cell at hand is not mineralized and it can only be a barrier to flow.

In Figure 9-4, cumulative gas productions (rescaled for confidentiality reasons) for the conventional well and the fishbone completed well are plotted for different grid resolutions. The cumulative

fishbone benefit at the end of the simulation (7000 days) results extremely low. Indeed, with the given petrophysical properties the conventional well is suitable to fully produce the sector taken into account.

Another observation arising from this case is that EDFM results to be consistent also with relatively coarse grid, as the few differences among the different resolution cases demonstrate.

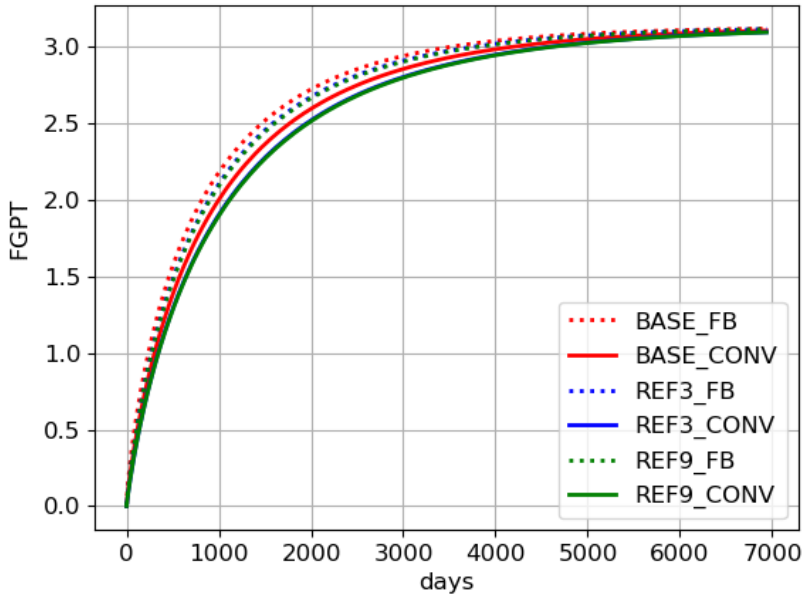

Figure 9-4: Cumulative gas production (or FGPT: field gas production total) in a homogeneous reservoir at different grid refinements. (In the legend, FB: fishbone completion, CONV: conventional completion).

As already mentioned, Field A is characterized by high vertical heterogeneity. In particular, the deeper layers of the reservoir are characterized by a permeability that is around one order of magnitude lower than the average values of the sector region considered. In order to evaluate the possible fishbone benefits, a second homogenous case is set up, where permeability are reduced of one order of magnitude. The results in terms of rescaled cumulative gas production are shown in Figure 9-5. It is possible to observe that, as expected, fishbone benefit is enhanced in low-permeability domains, resulting to be around 19% after 7000 days of depletion, while the production anticipation is around 2000 days (≈ 5.5 years).

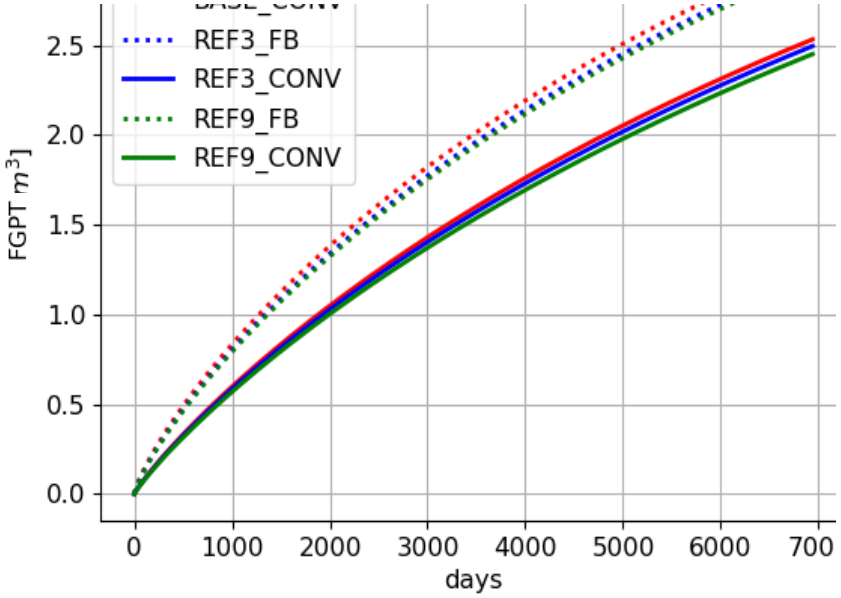

Figure 9-5: Cumulative gas production in a homogeneous reservoir with low permeability at different grid refinements. (in the legend, FB: fishbone completion, CONV: conventional completion).

9.1.2 Heterogeneous case

In this paragraph, the results are shown for the heterogeneous case, where the real sector property distributions (PERMX, PERMY, PERMZ, PORO, NTG) are used. In particular, as previously said, permeability of the bottom layers are extremely low (see Figure 9-6 for the horizontal permeability and Figure 9-7 for the vertical one in a I-slice of the model). The sector model is affected by the presence of layers and regions inactive to fluid flow (that is, null NTG), as highlighted in Figure 9-8, where a slice orthogonal to well trajectory shows the fishbone completed well crossing a section of the model (NTG is plotted).

Looking at Figure 9-9, the first observation is that the cumulative fishbone benefit – volume of fluid produced with fishbone over the volume of fluid produced with a conventional completion - is around 10% after 7000 days of production, and the production anticipation consists of 1500 days (≈ 4 years). The second comment is that EDFM fishbone modelling approach confirms to be consistent also with relatively coarse grids and heterogeneous properties.

It should be notice, that the cumulative fishbone benefit, at the end of the field production, is lower than the one expected according to the results obtained during previous sensitivities (through chapters 6, 7 and 8). However, if the rescaled flow rates are considered (as in Figure 9-10), it can be seen how in the first 1000 days, the flow rate of the fishbone completion is significantly higher than the one of the conventional well: the instantaneous fishbone benefit (see Figure 9-11) ranges from 2.2 to 1.12, while the cumulative production increment is 37%. After this first period, the instantaneous fishbone

benefit results to be lower than one. Actually, because of the well trajectory fishbone completions cannot contact reservoir regions untapped by the conventional completion. The additional productivity provides a way to anticipate production but the ultimate production for the time period of 7000 days is definitely given by the pressure target.

The analysis of alternative developments, with a reevaluation of the main bore path and fishbone completion configurations to contact also the bottom layers are left for future works.

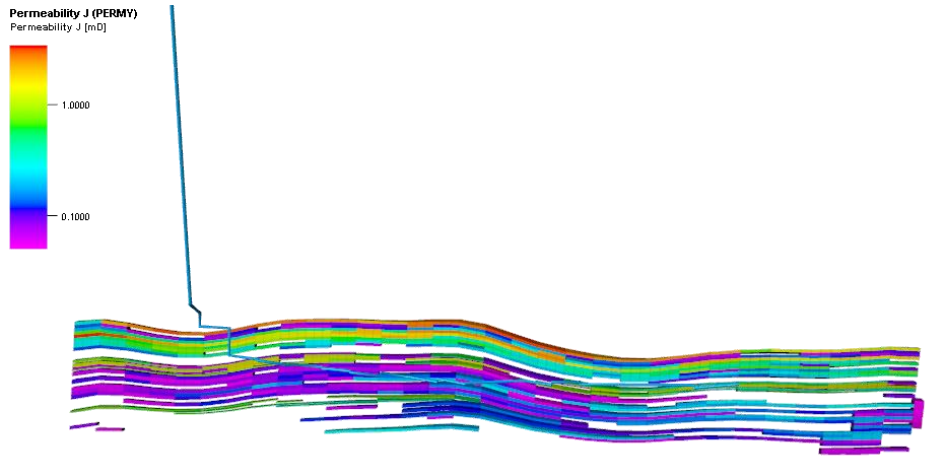

Figure 9-6: Horizontal permeability in the layers contacted by the fishbone completed well.

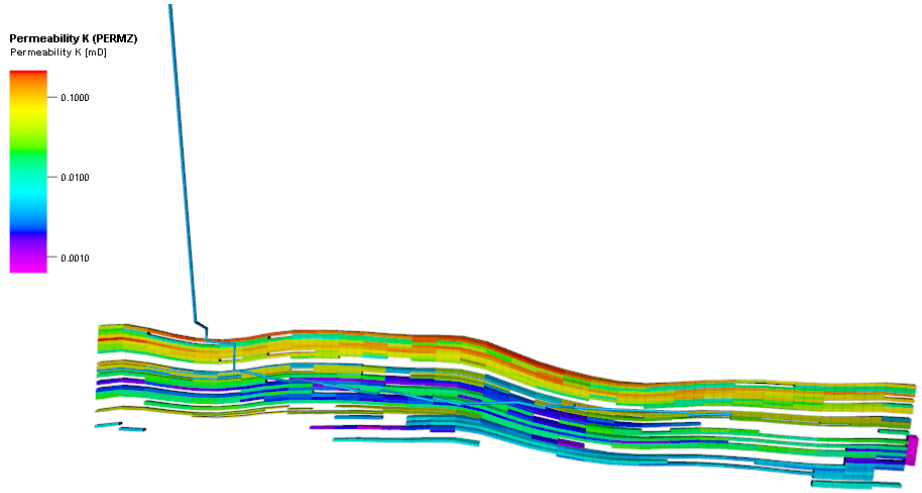

Figure 9-7: Vertical permeability in the layers contacted by the fishbone completed well. This permeability is one order of magnitude lower than the horizontal one.

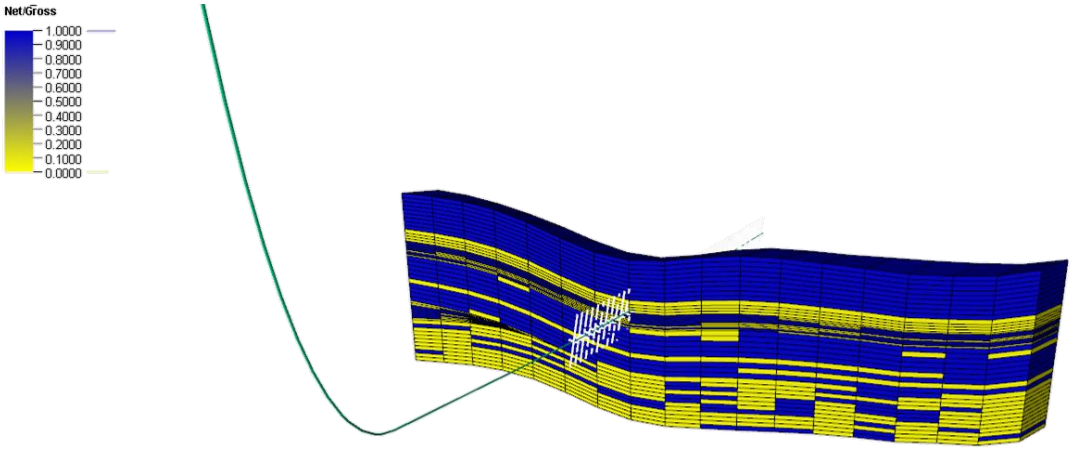

Figure 9-8: Net to gross values in a J-slice of the reservoir model. In the yellow blocks, the fluid flow is absent.

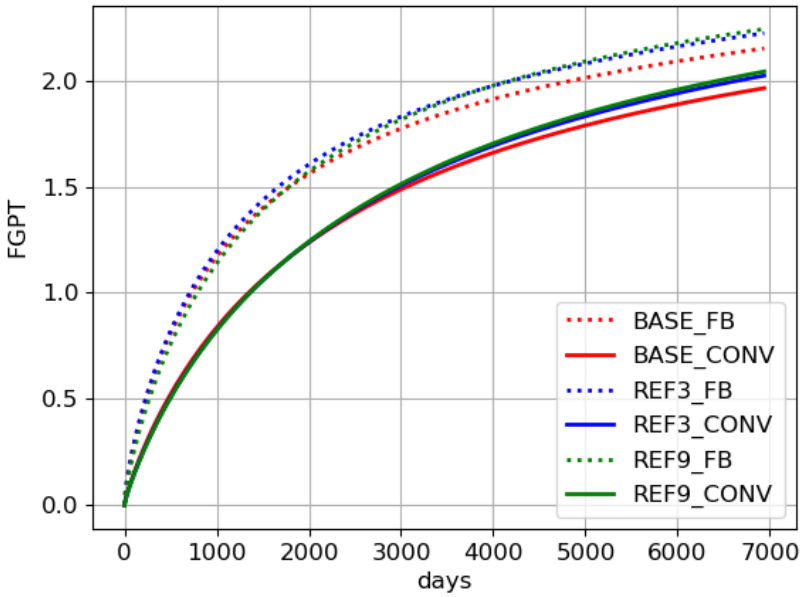

Figure 9-9: Cumulative gas production volume for the fishbone completion and the conventional well at different grid refinement.

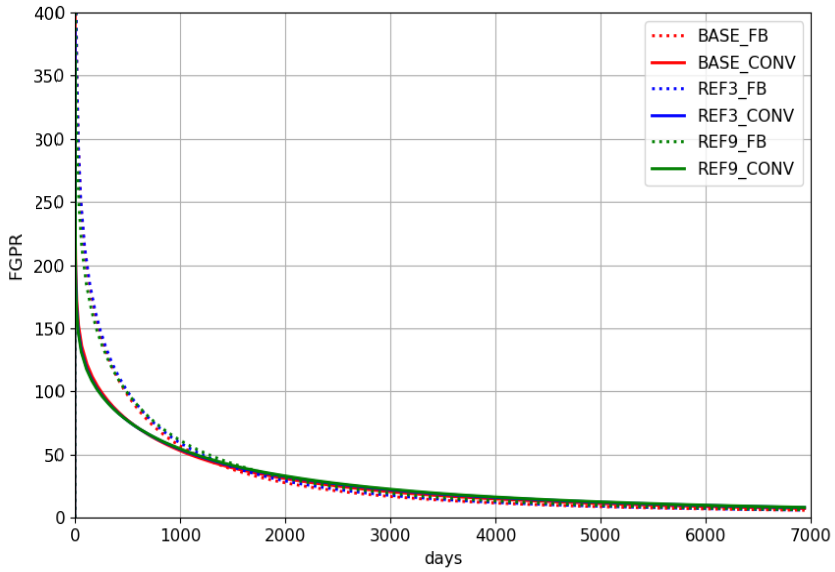

Figure 9-10: Rescaled gas production rates (or FGPR: field gas production rate) for a fishbone completion and a conventional well at different grid refinements.

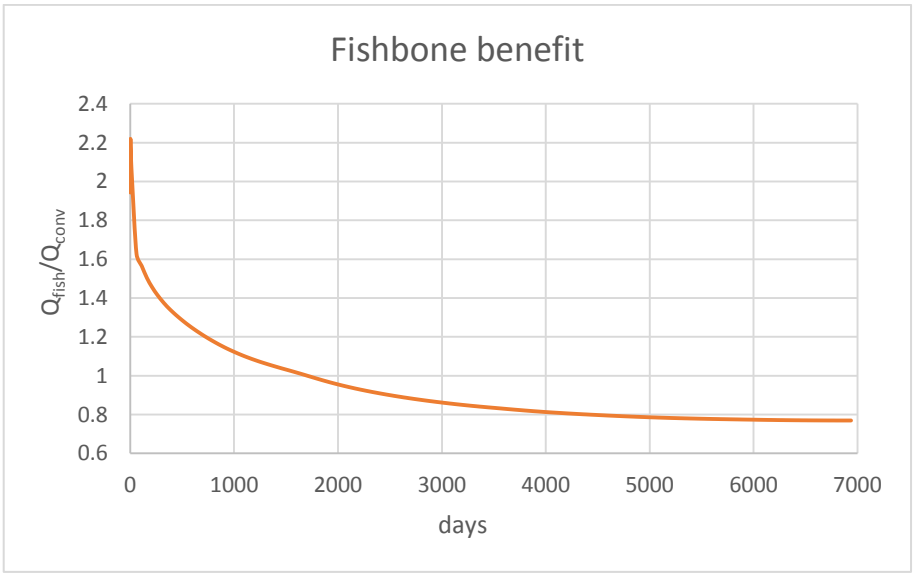

Figure 9-11: Instantaneous fishbone benefit along all the production period.

10 Conclusions

This thesis work was focused on the implementation of a methodology able to model branched completions, as a fishbone completed well, where the classical well modelling approach may not be optimal.

Three methodologies are proposed for modelling fishbone completions. All of them depart from the classic Peaceman's model used in reservoir simulations for conventional well modelling. The high resolution grid (HRG) and the Embedded Discrete Fracture Modelling (EDFM) both based on a finite volume formulation, and a detailed gridding which relies on finite element method (FEM). The latter method, available with the COMSOL Multiphysics environment, was thoroughly investigated using analytical and semi-analytical solutions to find the right grid size needed to simulate problems where wellbore and needles geometry are effectively and efficiently modelled.

These methods highlighted fishbone completion benefits for various combinations of reservoir properties, geometries and flow conditions. In particular, the production increment given by needles inflow with respect to conventional completions increases with an increase in the ratio k_h/k_v. As regards permeability/viscosity ratio, decreasing permeability or increasing viscosity does not alter the fishbone instantaneous benefit for steady state conditions. On the contrary, during transient flow, fishbone benefit is sensitive to the quoted ratio, leading to very large cumulative production increment in tight formations and with viscous fluids. As regards needle density, the main findings are two: i) the single sub performance decreases down to 75% going from 100 m to 12 m spacing due to interference and ii) the benefit per unit length of main bore increases linearly with the number of subs for a spacing between [12 m, 100 m]. In addition, fishbone completion makes the well much less sensitive to the presence of a damaged zones around wellbore.

It is worth noticing that inconsistencies between HRG on one side and FEM/EDFM on the other side posed questions on the accuracy of the former method. These differences could be ascribed to the limitation related to the use of a Cartesian grid around wellbore in a geometry where cell size is comparable with wellbore diameter and then, the Peaceman's model, which accounts for radiality of the inflow in the near-well region, cannot be used. EDFM, on the contrary, provided consistent results with FEM for problems that can be solved with both methods. This result is very important because EDFM solution is also easy to be developed for full field finite volume reservoir models. Since EDFM does not require extremely refined grids, also computational efficiency is guaranteed.

The achievements on EDFM motivated the application of this methodology to a real field. The problem is based on an high pressure/high temperature (792 bar, 150°C) off-shore gas field where hydraulic fracturing is risky. A comparison between the production of a 1 km horizontal well and a fishbone completed well (51 subs spaced by 20 m) was done. The final cumulative production increment due to Fishbones resulted to be 10% higher. than the conventional completion. However, the main advantage is the production anticipation (in the order of 4 years) due to a flow rate also doubled in the first production period.

Future works can be undertaken to improve accuracy and efficiency in the estimation of fishbone completion benefits:

- The main wellbore and needles were modelled with the same bottom hole pressure. However, pressure drops due to friction losses in the annulus and across production valves should be considered to obtain more accurate results. Exploiting COMSOL Multhipysics environment, Darcy's law and Navier-Stokes equations can be coupled to estimate pressure losses in the completions. Also temperature change impact on production can be incorporated in the model.
- The definition of an abacus that for given cell block dimensions and properties returns a geometric skin factor due to the fishbone completion. This abacus could be used whenever the grid size is too large for implementing fishbone using EDFM.

In conclusion, after a preliminary real field test, the findings of this thesis work will allow to define a fishbone completion based development plan. In fact, since the modified EDFM approach resulted to be accurate and robust also with mild grid refinement, there is the confidence to rely on this methodology once economic decisions must be taken.

Appendix

Table A 1: Saturated black-oil properties.

Dissolved gas-oil ratio (Rs)	Bubble point pressure [bar]	Bo [rm^3/Sm^3]	Viscosity [cP]
11.46	40	1.064	4.338
17.89	60	1.078	3.878
24.32	80	1.092	3.467
30.76	100	1.106	3.100
37.19	120	1.120	2.771
43.62	140	1.134	2.478
46.84	150	1.141	2.343
50.05	160	1.148	2.215
53.27	170	1.155	2.095
56.49	180	1.162	1.981
59.70	190	1.169	1.873
62.92	200	1.176	1.771
66.13	210	1.183	1.674
69.35	220	1.190	1.583
72.57	230	1.197	1.497
74.00	234	1.200	1.460
80.00	245	1.220	1.400
81.00	800	1.221	1.390

Table A 2: Undersaturated black-oil properties.

Dissolved gas-oil ratio (Rs)	Undersaturated pressure [bar]	Bo [rm^3/Sm^3]	Viscosity [cP]
Rs = 74	234	1.200	1.460
	250	1.198	1.541
	300	1.194	1.787
Rs = 80.00	245	1.220	1.400
	300	1.215	1.700
	800	1.210	1.800
Rs = 81.00	800	1.221	1.390
	810	1.210	1.400

Table A 3: Surface densities.

Oil [kg/Sm^3]	Water [kg/Sm^3]	Gas [kg/Sm^3]
912	1000	0.8266

Table A 4: Water properties

Ref pressure [bara]	B_w (Pref)	Compressibility [1/bara]	Viscosity [cP]	Water viscosibility [1/bara]
234.46	1.0042	5.43E-05	0.5	1.11E-04

Table A 5: Rock properties.

Ref pressure [bara]	Compressibility [1/bara]
300	1.42E-05

Table A 6: Dry gas properties.

P [bara]	Bg [rm^3/Sm^3]	Viscosity [cP]
120	0.011711	0.0173
201	0.007069	0.0198
241	0.005974	0.0213
276	0.005283	0.0228
311	0.004779	0.0243
401	0.003963	0.0285
440	0.003754	0.0301
451.7	0.003693	0.0306
477.5	0.003573	0.0317
501.8	0.003471	0.0327
526.7	0.003378	0.0337
552.4	0.003289	0.0347
576.9	0.003213	0.0357
600.5	0.003149	0.0366
628.6	0.003079	0.0377
652.5	0.003021	0.0386
676.7	0.002967	0.0396
702.1	0.002916	0.0405
726.5	0.002871	0.0414
751.4	0.002825	0.0424
776	0.002786	0.0433
792.2	0.002762	0.0438
800.4	0.002752	0.0441

References

(1) *alien-homepage.de.* 2018. http://alien-homepage.de/personal/environment/the_deepwater_horizon%20incident.html (accessed July 2018).

(2) Aziz, Khalid, and Antonin Settari. *Petroleum reservoir simulation.* Applied Science Publ. Ltd., London, UK, 1979.

(3) Borisov, J.P. *Oil Production Using Horizontal and Multiple Deviation Wells.* Bartlesville, Oklahoma, 1954.

(4) Brandt, A.R., et al. "Methane leaks from North American natural gas systems." *Science*, 2014: 733-735.

(5) Casciano, C., A. Cominelli, and M. Bianchi. "Latest Advances In Simulation Technology For High-resolution Reservoir Models: Achievements And Opportunities For Improvement. Society of Petroleum Engineers." 15/09/2015.

(6) Castro-Alvarez, Fernando, Peter Marsters, Diego Ponce de Leon Barido, and Daniel M. Kammen. "Sustainability lessons from shale development in the United States for Mexico and other emerging unconventional oil and gas developers." *Elsevier*, 2017.

(7) Cavalcante, Filho J. S. A., Y. Xu, K. Sepehrnoori, The University of Texas at Austin, H. Høgstøl, and Statoil. "Modeling Fishbones Using the Embedded Discrete Fracture Model Formulation: Sensitivity Analysis and History Matching." *Society of Petroleum Engineers*, 2015.

(8) Cavalcante, Filho Jose Sergio de Araujo, and Mahmood Shakiba. *Implementation of a Preprocessor for Embedded Discrete Fracture Modeling in an IMPEC Compositional Reservoir Simulator.* Society of Petroleum Engineers, 2015.

(9) Dake, L. P. *Fundamental of reservoir engineering.* Elsevier, 1978.

(10) *Drilling Contractor.* n.d. http://www.drillingcontractor.org/what-the-shales-have-taught-us-14454 (accessed July 2018).

(11) ExxonMobil. “2018 Outlook for Energy: A View to 2040.” 2018.

(12) Farrell, A. E., and A. R. Brandt. “Risks of the oil transition.” *Environmental Research Letters* 014004 (2006).

(13) *Fishbones AS.* n.d. http://fishbones.as/ (accessed august 2018).

(14) *Fishbones AS.* 2018. http://fishbones.as/case-study/ (accessed august 2018).

(15) Freyer, R., Fishbones, J.R. Shaoul, and StrataGen Delft. "Lateral Stimulation Method." *Society of Petroleum Engineers*, 2011.

(16) Hawkins, Murray F. JR. "A NOTE on the SKIN EFFECT." *Journal of Petroleum Technology*, 1956: 65-66.

(17) Heinemann, ZE, C Brand, M Munka, and Y.M. Chen. "Modeling Reservoir Geometry With Irregular Grids." *SPE Symposium on Reservoir Simulation*, 1989.

(18) Holmes, Jonathan A. "Well Modelling and Optimization." Abingdon, UK: Schlumberger, 2005.

(19) *https://www.comsol.it/multiphysics/finite-element-method#second.* n.d. (accessed October 20, 2018).

(20) *httpssanjaypaul70.wordpress.com20121116a-risk-for-fracking-workers.* n.d. (accessed August 2018).

(21) International Energy Agency. *World Energy Outlook 2016.* International Energy Agency, 2016.

(22) Jackson, Robert B., et al. "The Environmental Costs and Benefits of Fracking." *The Annual Review of Environment and Resources*, 2014: 327-337.

(23) Klovning, Carl-Ivar. *Simulation of Wells with Fishbones using ECLIPSE.* Norwegian University of Science and Technology, 2016.

(24) Kuuskraa, V., S. H. Stevens, and K. D. Moodhe. *Technically Recoverable Shale Oil and Shale Gas Resources: An Assessment of 137 Shale Formations in 41 Countries Outside the United States.* U.S. Energy Information Administration, US Department of Energy, 2013.

(25) Li, Liyong, Seong H. Lee, and Chevron Enegy Technology. *Efficient Field-Scale Simulation of Black Oil in a Naturally Fractured Reservoir Through Discrete Fracture Networks and Homogenized Media.* Society of Petroleum Engineers, 2008.

(26) LR Senergy. “Smørbukk Sør Well Modelling: Completion Design Study and Quantifying the Impact of Near Wellbore Formation Damage on Multi Lateral Well Performance.” LR Senergy Project Number: PW13STO049N, 10/06/2015.

(27) Miao, J., W. Yu, Z. Xia, W. Zhao, Y. Xu, and K. Sepehrnoori. "An Easy and Fasy EDFM Method for Production Simulation in Shale Reservoirs with Complex Fracture Geometry." (American Rock Mechanics Association) 2018.

(28) Muskat, Morris. “The Flow of Homogeneous Fluids Through Porous Media.” 194-240. McGraw-Hill, 1937.

(29) Panfili, P., A. Cominelli, and Eni E&P. "Simulation of Miscible Gas Injection in a Fractured Carbonate Reservoir using an Embedded Discrete Fracture Model." Society of Petroleum Engineers, 2014.

(30) Peaceman, D. W. "Interpretation of Well_block Pressures in Numerical Reservoir Simulation." Edited by Society of Petroleum Engineers Journal, 183-194. 1978.

(31) Peaceman, D. W. "Interpretation of Wellblock Pressures in Numerical Reservoir Simulation (includes associated paper 6988." 183-194. Society of Petroleum Engineers Journal, 1978.

(32) Peaceman, D. W. "Interpretation of Well-Block Pressures in Numerical Reservoir Simultator With Nonsquare Grid Blocks and Anisotropic Permeability." *SPE Journal*, 1983: 531-543.

(33) Petroleum Servicies Association of Canada. *Facts about Canada's Oil and Gas Industry.* 2018. https://oilandgasinfo.ca/all-about-fracking/fracking-explained/ (accessed august 2018).

(34) Quandalle , P. "The use of flexible gridding for improved reservoir modeling." *SPE Reservoir Simulation Symposium*, 1983.

(35) Quandalle, P, and P Besset. "Reduction of grid effects due to local sub-gridding in simulations using a composite grid." *SPE Reservoir Simulation Symposium*, 1985.

(36) Quarteroni, A., and A. Valli. *Numerical Approximation of Partial Differential Equations (Vol.23).* Springer Science & Business Media, 2008.

(37) Quarteroni, Z. Chen, G. Huan, and Y. Ma. *Computational methods for multiphase flows in porous media.* Vol. Vol. 2. Siam, 2006.

(38) Rice, K, T Jorgensen, Fishbones, Jeremy Waters, and EnerVest Operating LLC. "First Installation of Efficient and Accurate Multilaterals Stimulation Technology in Carbonate Oil Apllication." *Society of Petroleum Engineers*, 2014.

(39) Rosa, L., M. C. Rulli, K. F. Davis , and P. D'Odorico. “The water-energy nexus of hydraulic fracturing: a global hydrologic analysis for shale oil and gas extraction.” *Earth's Future*, 2018.

(40) Scanlon , Bridget R., Robert C. Reedy, Frank Male, and Michael Hove. "Managing the Increasing Water Footprint of Hydraulic Fracturing in the Bakken Play, United States." *Environmental Science and Technology*, 2016: 10273-10281.

(41) Schlumberger. "ECLIPSE user guide 2009.1." 2009.

(42) Shu, Jones. *COMPARISON OF VARIOUS TECHINQUES FOR COMPUTING WELL INDEX*. STANFORD UNIVERSITY, 2005.

(43) Sintef.no. *MRST - MATLAB Reservoir Simulation Toolbox.* 2015. https://www.spe-uk.org/aberdeen/wp-content/uploads/2015/11/SPE-Aberdeen-presentation-Oct-2015-for-web.pdf (accessed October 2018).

(44) *SlideServe.* n.d. https://www.slideserve.com/kris/fossil-fuels (accessed July 2018).

(45) Szanyi, Marton L., Casper S. Hemmingsen, Wei Yan, Jens H. Walther, and Stefan L. Glimberg. “Near-wellbore modeling of a horizontal well woth Computational Fluid Dynamics.” *Journal of Petroleum Science and Engineering*, 2017.

(46) Torvund, S., et al. "First Installation of Multilateral Drilling Stimulation Technology in Tight Sandstone Formation." *Society of Petroleum Engineers*, 2016.

(47) Wasserman, M.L. "Local Grid Refinement for Three-Dimensional Simulators." *SPE Symposium on Reservoir Simulation*, 1987.